

2023

# Deconstructing wound healing: in vitro models and factors affecting stromal tissue repair

---

<https://hdl.handle.net/2144/45474>

*"Downloaded from OpenBU. Boston University's institutional repository."*

BOSTON UNIVERSITY  
COLLEGE OF ENGINEERING

Dissertation

**DECONSTRUCTING WOUND HEALING:  
IN VITRO MODELS AND FACTORS AFFECTING STROMAL TISSUE REPAIR**

by

**MEGAN E. GRIEBEL**

B.S., University of Illinois at Urbana-Champaign, 2016  
M.S., Boston University, 2020

Submitted in partial fulfillment of the  
requirements for the degree of  
Doctor of Philosophy

2023



Approved by

First Reader

---

Christopher S. Chen, M.D., Ph.D.  
William Fairfield Warren Distinguished Professor  
Professor of Biomedical Engineering  
Professor of Materials Science and Engineering

Second Reader

---

Jeroen Eyckmans, Ph.D.  
Research Assistant Professor of Biomedical Engineering

Third Reader

---

Muhammad H. Zaman, Ph.D.  
Professor of Biomedical Engineering  
Professor of Materials Science and Engineering  
Professor, Howard Hughes Medical Institute

Fourth Reader

---

Elise F. Morgan, Ph.D.  
Associate Dean for Research and Faculty Development  
Maysarah K. Sukkar Professor of Engineering Design and  
Innovation  
Professor of Mechanical Engineering  
Professor of Materials Science and Engineering  
Professor of Biomedical Engineering

Fifth Reader

---

Daniel S. Roh, M.D., Ph.D.  
Laszlo N. Tauber Assistant Professor of Surgery  
Chobanian and Avedisian School of Medicine

## **DEDICATION**

I dedicate this work to my Mom, my Dad, and my brother.

Thank you for always believing in me and for supporting me as I have become the family scientist. I am so grateful to have a family full of love to call home.

## ACKNOWLEDGMENTS

Research is a community effort, and I therefore have many people to thank for their assistance, support, and helpful intellectual discussions that have buoyed me throughout my graduate work. First, I would like to thank both of my advisors, Dr. Chris Chen and Dr. Jeroen Eyckmans, for their unwavering encouragement and patience over the years, for their wise and helpful scientific guidance, and for creating a healthy lab culture that promotes natural curiosity, personal and professional growth, and the development of well-rounded scientists.

Second, I would like to thank Anish Vasan, my second author, right-hand man, and sanity check in lab. Without his inquisitive nature, calm and steady presence, and inclination to be in lab at odd hours, my graduate experience would not have been as positive. Next, I would like to thank the rest of the tissue repair team, including Hayden Myers, Emily Davis, and Winnie Wang for their community and help within the lab. In addition to my immediate team, I have benefitted from the help, support, guidance, and community of the entire lab. We are a big team, and at risk of accidentally leaving someone out, I will not list all of the lab member and alumni names. I am very grateful to each and every member of the lab for their companionship in science and personal friendships.

The work in Chapter 3 was supported by NIBIB (R21 EB028491) and NSF. The Transmission Electron Microscope was funded by NIH Award Number

S10OD028571. We would like to thank Dr. Maria Medalla, Dr. Haiyan Gong, and the rest of the TEM staff for their invaluable assistance with TEM experiments, and Prof. Jerome Mertz for his expert guidance in the design of the laser ablation setup.

I would also like to thank the members of my dissertation committee, Dr. Muhammad Zaman, Dr. Elise Morgan, and Dr. Daniel Roh. I am grateful for their helpful questions at my prospectus defense, in committee meetings, and at my dissertation defense.

Last, but not least, I would like to thank all of my friends and family for their continued love and encouragement throughout the years. I am very fortunate to have a network of amazing people in my life. I will not attempt to list everyone, but if you are reading this (unlikely), you know who you are. Thank you, and I love you.

**DECONSTRUCTING WOUND HEALING:  
IN VITRO MODELS AND FACTORS AFFECTING STROMAL TISSUE REPAIR**

**MEGAN E. GRIEBEL**

Boston University, College of Engineering, 2023

Major Professors: Christopher S. Chen, M.D., Ph.D., William Fairfield Warren  
Distinguished Professor, Professor of Biomedical  
Engineering, Professor of Materials Science and  
Engineering

Jeroen Eyckmans, Ph.D., Research Assistant Professor of  
Biomedical Engineering

**ABSTRACT**

Damage to our tissues occurs daily and must be repaired by the body in a timely manner in order to prevent infection and restore tissue integrity. Many cell types are involved in the healing process, but it is the cells of the stroma that are largely responsible for rebuilding fibrous tissue, which provides structure and support for all other cell types during healing. This dissertation focuses on stromal tissue repair, the rebuilding of fibrous tissue by fibroblasts following injury. Specifically, I focus on 1) models to study wound healing in vitro, and the specific biological processes of healing that each model captures, 2) the response of engineered stromal microtissues to different methods of injury, namely laceration and laser ablation, and the subsequent clearance and rebuilding of the extracellular matrix by fibroblasts, and 3) how different types of stromal cells and extracellular matrix proteins contribute to tissue repair in vitro.

## TABLE OF CONTENTS

DEDICATION.....	iv
ACKNOWLEDGMENTS.....	v
ABSTRACT.....	vii
TABLE OF CONTENTS .....	viii
LIST OF TABLES .....	xii
LIST OF FIGURES.....	xiii
LIST OF ABBREVIATIONS.....	xiv
CHAPTER ONE: Introduction .....	1
1.1. OVERVIEW .....	1
1.2. BACKGROUND: Wound healing .....	2
1.2.1. Structure of skin .....	2
1.2.2. Phases of wound healing .....	6
1.2.3. Pathological wound healing.....	13
1.2.4. Models to study wound healing.....	15
1.3. BACKGROUND: Fibroblasts.....	19
1.3.1. Phenotypic heterogeneity of fibroblasts .....	19
1.3.2. Fibroblasts in wound healing.....	20
1.3.3. Fibroblast differentiation to myofibroblasts .....	22
1.3.4. Myofibroblast role in tissue remodeling.....	24
1.4. OBJECTIVES: Outline of objectives by chapter.....	25

CHAPTER TWO: Deconstructing the wound healing process with in vitro models	
.....	28
2.1. INTRODUCTION .....	28
2.2. HEMOSTASIS .....	29
2.3. INFLAMMATION .....	31
2.4. GRANULATION TISSUE FORMATION .....	35
2.5. REEPITHELIALIZATION.....	41
2.6. REMODELING.....	42
2.7. DISCUSSION .....	43
CHAPTER THREE: Fibroblast clearance of damaged tissue following laser	
ablation in engineered microtissues .....	46
3.1 INTRODUCTION .....	47
3.2. RESULTS .....	50
3.2.1. Laser ablation creates holes in microtissues surrounded by non-viable	
tissue .....	50
3.2.2. Ablated microtissues close following an initial opening phase.....	54
3.2.3. Characterization of fiber damage and movement at gap periphery ...	57
3.2.4. Transmission electron microscopy reveals intracellular fibrillar	
structures, suggesting phagocytosis of ECM after ablation .....	62
3.3. DISCUSSION .....	65
3.4. METHODS.....	67
3.5. SUPPLEMENTAL MATERIAL .....	74

CHAPTER FOUR: Effects of fibroblast phenotype and ECM composition on repair potential in engineered stromal microtissues .....	78
4.1. INTRODUCTION .....	78
4.2. PILOT STUDY 1: Fibroblasts from different tissues have varying in vitro repair potentials .....	82
4.2.1. Motivation .....	82
4.2.2. Methods .....	82
4.2.3. Results .....	86
4.2.4. Discussion .....	90
4.3. PILOT STUDY 2: Effect of ECM composition on fibrous tissue healing in microtissues .....	92
4.3.1. Motivation .....	92
4.3.2. Methods .....	93
4.3.3. Results .....	96
4.3.4. Discussion .....	97
4.4. PILOT STUDY 3: Fibroblast activation to myofibroblast phenotype in standard cell culture .....	99
4.4.1. Motivation .....	99
4.4.2. Methods .....	100
4.4.3. Results .....	103
4.4.4. Discussion .....	107

CHAPTER FIVE: Perspectives .....	109
5.1. PERSPECTIVES: Fibroblast clearance after laser ablation (Chapter 3) .....	109
5.1.1. Summary of findings .....	109
5.1.2. Remaining questions .....	110
5.1.3. Broader context.....	113
5.2. PERSPECTIVES: Fibroblast type and ECM composition (Chapter 4) ...	114
5.2.1. Summary of findings .....	114
5.2.2. Future directions .....	115
5.3. CONCLUSION.....	118
APPENDIX: Supplemental Movies .....	119
REFERENCES .....	120
CURRICULUM VITAE .....	146

## LIST OF TABLES

Table 3.S1: Measured laser power and calculated laser fluence .....	77
Table 4.1: Cell sources and growth medias used in Pilot Study 1.....	84
Table 4.2: qPCR primer sequences used in Pilot Study 3. ....	102

## LIST OF FIGURES

Figure 1.1: Structure of human skin (Terese Winslow, NCI Visuals Online, 2008). .....	3
Figure 1.2: Schematic presentation of timing of the wound healing stages (Häkkinen, Larjava, & Koivisto, 2011). .....	7
Figure 1.3: Proposed models of keratinocyte migration (Rousselle, Braye, et al., 2019). .....	12
Figure 1.4: Myofibroblast differentiation (Tomasek et al., 2002). .....	23
Figure 3.1: Tissue injury by transection and laser ablation in stromal microtissues. ....	53
Figure 3.2: Closure of injured microtissues. ....	56
Figure 3.3: Fiber disruption and breakage following ablation. ....	61
Figure 3.4: Transmission electron microscopy suggests ECM fiber uptake after ablation. ....	64
Figure 3.S1: Quantification of damaged tissue area. ....	74
Figure 3.S2: Details of laser ablation system. ....	75
Figure 4.1: Injury responses in microtissues of various human cell types. ....	88
Figure 4.S1: Closure rates for various cell types colored by cell source. ....	89
Figure 4.2: ECM composition alters microtissue closure and compaction. ....	96
Figure 4.3: Fibroblast activation in standard cell culture. ....	106

## LIST OF ABBREVIATIONS

$\alpha$ SMA	alpha-smooth muscle actin
CTGF	connective tissue growth factor
DEJ	dermal-epidermal junction
DMSO	di-methyl sulfoxide
ECM	extracellular matrix
EGF	epidermal growth factor
EMT	epithelial-to-mesenchymal transition
FGF	fibroblast growth factor
FPCL	fibroblast-populated collagen lattice
GM-CSF	granulocyte-macrophage colony-stimulating factor
HCF	human cardiac fibroblast
HDF	human dermal fibroblast
HGF	hepatocyte growth factor
HLF	human lung fibroblast
IL	interleukin
iPSC	induced pluripotent stem cell
KGF	keratinocyte growth factor
MMP	matrix metalloproteinase
MSC	marrow-derived stromal cell
PDGF	platelet-derived growth factor
PDMS	poly dimethyl siloxane

qPCR .....quantitative polymerase chain reaction  
TEM..... transmission electron microscopy  
TGF $\beta$ .....transforming growth factor beta  
TIMP ..... tissue inhibitor of metalloproteinases  
TNF $\alpha$ ..... tumor necrosis factor alpha  
uPARAP ..... urokinase plasminogen activator receptor-associated protein  
VEGF .....vascular endothelial growth factor

## **CHAPTER ONE: Introduction**

### **1.1. OVERVIEW**

Damage to our tissues occurs daily. Bumps and bruises, air pollution, strenuous exercise, alcohol intoxication, and skin trauma like burns or surgical incisions, all result in tissue damage that must be repaired by the body. Other than development and pregnancy, tissue repair is perhaps the most complicated, dynamic, and highly coordinated set of physiological processes. There are several tissues that each participate in the healing process: vasculature, white blood cells, connective tissues, and epithelium. Each has an important role to play in order for the body to heal correctly. Immune cells clear pathogens and necrotic tissue, and release an abundance of signaling molecules that help direct other cells in healing. The vasculature supplies nutrients and oxygen and removes waste from the site of healing. The ultimate goal is to restore the integrity, and ideally the function, of the epithelium. But it is the cells of the stroma that are largely responsible for rebuilding the fibrous tissue that provides structure and support for all other cell types. This dissertation focuses on stromal tissue repair, the rebuilding of fibrous tissue by stromal cells following injury. Specifically, I focus on 1) models to study tissue repair in vitro, and the specific aspects of the healing process that each model captures, 2) the response of stromal microtissues to different methods of injury, and the subsequent clearance and rebuilding of the extracellular matrix, and 3) how different types of stromal cells and extracellular matrix proteins contribute to tissue repair in vitro.

The overall tissue repair process is generally considered the same regardless of where in the body it occurs. However, there are many differences between organs – stiffness, architecture, matrix composition, cell type composition, presence of stem cells, degree of vascularization, etc. – that lead to differences in the healing process. Because of these complexities, the first two chapters of this dissertation are mainly focused on tissue repair in the skin, also called wound healing. In Section 1.2, I describe the structure of skin and the classic phases of wound healing. The pathological outcomes of improper healing are described, as well as the models used to study wound healing. In Section 1.3, I expand on fibroblast biology and the role of the fibroblast – and its activated counterpart, the myofibroblast – in wound healing. In Section 1.4, I will state the questions explored in this dissertation and the goals for each of the subsequent chapters.

## **1.2. BACKGROUND: Wound healing**

### **1.2.1. Structure of skin**

The skin is the largest organ of the body. It serves two critical purposes – to prevent fluid loss and to protect the body from environmental threats, including physical insults, pathogens, and heat loss. The skin is composed of three layers, from the inside out, the subcutaneous tissue, the dermis, and the epidermis. For convention, we will consider the epidermis the top and subcutaneous tissue the bottom, as in Figure 1.1.

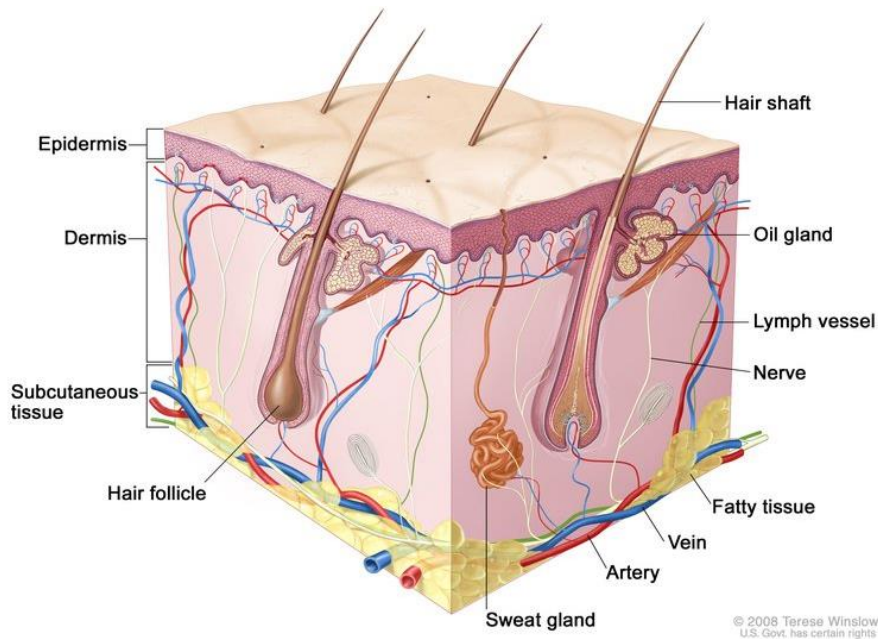


**Figure 1.1: Structure of human skin (Terese Winslow, NCI Visuals Online, 2008).**

**A. Subcutaneous tissue:** The subcutaneous tissue, or hypodermis, is mainly comprised of adipose tissue. The superficial fat layer sits beneath the dermis on all parts of the body. In some places, there is also an underlying deep fat layer, called visceral fat, separated from the superficial fat by the fascia superficialis. Where visceral fat is absent, the fascia superficialis is continuous with the muscle fascia. Atop the superficial fat layer is a network of neurons, blood vessels, and lymphatic vessels that border the dermis. The dermis and superficial fascia are linked by fibrous septa that are arranged vertically throughout the subcutaneous fat layer (Estève et al., 2019; Illouz, 1990). The hypodermis provides mechanical shock protection and thermal insulation (Baroni et al., 2012). It is also an active component of the endocrine system and is important for glucose and lipid

metabolism (Scheja & Heeren, 2019).

**B. Dermis:** The main cell type found in the dermis is the fibroblast. The dermis is composed of fibrillar extracellular matrix (ECM) proteins. This ECM is mainly collagen, about 90% collagen type I and 10% collagen type III in adults (Krieg & Aumailley, 2011). Several other fibrillar ECM proteins are also found in the dermis, including elastin, fibronectin, vitronectin, and fibrillin. These fibrillar proteins determine the rigidity and elasticity of the dermis (Tracy, Minasian, & Caterson, 2016). The dermis is formed of two layers, the lower reticular dermis and the upper papillary dermis, which differ in their cell density, degree of fiber organization, and quantity of proteoglycans. The papillary dermis has a higher density of cells, and loose connective tissue with more proteoglycans, denser near the dermal-epidermal junction (DEJ) and decreasing in density towards the reticular dermis. The reticular dermis has more organized and denser collagen bundles than does the papillary dermis, but has a lower cell density (Korosec et al., 2019; Rippa, Kalabusheva, & Vorotelyak, 2019).

The dermis also contains blood vessels, nerves, and several appendages: hair follicles, sweat glands, and sebaceous glands. The appendages are derived from the epidermis during development, and extend down into the dermis. Sweat glands are responsible for sweat and waste excretion and temperature regulation. Sebaceous glands contain specialized keratinocytes that make

sebum, a lipid mixture that protects against fluid loss in the epidermis. Hair follicles disperse sweat and sebum and aid in thermal regulation. They also serve as a repository for self-renewing progenitor cells. During wound healing in adult humans, these appendages are not regenerated but are instead replaced with scar tissue (Hosseini, Koehler, & Shafiee, 2022; Weng et al., 2020).

**C. Epidermis:** The epidermis consists of stratified layers (strata) of specialized epithelial cells called keratinocytes. The layer closest to the dermis is the stratum basale, followed by the stratum spinosum, the stratum granulosum, the stratum lucidum, and the outermost stratum corneum. The keratinocytes of the basal layer are the most proliferative, a capacity which is lost as the keratinocytes differentiate and move up through the spinous and granular layers (Baroni et al., 2012). The basal layer is just one cell thick and is adhered to the basement membrane. The basement membrane is a layer of specialized ECM, composed of collagen type IV, laminin, nidocan, and perlecan, which forms the DEJ and is anchored to the dermis below and the epidermis above (Aumailley, 2021). Dispersed among the keratinocytes of the basal layer are melanocytes, the pigment producing cells of the hair and skin (Wickett & Visscher, 2006). As keratinocytes mature and move up through the strata spinosum, they produce structural proteins called keratins and lamellar bodies containing lipids. The strata spinosum also contains Langerhans cells, the specialized dendritic cells of the skin that protect against pathogens. Keratinocytes accumulate lipid and

keratin filled granules, which give the stratum granulosum its characteristic granular appearance. In the granular layer, keratinocytes transform into corneocytes, the anuclear, flat, squamous cells of the outermost layer of the epidermis, the stratum corneum. The cells release their lipids, and after transformation, corneocytes are composed of flattened keratin microfilaments surrounded by a cell envelop of covalently linked proteins and lipids, with desmosomes linking adjacent cells. The stratum corneum is made up of 9-25 alternating lipid layers containing cholesterol and ceramides and keratin-rich squamous cell layers. The lipids of the stratum corneum are critical for fluid retention and protection against pathogens, the main functions of skin (Baroni et al., 2012; Wickett & Visscher, 2006).

### **1.2.2. Phases of wound healing**

Wound healing is classically divided into four, partially overlapping phases: hemostasis, inflammation, new tissue formation (sometimes called the proliferation and migration phase), and remodeling. Hemostasis and inflammation are described briefly, and a larger focus is given to new tissue formation and remodeling, as these are the functions of the stroma. The relative timing of each wound healing stage is depicted in Figure 1.2.

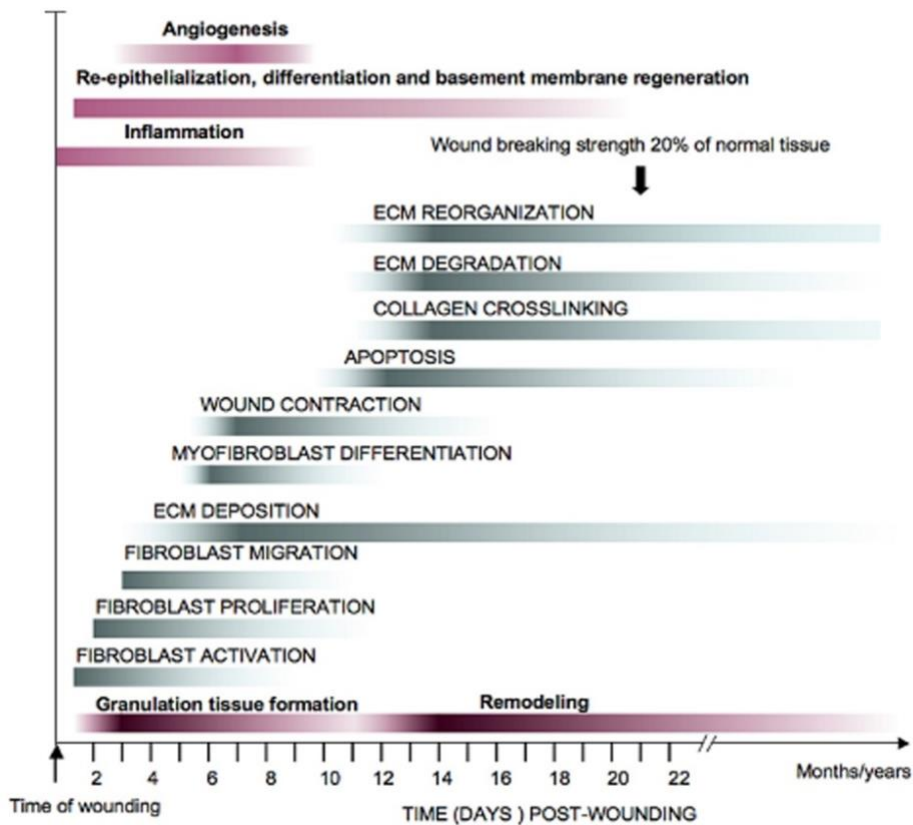


**Figure 1.2: Schematic presentation of timing of the wound healing stages (Häkkinen, Larjava, & Koivisto, 2011).**

**A. Hemostasis and inflammation:** An injury or wound damages blood vessels, exposing plasma to tissue outside of the blood, which triggers the clotting cascade and activation of thrombin. Within seconds, thrombin converts soluble fibrinogen into a thrombin clot, and initiates the aggregation of platelets to form a platelet plug (Smith, Travers, & Morrissey, 2015). Together, these processes are called hemostasis, and function to stop blood loss. Additionally, the thrombin clot serves as a reservoir for cytokines and growth factors released by damaged cells and platelets, including platelet-derived growth factor (PDGF), epidermal growth

factor (EGF), and transforming growth factor-beta (TGF $\beta$ ). The thrombin meshwork, together with plasma fibronectin, vitronectin, and thrombospondin, serve as the initial provisional matrix for immune cells, fibroblasts, and endothelial cells that follow (Opneja, Kapoor, & Stavrou, 2019).

Concurrent with hemostasis, the inflammatory phase begins within seconds of injury and lasts for several days. The wound milieu contains cytokines such as interleukin (IL)-1, tumor necrosis factor-alpha (TNF $\alpha$ ), and TGF $\beta$  that attract immune cells. Neutrophils are the first immune cells on the scene, and they release more chemoattractants and begin to clear bacteria and non-viable tissue in the wound bed (Broughton, Janis, & Attinger, 2006). Monocytes migrate into the wound and transform into macrophages, which are critical for wound healing. Macrophages, like neutrophils, release matrix metalloproteinases (MMPs), including collagenase, and contribute to the clearance of non-viable tissue via phagocytosis. Macrophages also release many cytokines and growth factors that stimulate angiogenesis, fibroblast proliferation and migration, and keratinocyte proliferation (J. E. Park & Barbul, 2004). Macrophages are classically divided into two subtypes, M1 and M2, which have different effects on the healing process. Early on, M1 macrophages are dominant and promote inflammation. M1 macrophages then induce neutrophil apoptosis and phagocytose dead neutrophils. This phagocytosis initiates a transformation to the M2 macrophage subtype, which reduces inflammation and promotes tissue repair (Opneja et al.,

2019). There is also evidence of roles for other lymphocytes, including T cells, B cells, and natural killer cells, in wound healing (Cañedo-Dorantes & Cañedo-Ayala, 2019).

**B. New tissue formation:** As the inflammatory phase begins to subside, around day three or four post-injury, the new tissue formation phase of healing begins. This phase consists of three fairly distinct biological processes that overlap in time and space: angiogenesis, or the formation of new blood vessels, fibroplasia, or the construction of fibrous granulation tissue by fibroblasts, and reepithelialization to restore the epidermal barrier.

In response to the numerous stimuli released during the inflammatory phase, including  $\text{TNF}\alpha$ ,  $\text{TGF}\beta$ , EGF, PDGF, and IL-1, fibroblasts increase proliferation and migrate into the early provisional matrix of the wound bed. Fibroblasts replace the fibrin clot with fibronectin and collagen, specifically collagen type III at this stage, to serve as the mature provisional matrix of the newly forming granulation tissue. Additionally, fibroblasts in the wound bed generate contractile forces that contribute to drawing the wound margins closer together. Wound contraction decreases both the amount of granulation tissue that must be made and the distance that epithelial cells must travel (Broughton et al., 2006; Enoch & Leaper, 2008; Gurtner, Werner, Barrandon, & Longaker, 2008; Häkkinen et al., 2011). Wound contraction and ECM production by fibroblasts will be discussed in

more depth in Section 1.3.2.

As the granulation tissue matures and is remodeled, collagen I is deposited and replaces the collagen III. During this stage, about four to seven days post-injury, persistent fibroblast activation causes their differentiation first to proto-myofibroblasts and then to myofibroblasts. The myofibroblast is an enigmatic cell type characterized by an increased production of extracellular matrix proteins and high cell contractility, often accompanied by the de novo expression of alpha-smooth muscle actin ( $\alpha$ SMA) in stress fibers. The differentiation of myofibroblasts is discussed in detail in Section 1.3.3.

Granulation tissue achieves its characteristic red granular appearance due to the abundant growth of new blood vessels during this phase of healing.

Angiogenesis, the formation of new blood vessels from preexisting ones, is important for supplying the healing tissue with oxygen and nutrients and removing waste products from the wound. Endothelial cells are stimulated to begin angiogenesis by growth factors including vascular endothelial growth factor (VEGF)-A released by keratinocytes at the wound edges and EGF, PDGF, and fibroblast growth factors (FGFs) released by platelets and macrophages in the wound bed (Enoch & Leaper, 2008; Opneja et al., 2019). Endothelial cells first break down their basement membrane using secreted MMPs, then migrate into the wound bed. Endothelial cells behind the tip cells proliferate, and new

capillaries with functional lumens are formed (Enoch & Leaper, 2008).

The new tissue formation phase cannot conclude until the epidermal layer is replaced and its barrier function restored. The process of epithelial cell migration in order to restore tissue barrier is called reepithelialization. Keratinocytes are attracted to many of the cytokines present in the wound milieu, including FGF, EGF, hepatocyte growth factor (HGF), and keratinocyte growth factor (KGF). In order to begin migration, keratinocytes undergo epithelial-to-mesenchymal transition (EMT) and disband their adhesions to the basement membrane ( $\alpha6\beta4$  integrins) in favor of integrins specific to fibronectin ( $\alpha5\beta1$  and  $\alpha v\beta6$  integrins) to enable migration on the provisional matrix of the granulation tissue (Breuss et al., 1995; Gurtner et al., 2008; Martin, 1997). As shown in Figure 1.3 from Rousselle, Braye, & Dayan, 2019, researches have proposed several models of keratinocyte migration. Following migration, the epithelial cells synthesize and form strong adhesions to a mature basement membrane, resuming their apical-basal polarity. The stratification of the epidermis is restored as basal keratinocytes terminally differentiate and move into the upper layers of the epidermis at the air interface and restore barrier function. Reepithelialization is not complete until the stratum corneum has been replaced over the entire wound bed.

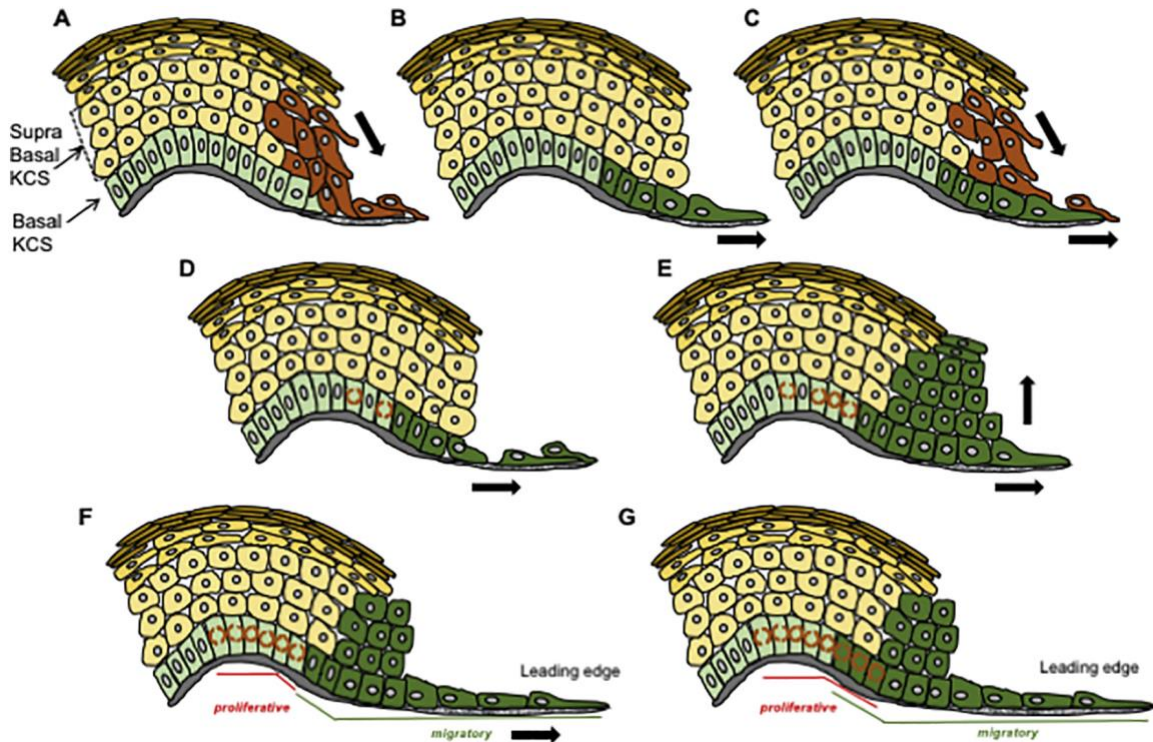


**Figure 1.3: Proposed models of keratinocyte migration** (Rousselle, Braye, et al., 2019). “(A) According to the rolling mechanism, the migrating suprabasal cells roll over leading basal cells and dedifferentiate to form new leaders at the epidermal tongue that migrate as a cohesive sheet (Bereiter-Hahn, 1986; Clark, 1993; Gibbins, 1978; Krawczyk, 1971; Winter, 1972). (B) According to the sliding mechanism, keratinocytes from the basal layer move forward in a cohesive block at the leading edge, whereas the above cluster of superficial cells is passively dragged along (Buck, 1979; Radice, 1980; R. B. Vaughan & Trinkaus, 1966; Woodley, 1996). (C) The model of Usui et al. is an alternative to both previous models suggesting that suprabasal cells de-differentiate and participate, together with the basal cells, in reconstituting the new wound epithelium (Usui et al., 2005). (D) The model of LaPlante et al. involves the passive displacement of the superficial layers over the basal layers of keratinocytes which migrate individually over each other in agreement with the rolling model of migration. Pushing force is provided by dividing keratinocytes from the adjacent unwounded epidermis (Laplante, Germain, Auger, & Moulin, 2001). (E) The model of Safferling et al. suggested that collectively migrating basal keratinocytes of the epidermal tongue continuously build a multilayered epithelium in which suprabasal cells never contact the ECM. Keratinocyte proliferation occurs in a concentric pattern around the wound, producing new cells that migrate into the direction of the wound (Safferling et al., 2013). (F) The molecular profiling of the migrating leading edge of a re-epithelializing wound in mice revealed that this zone is distinctive from a proliferative zone located behind (Aragona et al., 2017). (G) The proliferative and migratory zones overlap, and this area is the major source of surface expansion. Arrow indicates movement of basal and/or suprabasal keratinocytes. Dark green or orange colors mean that basal (dark green) or suprabasal (orange) keratinocytes are activated.”

**C. Remodeling:** The final stage of wound healing, which can last for months to years, is driven by myofibroblasts and consists of the continued remodeling of the tissue until a mostly acellular scar is left. Unlike the basket-weave configuration of collagen fibers found in healthy dermis, scar tissue consists of highly aligned and highly crosslinked collagen fibers that are parallel to the skin (Gurtner et al., 2008; Rousselle, Montmasson, & Garnier, 2019). ECM remodeling by myofibroblasts is discussed further in Section 1.3.4. At the conclusion of scar remodeling, myofibroblasts likely leave the wound by several methods, although it is still an area of active research. It was long believed that they undergo apoptosis; however, more recent studies suggest that myofibroblasts are not terminally differentiated and can revert to a quiescent state (Pakshir & Hinz, 2018).

### **1.2.3. Pathological wound healing**

Given the complexity of wound healing, it is unsurprising that the process sometimes goes awry. Pathological wound healing outcomes can be divided into two categories: under-healing and over-healing. Under-healing describes delayed wound healing and chronic or recurring wounds. Over-healing describes the formation of excessive scar tissue and encompasses fibrosis, hypertrophic scarring, and keloid scars.

**A. Under-healing:** Impaired wound healing is a major clinical problem that affects 3-6 million Americans annually, resulting in enormous health care expenditures estimated at more than \$25 billion USD per year in the US alone (Gosain & DiPietro, 2004; Han & Ceilley, 2017). The etiology of chronic wounds is varied and often related to underlying comorbidities such as diabetes, obesity, and advanced age. Venous ulcers, pressure ulcers, and diabetic foot ulcers are the most common types of chronic wounds. In these settings, a chronic inflammatory state prevents progression through the new tissue formation phase (Zhao, Liang, Clarke, Jackson, & Xue, 2016). The persistence of neutrophils and M1 macrophages in a wound causes an excess of pro-inflammatory cytokines, such as  $TNF\alpha$ , and matrix-degrading MMPs, which favor ECM degradation rather than assembly. This in turn stalls future phases of healing; in particular, reepithelialization is prevented because keratinocytes lack an adhesive matrix for migration (Raziyeva et al., 2021).

**B. Over-healing:** Hypertrophic scarring and fibrosis are characterized by the excessive deposition of dense, aligned collagenous matrix and painful wound contracture. Myfibroblasts are considered the main culprits in these disorders because of their ability to produce and contract ECM. In physiological healing, myfibroblasts undergo apoptosis or transdifferentiate and leave the wound setting after the conclusion of healing. However, in fibrosis and scarring, myfibroblasts persist due to an excess of pro-fibrotic cytokines, including  $TGF\beta$

and connective tissue growth factor (CTGF). Additionally, tissue inhibitors of metalloproteinases (TIMPs) are upregulated in fibrosis and hypertrophic scarring (Zhu, Ding, Shankowsky, & Tredget, 2013). Scar tissue is stiffer than healthy skin, and this stiffness also contributes to further myofibroblast differentiation and persistence (Pakshir & Hinz, 2018). Altogether, these factors favor ECM production over degradation. This balance between ECM deposition and degradation is an important theme for proper wound healing: too much ECM degradation results in chronic wounds, but too much ECM deposition results in fibrosis.

#### **1.2.4. Models to study wound healing**

Various experimental models have been developed to study wound healing, ranging from simple cell culture, to three-dimensional (3D) skin equivalents, to animal models. Here, I will delineate two categories of experimental models: in vivo (animal) and in vitro models. Additionally, many in silico (computational) models of wound healing have been developed (Adra, Sun, MacNeil, Holcombe, & Smallwood, 2010; Buganza Tepole & Kuhl, 2013; Guerra, Belinha, & Jorge, 2018; Jorgensen & Sanders, 2016; Kuhl & Steinmann, 2004; Menke et al., 2010; Sami, Heiba, & Abdellatif, 2019; Ud-Din & Bayat, 2017), but will not be discussed here.

**A. In vivo models:** The simplest animal models used to study wound healing are non-mammalian animals. Simple organisms, such as sponges, roundworms, and fruit flies can be used to study very specific physiological processes, such as cell patterning and dorsal closure. These processes rely on the same cell-adhesion and intracellular signaling pathways as does mammalian wound healing (Gurtner et al., 2008). Additionally, the study of amphibians is particularly exciting because of their capacity for total limb regeneration (limited to newts and salamanders) and perfect skin regeneration (seen in most amphibians including frogs). Amphibious healing displays extremely fast reepithelialization, followed by dedifferentiation and redevelopment of lost anatomical structures (Gurtner et al., 2008; Kawasumi, Sagawa, Hayashi, Yokoyama, & Tamura, 2012). Study of these creatures may provide insights that inform strategies to achieve skin regeneration in humans.

The most widely used animal to study wound healing are rodents. The use of rodents is advantageous because it enables study of the interaction of multiple tissues that contribute to healing. Additionally, the genetic background of rodents can be tightly controlled, and genes can be knocked out or modified as necessary for experimentation. However, the anatomy of murine skin differs somewhat from human skin, and the mode of wound healing in rodents is different than in humans. Rodent skin has a thin epidermis and dense hair, which is believed to aid in wound healing. The panniculus carnosus is a subcutaneous

muscle in rodents that contributes to wound contraction. Thereby, rodent wounds heal rapidly by contraction, rather than by granulation tissue formation and reepithelialization, and require splinting after wounding in order to mimic human wound healing (Galiano, Michaels V, Dobryansky, Levine, & Gurtner, 2004). Furthermore, although the cellular players and their roles in the inflammatory responses of rodents and humans overlap, there are differences in the transcription level responses between rodents and humans (Seok et al., 2013).

Large mammals, including pigs, serve as more faithful models of human wound healing. Like humans, pigs have thick epidermis and sparse hair, and they lack a panniculus carnosus. Both pigs and humans heal wounds primarily via reepithelialization, and the turnover time of the epidermis is similar between the two mammals (Sullivan, Eaglstein, Davis, & Mertz, 2001). Pigs can also be used to study wound healing in animals with comorbidities, particularly diabetes, which makes them an advantageous preclinical tool (Seaton, Hocking, & Gibran, 2015). However, because of their size and expense, pig models have not been widely adapted.

**B. In vitro models:** Unlike in vivo wound healing assays, in vitro wound healing models capture specific aspects of wound healing in isolation and have therefore been instrumental tools to investigate underlying wound healing mechanisms. Here I provide a brief description of the most commonly used in vitro wound

healing models; an elaborate discussion on this topic is provided in Chapter 2. The first category of in vitro models includes two-dimensional (2D) culture settings. Perhaps most common is the traditional 2D scratch wound assay, in which a monolayer of cells is scratched with a pipet tip to create a gap devoid of cells, and cell migration into this space is measured as a proxy for healing (Liang, Park, & Guan, 2007; Poujade et al., 2007). Basic biological mechanisms, such as rate of proliferation and migration under various conditions, can be easily measured. However, 2D settings do not capture the composition, architecture, or mechanical properties of 3D soft tissue. To address this drawback, cells can be cultured on or in 3D hydrogels. Multiple cell types can also be combined in culture to study paracrine interactions. For example, keratinocytes and fibroblasts can be cultured in different sections of a trans-well plate, and the changes in ECM expression and hydrogel contracture measured across conditions (Butler, Ly, Longaker, & Yang, 2008).

The second category of in vitro models includes organotypic models. One common example is skin equivalents, which are generated by culturing fibroblasts in a natural matrix, typically collagen I, for a week or more, followed by the seeding of keratinocytes on top of the hydrogel that are then allowed to differentiate for two to three weeks. This model recapitulates the stratification of the epidermal layer as seen in vivo, the migration of keratinocytes, and the formation of basement membrane. However, the dermal layer remains inactive

upon injury. This is likely due to the lack of mechanical loading necessary for fibroblast activation, which is important for rapid wound closure (Grinnell, 2003; M. B. Vaughan et al., 2004). Our lab has previously developed a stromal healing model where fibrous microtissues under tension are injured, and fibroblasts contract the tissue and synthesize ECM in order to repair the microtissue (Sakar et al., 2016). This model is used throughout Chapters 3 and 4 of this dissertation.

### **1.3. BACKGROUND: Fibroblasts**

#### **1.3.1. Phenotypic heterogeneity of fibroblasts**

“Stromal cells” is an umbrella term for a very diverse set of fibroblasts and fibroblast-like cells. In the skin, we call these cells dermal fibroblasts. In other organs there are specialized mesenchymal cells; for example, in the liver, these are hepatic stellate cells. There are also marrow-derived stromal cells (MSC), previously called mesenchymal stem cells, which can migrate in the circulatory system. MSC have similar morphology and perform similar functions to fibroblasts. Because they are relatively easy to collect, self-renewing, and can differentiate into osteogenic and adipogenic lineages, MSC are of great interest for potential cell therapies (Ugurlu & Karaoz, 2020).

Even within one type of fibroblast, say dermal fibroblasts, there is considerable variability depending on the site of the body, because they have different developmental origins. For example, dermal fibroblasts from the face arise from

the neural crest, whereas those from the ventral skin arise from the lateral plate mesoderm (Driskell & Watt, 2015). To further add to the heterogeneity, dermal fibroblasts (DF) from the same site can vary depending on whether they come from the papillary or the reticular dermis. For example, they differ in their ECM expression: papillary DF make more proteoglycans, whereas reticular DF make more collagens. Papillary DF are spindle-shaped; reticular DF are stellate-shaped. Reticular DF have a larger fraction of  $\alpha$ SMA-positive cells. When cultured with keratinocytes, papillary DF, but not reticular DF, support keratinocyte differentiation and stratification (Rippa et al., 2019). Fibroblast heterogeneity is important to keep in mind, particularly when using cells from an unknown or a pooled source. For example, when we purchase adult dermal fibroblasts from Lonza, we only know that they came from healthy dermis, but not which dermal layer or anatomical site.

### **1.3.2. Fibroblasts in wound healing**

Fibroblasts have many important roles in wound healing including cytokine secretion, matrix deposition and remodeling, and force generation for wound contraction. Early during wound healing, fibroblasts are activated by cytokines EGF and PDGF to increase their proliferation and migrate into the wound bed. In turn, fibroblasts secrete more PDGF, TGF $\beta$ , FGF, and keratinocyte growth factor (KGF). KGF is only made by fibroblasts and is important because it stimulates keratinocyte proliferation and migration, which are necessary for

reepithelialization (Broughton et al., 2006).

Once in the wound bed, fibroblasts replace the initial fibrin matrix with a more mature provisional matrix made of fibronectin and collagen type III. This matrix is critical because it provides a substrate over which reepithelialization can occur. In full-thickness wounds where fat is exposed, epithelial cells are unable to migrate into the wound because fat is a poor adhesive surface. Keratinocytes require first the production of a fibrous matrix to which they can adhere (Rittié, 2016). Cellular fibronectin is particularly important as its active polymerization is required for the deposition of other ECM such as collagen (Sottile & Hocking, 2002).

In addition to synthesizing and depositing ECM, fibroblasts also contribute to ECM remodeling and wound contraction via production of cellular contractility forces. Fibroblast-mediated contractility has been compared to a treadmill, where traction forces are produced as fibroblasts attempt to migrate through the ECM (Porter, 2007). This process involves cell extension, adhesion to the ECM, force generation via RhoA activation and the activity of myosin II to draw the cell towards the leading edge, and finally release of matrix adhesions in the trailing edge (Humphrey, Dufresne, & Schwartz, 2014).

### 1.3.3. Fibroblast differentiation to myofibroblasts

During wound healing, beginning about four days post injury, a new cell type begins to appear. These cells produce abundant ECM and exert relatively large amounts of force on their surrounding matrix. Because these cells often display alpha-smooth muscle actin stress fibers, they are called myofibroblasts. The expression of  $\alpha$ SMA in mouse embryonic fibroblasts is sufficient to dramatically increase their force production on soft substrates (Hinz, Celetta, Tomasek, Gabbiani, & Chaponnier, 2001), although it is unknown how this actin isoform contributes to increased contractility. This feature is not limited to  $\alpha$ SMA; in a whole-animal  $\alpha$ SMA knockout, gamma-smooth muscle actin and alpha-skeletal muscle actin were able to functionally compensate for  $\alpha$ SMA (Tomasek, Haaksma, Schwartz, & Howard, 2013).

Myofibroblast differentiation is gradual, occurring over the course of days. In the first phase, fibroblasts and other stromal cells become proto-myofibroblasts. Proto-myofibroblasts exhibit increased mechanical tension along with the formation of beta-cytoplasmic actin stress fibers. With further stimulation, these cells will then fully differentiate into myofibroblasts, characterized by  $\alpha$ SMA stress fibers (Tomasek, Gabbiani, Hinz, Chaponnier, & Brown, 2002). This process is depicted in Figure 1.4 from Tomasek et al., 2002.

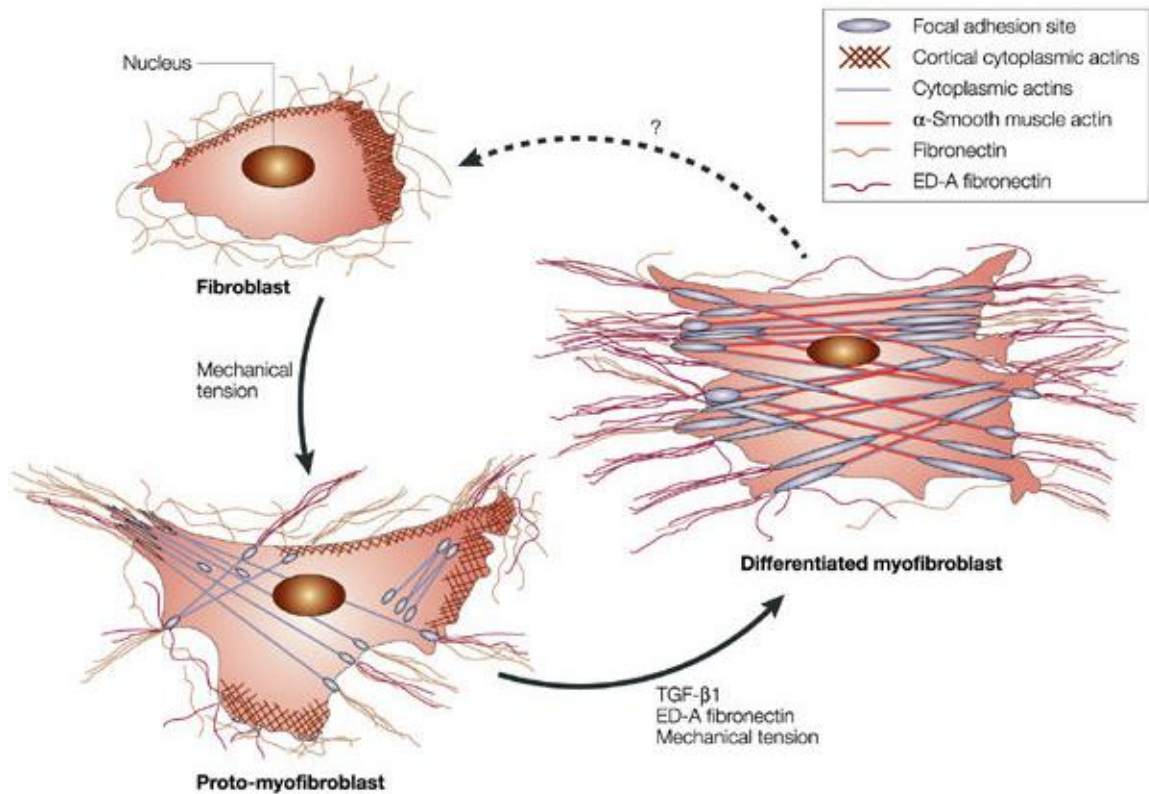


**Figure 1.4: Myofibroblast differentiation (Tomasek et al., 2002).**

*"In vivo, fibroblasts might contain actin in their cortex but they neither show stress fibres nor do they form adhesion complexes with the extracellular matrix. Under mechanical stress, fibroblasts will differentiate into proto-myofibroblasts, which form cytoplasmic actin-containing stress fibres that terminate in fibronexus adhesion complexes. Proto-myofibroblasts also express and organize cellular fibronectin — including the ED-A splice variant — at the cell surface. Functionally, these cells can generate contractile force. Transforming growth factor  $\beta$ 1 (TGF- $\beta$ 1) increases the expression of ED-A fibronectin. Both factors, in the presence of mechanical stress, promote the modulation of proto-myofibroblasts into differentiated myofibroblasts that are characterized by the de novo expression of  $\alpha$ -smooth muscle actin in more extensively developed stress fibres and by large fibronexus adhesion complexes (in vivo) or supermature focal adhesions (in vitro). Functionally, differentiated myofibroblasts generate greater contractile force than proto-myofibroblasts, which is reflected by a higher organization of extracellular fibronectin into fibrils."*

TGF $\beta$ 1 is the main mediator of this differentiation, ultimately activating the Smad family of transcription factors, which cause the aforementioned shift in protein expression. Additionally, myofibroblast differentiation is dependent on the ED-A splice variant of fibronectin. Substrate stiffness and mechanical loading are also

important for myofibroblast differentiation. Culture on soft matrices can prevent myofibroblast differentiation in multiple cell types (Olsen et al., 2011; Wang, Haeger, Kloxin, Leinwand, & Anseth, 2012). It is important to note that in the absence of regulating anti-inflammatory factors, myofibroblast differentiation becomes a positive feedback loop. Myofibroblasts synthesize more TGF $\beta$ 1 and CTGF, generate stiffer matrices, and produce increased amounts of matrix-bound latent TGF $\beta$ , thus causing further myofibroblast differentiation (Pakshir & Hinz, 2018).

#### **1.3.4. Myofibroblast role in tissue remodeling**

Myofibroblasts remodel granulation tissue in skin wounds into scar tissue. In other organs, myofibroblasts are also responsible for the development of fibrosis. ECM produced by myofibroblasts is stiffer and more highly cross-linked than typical dermal ECM. The differentiation and subsequent changes in expression profiles of myofibroblasts have been well described (Wynn, 2008). Indeed, the matrisomes of fibroblasts and myofibroblasts differ substantially, and these differences contribute to fibrosis (Bergmeier et al., 2018). More mechanistic studies are needed, however, and are particularly challenging because of the very heterogeneous population of myofibroblasts and the difficulty in maintaining their phenotype in culture (Kunz-Schughart, Wenninger, Neumeier, Seidl, & Knuechel, 2003; Oda, Gown, Vande Berg, & Stern, 1990).

#### **1.4. OBJECTIVES: Outline of objectives by chapter**

In 2018, the estimated Medicare cost for wound care, including acute and chronic wounds, ranged from \$28 billion to \$97 billion (Sen, 2019). This value is expected to increase in coming years as the aging population expands and the instances of comorbidities rises. Improved treatments for pathological wounds are needed, as are preclinical platforms required to screen potential therapies. In Chapter 2, we review the in vitro models available to study wound healing. Specifically, we deconstruct the wound healing process, and examine which models capture which subprocesses within healing. For example, compaction of unconfined collagen hydrogels by fibroblasts can be used to study factors affecting wound contraction, but cannot capture fibroblast migration or the production of a provisional matrix. In this context, we introduce our stromal healing model.

In Chapter 3, we elaborate our stromal healing model to investigate the repair response of fibroblasts in the presence of tissue damage. Clearance of damaged ECM from the wound site is an important early step of the wound healing process, and is often attributed to immune cells such as macrophages. The extent of damaged tissue in wounds is dependent on the mode of injury. For example, lesions caused by thermal injury contain more denatured collagen than do lacerations, which may cause a delay in healing. To create injuries with variable degrees of tissue damage, we inflicted wounds in engineered stromal

microtissues using two injury methods – laser ablation and laceration. In our experiments, laser ablation induced more necrosis and damage to the surrounding matrix than did laceration. Interestingly, tissue repair was delayed in laser ablated wounds as the damaged ECM was first cleared by the remaining fibroblasts. Inhibition studies targeting phagocytic pathways and transmission electron microscopy further confirmed that fibroblasts removed damaged extracellular matrix through engulfment before laying down a new provisional matrix. Together, our work presents a new bioengineered model system to study wound clearance in 3D microtissues and reveals a previously unappreciated role for fibroblasts in this process.

In Chapter 4, I describe a series of pilot experiments that were performed to begin to understand the relationships between fibroblast type and phenotype, ECM composition, and tissue repair potential. In Pilot Study 1, I examined microtissue repair responses of several primary human fibroblast types. Additionally, human dermal fibroblasts from neonatal tissue were compared to those from adult tissue. In Pilot Study 2, the initial ECM composition of the microtissues was altered slightly, and changes in injury closure rate and tissue compaction were observed. In Pilot Study 3, the activation of fibroblast to myofibroblast phenotype in 2D cell culture was examined. Different cell types were observed to have varying activation potential.

In Chapter 5, I provide a summary for each of the data-driven chapters (3 and 4) and discuss questions that are remaining from each study. To conclude this dissertation, I describe potential elaborations for the stromal healing model.

## **CHAPTER TWO: Deconstructing the wound healing process with in vitro models**

### **2.1. INTRODUCTION**

Wound care intersects with most areas of medicine and has a large market globally. Although many treatments have been developed to aid in wound healing, there is still a pressing need for improved therapies, particularly for chronic and hard to heal wounds (Ansell, Holden, & Hardman, 2012). In order to identify new therapeutic targets and screen potential drugs, researchers utilize preclinical models of wound healing. These fall into two main categories: animal models and non-animal models. Each category has its benefits and drawbacks. Animal models enable the study of the wound healing process from injury to resolution, including all participating cell types and accurate tissue architecture. However, animal wound models either poorly capture the healing process in humans (as is the case for rodent models) or are difficult, expensive, and time-consuming to adapt (as are pig models) (Sami et al., 2019). Non-animal models include in vitro studies with varying degrees of complexity. In vitro studies are less expensive, higher throughput, and more easily adapted than are animal models. Although unable to capture the full complexity of in vivo wound healing, in vitro models enable detailed mechanistic studies of specific biological processes within wound healing. In this chapter, I examine recently published wound healing studies, and categorize the in vitro models by which phase(s) of the healing process that they capture. I conclude with a discussion of potential

elaborations on in vitro wound healing models.

## **2.2. HEMOSTASIS**

Nearly all cells in the body must be located within 200  $\mu\text{m}$  of a blood vessel in order to have an efficient exchange of oxygen, carbon dioxide, nutrients, and waste. Therefore, during wounding, capillaries are inevitably damaged, allowing platelets to contact materials outside of the vascular system which causes them to adhere, aggregate, and release their cytokine-rich contents. Experiments involving platelet adhesion and aggregation can be performed using microfluidic devices. For example, one group utilized microcontact printed thin collagen films within microfluidic channels. By varying the size of collagen patches presented to platelets, they determined that a minimum “injury size” of 50  $\mu\text{m}$  is required to initiate platelet adhesion and aggregation (Hansen et al., 2013). One main advantage of these microfluidic systems is the ability to alter the shear stress by changing channel geometry. Gutierrez et. al. designed a device with eight parallel channels that encompassed a 100-fold range of shear stress values. Because of the very low volume of blood required for experimentation, they were able to use whole blood from transgenic mice in their system to determine how shear stress affects coagulation (Gutierrez et al., 2008).

While microfluidic devices, as described above, have been very useful for learning about platelet activation and the formation of thromboses, these models

lack endothelial cells and do not capture the mechanical aspects of hemostasis, such as pressure changes that occur with injury. Recently, a model of hemostasis has been developed where a pneumatic valve opens a side channel and mechanically disrupts an established endothelial monolayer. Using whole blood in this device, the authors were able to measure “bleeding time” in vitro (Sakurai et al., 2018). A very similar model has been expanded to include culture of endothelial cells on a more biomimetic collagen hydrogel channel, rather than on glass or PDMS (Poventud-Fuentes et al., 2021). These model systems have made strides in capturing hemostasis in vitro. However, as no other tissue components were incorporated, the interactions between hemostasis and downstream aspects of the healing process were not captured.

In an effort to combine aspects of coagulation with subsequent healing phases, Liu et. al. established an in vitro scab model by combining whole blood with cultured keratinocytes and initiating coagulation to form a fibrin clot. They observed scab resorption over the course of two weeks (C. Liu et al., 2022). As the keratinocytes were mixed with blood prior to coagulation, this model does not capture the migration or invasion of keratinocytes into the fibrin clot. To capture the interactions between keratinocytes and the clot matrix in an organotypic environment, skin equivalent models have been used. Briefly, skin equivalents include a dermal layer formed from decellularized dermal explants or fibroblast-laden collagenous hydrogels, which serves as the scaffold for an epidermal layer

composed of cultured keratinocytes. Following injury by scalpel or biopsy punch, the wounded region was filled with fibrin (Geer, Swartz, & Andreadis, 2002), with vitronectin, or with a synthetic matrix (Xie et al., 2010). These studies found that addition of a matrix to the wound bed which mimicked the presence of a clot promoted keratinocyte migration (Geer et al., 2002; Xie et al., 2010). Skin equivalent models will be discussed more throughout this chapter as these are very popular for studying interactions between keratinocytes and other cells, as well as the reepithelialization process.

### **2.3. INFLAMMATION**

Inflammation follows hemostasis within minutes; neutrophils arrive in the wound first, followed by monocytes that differentiate into macrophages. Because of the difficulty in maintaining the phenotype of immune cells in vitro, models that capture the interaction of neutrophils and macrophages with other skin components are rare (Urciuolo, Passariello, Imperato, Casale, & Netti, 2022). In fact, a recent model of inflammation and edema in a skin-on-chip model used only exogenous cytokines without the presence of immune cells to simulate inflammation. In a microfluidic device, porous membranes separated three cell compartments: endothelial cells, fibroblasts, and epithelial cells to mimic vasculature, dermis, and epidermis, respectively. Following addition of  $\text{TNF}\alpha$ , cytokine production and changes in endothelial permeability were measured (Wufuer et al., 2016). More recently, a similar model was established which also

incorporated M1 and M2 macrophages. This microfluidic device consisted of three parallel compartments; the central channel contained endothelial cells embedded in Matrigel™, and external compartments contained either fibroblasts or macrophages. The authors found that the presence of macrophages reduced the time it took endothelial cells to vascularize Matrigel™ (Biglari et al., 2019). The effect of neutrophils has also been investigated using the scratch wound assay (Sumagin et al., 2016) and the transwell assay (R. Menon, Krzyszczyk, & Berthiaume, 2017). Neutrophils produce neutrophil extracellular traps (NETs), a phenomena that has garnered attention in animal wound healing models (Wong et al., 2015) and which can also be studied in vitro using 3D hydrogels (Kaur, Dumoga, Koul, & Singh, 2020). These reductionist platforms are useful tools for probing the paracrine interactions between multiple cell types. However, they do not incorporate tissue architecture, physical cell interactions such as invasion and migration, or the repair process following tissue damage. To address these limitations, we turn again to biomimetic skin equivalent models.

Immune cells have been incorporated into a handful of full-thickness skin equivalent models (Pupovac et al., 2018; Urciuolo et al., 2022). As described in the previous section, skin equivalent models contain a dermal layer, comprised of fibroblasts embedded in a 3D collagen hydrogel, and an epidermal layer, formed by culturing keratinocytes on top of the dermal layer, which is raised to the air-liquid interface (ALI) in order to promote keratinocyte differentiation and

stratification. In order to facilitate movement of the skin equivalent to the ALL, they are often grown in Transwell (Chung, Choi, Lim, & Son, 2014; Kühbacher et al., 2017; Linde, Gutschalk, Hoffmann, Yilmaz, & Mueller, 2012; Ouwehand et al., 2011), Snapwell (Bechetoille et al., 2007), or Cell Crown (Chau, Johnson, Macneil, Haycock, & Ghaemmaghami, 2013) culture plates with inserts. Alternately, instead of cultured keratinocytes, explanted epidermal cell sheets have been used (Ouwehand et al., 2012).

Each of the aforementioned models incorporated one or two immune cell types to generate immunocompetent skin equivalents. Chung et. al. included macrophages in the bottom of a transwell, and recorded changes in macrophage phenotype and cytokine production in response to lipopolysaccharide stimulation (Chung et al., 2014). Linde et. al. developed a similar model, although cancerous cells instead of healthy keratinocytes were seeded on top of a fibroblast-populated collagen gel. Macrophages were included in the gel and polarized towards an M1 or an M2 phenotype, and M2 macrophages were found to promote invasion of cancer cells (Linde et al., 2012). Kreimendahl et. al. developed a wound healing assay utilizing a skin equivalent model where the dermal layers additionally contain endothelial cells, and the epidermal layers contain macrophages. After injury by CO<sub>2</sub> laser ablation, macrophage activation, angiogenic remodeling, and epidermal repair were characterized (Kreimendahl et al., 2019). As this model contains four cell types, it is one of the more complex

skin equivalent studies available. Isolated T cells and whole blood were used by Kübacher et. al. in a transwell format in order to study the response of skin equivalents to infection by a pathogenic yeast (Kühbacher et al., 2017). Studies have also incorporated T cells into skin equivalent models in the context of psoriasis and the cytokine profile was characterized, as well as keratinocyte proliferation and differentiation (Lorthoïs, Simard, Morin, & Pouliot, 2019; Shin et al., 2020).

Several models that investigate aspects of inflammation in skin equivalents incorporate tissue-resident dendritic cells and Langerhans cells. Bechetoille et. al. incorporated both of these cell types into skin equivalents and characterized the inflammatory response to tissue damage via UV irradiation (Bechetoille et al., 2007). Similarly, Chau et. al. have incorporated dendritic cells into a multilayer 3D culture for study of cytokine production, epidermal barrier changes, and dendritic cell migration in response to skin irritants (Chau et al., 2013). Several studies have incorporated Langerhans cells into dermal equivalents (Laubach et al., 2011) and measured their migration either out of the epidermal layer in response to an allergen (Kosten, Spiekstra, de Gruijl, & Gibbs, 2015; Ouwehand et al., 2011), or into the epidermal layer to mimic repopulation of the epidermis (Ouwehand et al., 2012).

In this section, I have presented several studies that incorporate immune cells

into skin equivalent models. Most of these studies described cytokine production and migration of immune cells, and some characterized keratinocyte behavior (including proliferation, migration, differentiation, and epidermal barrier function), in response to tissue damage caused by chemical irritants, UV irradiation, or the presence of pathogens. Although the dermal compartment is present in each of these models, it is unclear how fibroblast behavior was affected by the altered inflammatory states, as most of the focus is given to the epidermal compartment. Furthermore, while these studies included tissue damage and subsequent inflammatory responses, most of them did not include true wounds in which the epidermis is compromised and must undergo reepithelialization (with the exception of Kreimendahl et. al.). Future elaborations of the immunocompetent skin equivalent models could combine with models of wound healing that include injury, dermal repair, and/or reepithelialization.

#### **2.4. GRANULATION TISSUE FORMATION**

While the inflammatory phase is in full swing, two key cell types are attracted to the now abundant presence of cytokines and growth factors in the wound: stromal cells and vascular cells. Together, these cells generate granulation tissue, which replaces the clot in the wound bed, and serves as an adhesive substrate for reepithelialization. Fibroblasts and other stromal cells are responsible for replacing the early matrix of fibrin-rich clot with a more mature provisional matrix, while endothelial cells undergo angiogenesis in order to

vascularize the new granulation tissue. There are many biological processes that occur during this phase, as represented in Figure 1.2: fibroblast activation, migration, proliferation, ECM deposition, crosslinking, remodeling, myofibroblast activation, tissue contraction, and angiogenesis.

Most of the above processes are studied in isolation in various contexts. Due to the ubiquitous presence and necessity of the vascular system, the study of angiogenesis is important for many areas of research, including development, cancer, tissue repair in all organs, and many tissue engineering applications. In vitro assays of angiogenic processes, and in particular tissue engineering approaches to capture angiogenesis in biomimetic environments, have been extensively reviewed (Fetz, Radic, & Bowlin, 2021; Mastrullo, Cathery, Velliou, Madeddu, & Campagnolo, 2020; Moore & West, 2019; Reddy, Murugan, Mullick, Begum Moghal, & Sen, 2019; Rouwkema & Khademhosseini, 2016; Song, Rumma, Ozaki, Edelman, & Chen, 2018; Staton et al., 2004; Stryker, Rajabi, Davis, & Mousa, 2019; Yang, Mahadik, Choi, & Fisher, 2020).

With the exception of angiogenesis, the vast majority of activity that occurs during the formation of granulation tissue is performed by fibroblasts. Like angiogenesis, many of these processes are studied in vitro in isolation. In the following paragraphs, I will describe models that capture three main activities of fibroblasts during wound healing: migration, tissue contraction, and the synthesis

of extracellular matrix.

Upon stimulation by cytokines and growth factors released during the inflammatory phase, fibroblasts begin migration into the wound bed. Fibroblast migration over 2D surfaces can be studied using the classic scratch wound assay in which a monolayer of cells is disrupted, and migration into the cleared “wound” is measured (Gouzos et al., 2020; M. B. Menon, Ronkina, Schwermann, Kotlyarov, & Gaestel, 2009; Monsuur et al., 2016). These assays are widely used because they are simple, easy to perform, and provide direct readouts, such as migration speed and direction, that can be easily interpreted. The main drawback of 2D migration studies is that many factors affecting fibroblast migration in 3D are lacking. These factors include dimensionality, matrix architecture and topography, and physiologically relevant mechanical properties of the substrate, which are known to alter cell morphology, migration modes, cell adhesion, and contractility (Doyle, Carvajal, Jin, Matsumoto, & Yamada, 2015; Doyle, Petrie, Kutys, & Yamada, 2013; Ghibaud et al., 2009; Grinnell, 2003; Hakkinen, Harunaga, Doyle, & Yamada, 2011; Rhee, 2009). Therefore, fibroblast migration is also studied in vitro using 3D hydrogel assays. In the simplest of these models, fibroblasts are embedded into a matrix (collagen, Matrigel™, and fibrin are most common) and the speed of their random migration measured (Doyle et al., 2015; Hakkinen et al., 2011). A different platform to study directed 3D fibroblast migration relies on nested matrices. The innermost matrix is cell laden and is

embedded into a surrounding acellular matrix. In this manner, fibroblast migration out of the central tissue is measured (Grinnell, B. Rocha, Iucu, Rhee, & Jiang, 2006; Karamichos, Lakshman, & Petroll, 2009; Miron-Mendoza, Lin, Ma, Ririe, & Petroll, 2012).

As fibroblasts migrate into the wound, they contract the wound bed and surrounding tissue in order to draw the wound margins closer together. Tissue contraction has long been studied using fibroblast-populated collagen lattices (FPCL; Bell, Ivarsson, & Merrill, 1979; Carlson & Longaker, 2004), and these assays are useful for probing cell-ECM interactions and for measurement of cell-generated forces (Zhang et al., 2022). Due to fibroblasts' primary role in facilitating tissue contraction, several methods have been developed to measure tissue-level forces in FPCL and similar models. The earliest of these methods is the culture force monitor developed by Kasugai et al., in which a collagen gel is uniaxially constrained between a rigid wall and a strain-gauge that measures the force exerted by the tissue (Kasugai et al., 1990). This platform has been expanded to test multiple tissues in one device with improved contractile force measurements (Tiraravesit et al., 2017). Similar platforms have been developed with different geometries to impart multiaxial loading on the tissues, rather than uniaxial (Hu, Liu, Chen, Wang, & Lee, 2013; John, Throm Quinlan, Silvestri, & Billiar, 2010). An alternate method to measure tissue level forces relies on microfabricated tissue gauges. In these devices, cells remodel and compact

collagen around PDMS cantilevers to form suspended microtissues. Cantilever deflection is measured via microscopy, and device geometry and material properties are used to calculate the tissue force (Legant et al., 2009). Polacheck and Chen have reviewed these methods to measure tissue-level forces, as well as several methods for measuring single-cell forces (Polacheck & Chen, 2016).

Once they have entered the wound scene, fibroblasts have the very important task of depositing ECM, thereby replacing the fibrin-rich matrix of the clot with the provisional matrix of granulation tissue, rich in fibronectin and collagen type III. Assays involving treatment of standard cell cultures followed by Western Blotting or qPCR can be used to determine changes in expression of ECM proteins. However, to learn much about the synthesis of fibrillar ECM beyond protein expression, a 3D biomimetic environment is necessary. Again, we turn to the FPCL, researchers' favorite fibroblast assay since 1979, to study ECM deposition and remodeling. Fibroblasts embedded in collagen have been used to study altered ECM production by diabetic foot ulcer fibroblasts (Maione et al., 2016), to characterize improved ECM production in iPSC-derived fibroblasts (Shamis et al., 2012), to model ligament wound healing (Frahs et al., 2018), and more. These types of in vitro models are versatile and can be used to study a number of different aspects of ECM deposition. In the wound healing setting, fibronectin is an important ECM molecule that is produced by fibroblasts. Fibronectin can regulate fibroblast migration (Sottile et al., 2007), and its active polymerization is

required for the deposition of other ECM proteins (Sottile & Hocking, 2002). Our group has previously developed a model of provisional matrix formation by fibroblasts in a 3D microtissue, where the provisional matrix is composed primarily of fibrillar fibronectin (Sakar et al., 2016). This system is advantageous because it enables the simultaneous study of each of the fibroblast processes described above: migration, tissue contraction, and ECM deposition. Various mechanical aspects such as tissue tension and fiber alignment can be adjusted by changing the geometry of the device (Das et al., 2021), and force output can be readily measured (Sakar et al., 2016). In this dissertation, I use this model of fibrous wound healing for the studies in Chapters 3 and 4.

Because fibroblast activity overlaps with angiogenesis in time and space during healing, there is a focus on creating 3D biomimetic models of wound healing that also capture vascularization and angiogenesis (Grambow, Sorg, Sorg, & Strüder, 2021). For example, Tefft et. al. utilized a capillary network embedded in fibroblast-laden fibrin hydrogel to study the response of blood vessels to tissue injury. They found that fibroblasts were critical for building new tissue, but were insufficient to promote angiogenesis into the wound bed (Tefft, Chen, & Eyckmans, 2021). This model is an exciting new tool to study multiple cellular processes that contribute to the formation of granulation tissue.

## 2.5. REEPITHELIALIZATION

Reepithelialization encompasses keratinocyte activation, migration, deposition of a basement membrane, differentiation, and stratification. Keratinocyte migration is perhaps the most commonly studied aspect of wound healing thanks to the pervasiveness of the scratch wound assay. Many studies still rely on this simple technique or modified versions utilizing different methods to generate the “wound” (Costantini et al., 2022, 2019; Vedula et al., 2015; Vidmar, Chingwaru, & Chingwaru, 2017). However, these assays lack many components of the complex wound microenvironment, in particular the architecture and mechanical properties of soft tissue. To account for this, 3D skin equivalent models have been generated, which capture both the fibroblast-laden, collagenous dermis, and the multi-layered, keratinocyte-rich epidermis (Iljas et al., 2021; Maione et al., 2015; Marquardt et al., 2015; Monfared, Ertl, & Rothbauer, 2021; Ponmozhi et al., 2021; Randall, Jüngel, Rimann, & Wuertz-Kozak, 2018; Shravani, Agrawal, & Raksha, 2021). These models capture the migration of keratinocytes, and sometimes subsequent stratification, in partial-thickness biomimetic wounds. Regardless of the method of injury in these models, typically some amount of the dermis tissue compartment remains and provides a ready-made substrate over which keratinocytes can migrate. However, the dermal tissue is not actively rebuilt in these models, likely because mechanical loading is required to activate fibroblasts but is missing in skin equivalent models (Grinnell, 2003; M. B. Vaughan et al., 2004). Unlike partial-thickness wounds, in full-thickness wounds,

reepithelialization cannot progress until the fibroblasts have generated the adhesive substrate of the granulation tissue (Rittié, 2016). An important elaboration of the study of reepithelialization is the combination with stromal tissues that actively remodel following injury.

## **2.6. REMODELING**

The longest phase of wound healing, extending weeks to months beyond reepithelialization, is the remodeling phase, during which granulation tissue is transformed to scar tissue. Myfibroblasts are the main effectors of wound remodeling. I will discuss methods to study myofibroblast differentiation here, although this process overlaps temporally with granulation tissue formation, beginning three to seven days following injury. The most common approach to recapitulate and study myofibroblast differentiation in vitro is to treat cultured fibroblasts with cytokines or growth factors, usually TGF $\beta$ , although PDGF, FGF, TNF $\alpha$ , and interferon  $\gamma$  can also stimulate myofibroblast differentiation (Amadeu, Coulomb, Desmouliere, & Costa, 2003). Mechanical components of the cellular microenvironment, including matrix stiffness and architecture, also play an important role in myofibroblast differentiation (Hinz, McCulloch, & Coelho, 2019; Klingberg, Hinz, & White, 2013; Loomis et al., 2022; Quinlan & Billiar, 2012; van Putten, Shafieyan, & Hinz, 2016). Therefore, 3D hydrogel platforms that enable control over material properties are good models for studying myofibroblast activation and subsequent ECM remodeling (Smithmyer, Sawicki, & Kloxin,

2014). Kollmannsberger et. al. published an interesting study that utilized FN-coated PDMS rectangular wells to measure new tissue growth into the tissue cavity, ECM stretch, and myofibroblast activation. They saw that cell contractility agreed with degree of FN stretch, and that myofibroblast activation was highest in tissue regions with high tension (Kollmannsberger, Bidan, Dunlop, Fratzl, & Vogel, 2018).

The remodeling phase and formation of scar tissue is the hardest aspect of wound healing to capture in vitro, likely for two reasons. First, myofibroblasts are not particularly well-defined cell types, arising from multiple sources, and maintaining their phenotype in culture is notoriously difficult. Second, in order to capture remodeling, a 3D culture system which lasts for weeks is required. This requirement poses a challenge because, in engineered systems where tissues are under tension, such as in the microfabricated tissue gauges (Legant et al., 2009), the high cell contractility tends to cause microtissue collapse.

## **2.7. DISCUSSION**

In this chapter, I have reviewed in vitro approaches to study various aspects of wound healing, with a particular focus on bioengineered, biomimetic models. The most common of these organotypic wound healing models, revisited several times, is the skin equivalent model. Although skin equivalents are useful for studying reepithelialization of partial-thickness wounds, they do not capture full-

thickness healing. Even when full-thickness wounds are generated in skin equivalents, a matrix such as fibrin must be added to the wound bed in these models to provide a substrate for keratinocyte migration and fibroblasts remain inactive (Geer et al., 2002). Therefore, this common preclinical model fails to capture granulation tissue formation. Other models with mechanically constrained hydrogels perform better at capturing new tissue formation by activated fibroblasts (Sakar et al., 2016; Tefft et al., 2021), but these platforms lack keratinocytes and do not recapitulate reepithelialization. Future directions for the field include the incorporation of both granulation tissue formation and reepithelialization into the same in vitro biomimetic model.

Another limitation of skin equivalents and similar models is that they lack key anatomical structures of the skin. There have been recent attempts to build skin equivalent models which incorporate some of the appendages found in skin: sweat glands, sebaceous glands, and hair follicles (Hosseini et al., 2022; Weng et al., 2020). Since the hair follicle is an important microenvironment for multipotent cells, these structures will likely be very important for studying and improving wound healing outcomes.

Another component of wound healing that ought to be considered is the type of injury. Different injury methods are used in each of the above models; excision, incision, burning, and ablation are the most common, but effects of the injury

method itself on subsequent repair processes are often overlooked, or at least not systematically compared. The effects of injury mode and subsequent healing outcomes will be discussed and explored in Chapter 3.

### **CHAPTER THREE: Fibroblast clearance of damaged tissue following laser ablation in engineered microtissues**

*The work in this chapter has been submitted for peer review at APL Bioengineering. The experiments and analysis in this study were led by me, with support from my second author, Anish Vasani, and experimental advice and guidance provided by both of my advisors. The manuscript was written by me, with revisions and edits from my co-authors.*

#### **ABSTRACT**

Although the mechanisms underlying wound healing are largely preserved across wound types, the method of injury can affect the healing process. For example, burn wounds are more likely to undergo hypertrophic scarring than are lacerations, perhaps due to the increased underlying damage that needs to be cleared. This tissue clearance is thought to be mainly managed by immune cells, but it is unclear if fibroblasts contribute to this process. Herein, we utilize a 3D in vitro model of stromal wound healing to investigate the differences between two modes of injury: laceration and laser ablation. We demonstrate that laser ablation creates a ring of damaged tissue around the wound that is cleared by fibroblasts prior to wound closure. This process is dependent on ROCK and dynamin activity, suggesting a phagocytic or endocytic process. Transmission electron microscopy of fibroblasts that have entered the wound area reveals large intracellular vacuoles containing fibrillar extracellular matrix. These results demonstrate a new model to study matrix clearance by fibroblasts in a 3D soft tissue. Because aberrant wound healing is thought to be caused by an imbalance

between matrix degradation and production, this model, which captures both aspects, will be a valuable addition to the study of wound healing.

### **3.1 INTRODUCTION**

Dermal wound healing is a sequential process characterized by hemostasis, inflammation, new tissue formation, and remodeling, four overlapping phases that must occur in a timely manner to restore barrier function and prevent infection. While these phases are considered to be preserved regardless of the type and location of the wound (Velnar, Bailey, & Smrkolj, 2009), the duration and clinical outcome of healing depend on the cause of injury, type and size of the wound, and contamination state. As such, different wound care strategies to achieve the optimal outcome have been developed (Abazari, Ghaffari, Rashidzadeh, Badeleh, & Maleki, 2022; Percival, 2002). Yet, the mechanisms by which injury modality affect the healing process remain poorly understood.

Despite the pervasive clinical presentation of various types of wounds, such as ulcers, abrasions, lacerations, and burns, there are few studies comparing tissue damage and the wound healing response between different injury modalities. Early animal studies comparing burn wounds to excision wounds show that burns heal more slowly than skin excision wounds (Monsaingeon & Molimard, 1976) and suggest that the proliferation phase of healing is delayed in burns compared to size-controlled cuts (Hell & Lawrence, 1979). Unlike cuts and

lacerations, burns do not exhibit hemostasis (Abazari et al., 2022) and also have substantially more damaged tissue to be cleared, both of which may contribute to the slower healing process of burns. In a zebrafish injury model, comparisons have also been made: delayed healing of thermal injuries compared to transection injuries was attributed to a disruption in the structure of collagen fibers (Miskolci et al., 2019). Close examination of the extracellular matrix (ECM) in skin tissue in multiple animals models showed that thermal injuries created a region of denatured collagen detected by Second Harmonic Generation (SHG) imaging (Tanaka et al., 2013), loss of birefringence (Pierce, Sheridan, Hyle Park, Cense, & De Boer, 2004), and a Cy5 labeled collagen-mimetic peptide that specifically binds denatured collagen (Schroeder et al., 2020). These studies suggest that injury modalities can cause different degrees of tissue damage which may affect the progression of the healing stages.

During the inflammatory phase, necrotic tissue, including dead cells and damaged ECM, and pathogens are removed from the wound bed (Gurtner et al., 2008), a process hereinafter referred to as wound clearance. Wound clearance has been mainly attributed to immune cells, particularly neutrophils and macrophages that engulf bacteria and apoptotic cells via a process called phagocytosis. When phagocytic clearance of apoptotic cells by macrophages is impaired, wound healing is delayed (Chen et al., 2015; Sindrilaru et al., 2009). Interestingly, phagocytic behavior is not limited to immune cells; other cell types,

including epithelial cells and fibroblasts, can clear apoptotic cells through phagocytosis (J. Lee, Wang, Ren, & Lele, 2010; E. J. Park, Park, Kim, Lee, & Chang, 2018; Seeberg et al., 2019). In addition to clearance of apoptotic cells, damaged ECM must also be removed from the wound bed. Both macrophages and fibroblasts secrete proteolytic enzymes such as matrix metalloproteinases (MMPs) that cleave ECM molecules (Caley, Martins, & O'Toole, 2015). However, how the degraded matrix leaves the wound scene is less clear. In healthy tissues, fibroblasts engulf collagen and other ECM proteins to regulate collagen maintenance and turnover (W. Lee, Sodek, & McCulloch, 1996; Sprangers & Everts, 2019). Whether fibroblasts actively contribute to the clearance of damaged ECM following tissue injury remains elusive.

To begin to address this question, we set out to study tissue repair in the presence of varying amounts of damaged tissue in our previously reported biomimetic model for stromal tissue repair (Sakar et al., 2016). This model uses 3T3 fibroblasts that compact a collagen type I hydrogel around elastomer pillars to form a fibrous microtissue. Upon injury with a microdissection knife, fibroblasts migrate into the gap, smoothen the wound edge, and subsequently repair the gap through assembly of a fibronectin-rich provisional matrix (Sakar et al., 2016). In this study, we selected laser ablation as an alternate mode of injury because of its amenability to create wounds at the desired scale (on the order of 100-400  $\mu\text{m}$ ) without breaking the suspended microtissue. We first demonstrate

that transection and laser ablation cause different degrees of tissue damage, which results in altered wound healing dynamics. While healing occurred in both wound types, laser ablated wounds exhibited a prolonged opening phase after injury compared to transected wounds, wherein fibroblasts invade and remodel the damaged tissue surrounding the wound. Closer examination with transmission electron microscopy revealed that fibroblasts engulfed damaged ECM from laser ablated wounds through a process that is mediated by RhoA and dynamin activity. These data suggest a previously unappreciated role for fibroblasts in wound clearance.

## **3.2. RESULTS**

### **3.2.1. Laser ablation creates holes in microtissues surrounded by non-viable tissue**

In our previous studies, stromal microtissues were injured using a microdissection knife mounted to an xyz-micromanipulator (Das et al., 2021; Sakar et al., 2016; Tefft et al., 2021). Due to the soft and compliant properties of microtissues, mechanical injury often resulted in slipping of the microtissue from the pillars before a gap was created. To overcome this limitation, we sought to deploy a Q-switched Nd:YAG nanosecond-pulsed laser to inflict wounds with laser ablation (Fig 3.1A). The Nd:YAG laser operates at 1064 nm and our setup include a removable KTP crystal capable of generating the second harmonic at 532 nm. Each pulse width is 5 ns. Given the different mode of injury, transection

versus ablation, we set out to characterize the two wound types and performed a viability assay on microtissues injured with either a microdissection knife or laser pulse. Interestingly, we observed a key difference in cell viability at the wound periphery. In knife-injured tissues, the long edges of the wound were largely free of dead cells as if the dead tissue is almost entirely removed, leaving only a small patch of dead cells at the end of the incision (Fig 3.1C). In contrast, laser-injured microtissues showed a band of dead cells around the perimeter of the wound (Fig 3.1C) indicating that tissue damage extended beyond the wound margins into the surrounding tissue.

To establish a protocol for reproducibly inflicting full-thickness gaps with laser light, microtissues were injured with laser pulses of different wavelengths (532 nm or 1064 nm) and pulse energies ranging from 0.25 to 3 mJ, two parameters that affect the energy density of the focused laser pulse. Phase contrast images were captured following injury (Fig 3.1A), and the initial gap area was quantified (Fig 3.1B). At both wavelengths, 532 nm and 1064 nm, there was a threshold energy below which no tissue gap was created, which was about 0.25 mJ at 532 nm and 1.5 mJ at 1064 nm. These laser pulse energies correspond to a fluence, that is the energy density at the focal point in the tissue, of 19 kJ/cm<sup>2</sup> and 17.6 kJ/cm<sup>2</sup> for 532nm and 1064nm, respectively (Supplemental Material, Table 3.S1). Thus, the ablation threshold of collagenous microtissues is similar for both wavelengths. Because laser pulse energies are

measured before each experiment, we report laser pulse energies, and not estimated fluences, in the x-axis of the graphs. At the minimum energies, the gaps created are smaller (mean values of  $17,600 \pm 1540 \mu\text{m}^2$  at 532 nm and  $14,300 \pm 3000 \mu\text{m}^2$  at 1064 nm) than those created by knife ( $41,600 \pm 3980 \mu\text{m}^2$ ). At intermediate energies, 0.4 mJ and 0.55 mJ at 532 nm and 2 mJ at 1064 nm, the average gap size ( $34,200 \pm 4270 \mu\text{m}^2$ ;  $53,800 \pm 8500 \mu\text{m}^2$ ; and  $30,100 \pm 6670 \mu\text{m}^2$ , respectively) is on the same scale as knife injuries. Further increase of the pulse energy for both wavelengths yielded initial gap areas that were much larger than what the knife was capable of creating (Fig 3.1B). To assess damage to the tissue surrounding the gap area, knife and laser injured microtissues were stained with Ethidium homodimer-1 to detect dead cells with damaged cell membranes and the percentage area that contained dead cells was quantified for different wavelengths and pulse energies (Fig 3.1C,D). The area of non-viable tissue in all but the lowest energy injuries was significantly larger than in the knife injuries, although there was a large range in size of the damaged zone (Fig 3.1D). Together, these data show that laser ablation can be used to reliably create gaps in microtissues with sizes comparable to knife inflicted wounds, but with more cell damage in the adjacent tissue.

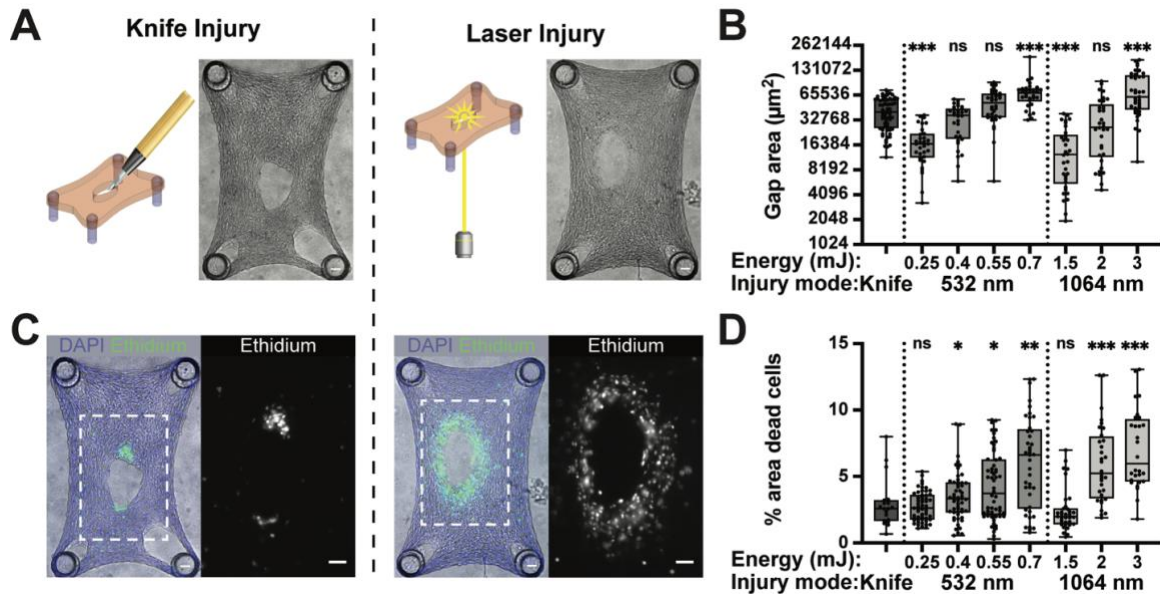


**Figure 3.1: Tissue injury by transection and laser ablation in stromal microtissues.**

(A) Two modes of injury are used to generate full-thickness gaps in microtissues. Phase contrast images show tissues immediately following injury. Scale bars 100  $\mu\text{m}$ . (Left) A diamond microdissection knife is used to manually create gaps in tissues. (Right) An Nd:YAG laser pulse, at 532 nm or 1064 nm, focused through a 10x objective, ablates a gap in the tissues. (B) Quantification of initial gap area following injury. Laser gap sizes are shown for distinct energy levels. (C) Epifluorescence images showing Hoechst stain for all cell nuclei (blue) and Ethidium Homodimer-1 stain for nuclei of dead cells (green/white). Scale bars 100  $\mu\text{m}$ . (D) Quantification of percent of tissue area covered by dead cells (from C, white area/blue area). Data in panels B & D were compared to the knife injury condition using the non-parametric Steel test with control.

\*  $p < 0.05$ , \*\*  $p < 0.01$ , \*\*\*  $p < 0.001$ , ns: not significant.

### **3.2.2. Ablated microtissues close following an initial opening phase**

Gap closure in our model system is initiated by the fibroblasts adjacent to the wound edge (Mailand, Li, Eyckmans, Bouklas, & Sakar, 2019). Given the increased levels of cell death in laser-ablated wounds versus knife wounds (Figure 3.1C,D), we hypothesized that ablation wounds would show impaired closure. To investigate this hypothesis, we monitored gap closure for stromal microtissues injured by knife and by laser, both 532 and 1064 nm, using time-lapse microscopy. As previously reported, knife-injured tissues smoothed the wound margins and commenced closure within minutes, and closure finished in about 24 hours (Sakar et al., 2016; Fig 3.2A,B). The laser-ablated tissues displayed a prolonged smoothing phase that was characterized by opening of the gap that lasted between 4 and 6 hours which was then followed by closure similar to knife-injured tissues (Fig 3.2B, Supplemental Movie 3.1).

To quantitatively assess tissue closure between the different conditions, we compared closure rates during two phases of the healing process. We defined the initial phase between 0 and 4 hours as ~80% of tissue gaps reached their maximum area by 4 hours. We considered the closure phase to occur between 6 and 16 hours post injury as most tissue gaps (>90%) reached maximum area by 6 hours, and the closure rate was linear for the ensuing 10 hours (Fig 3.2B). The rate of closure during each phase was quantified as change in gap area per hour, where a negative value indicates the gap was opening rather than closing (Fig

3.2C). During the initial phase (Fig 3.2C, left), knife injured tissues displayed an average closure rate of  $1380 \pm 270 \mu\text{m}^2/\text{hour}$ . For 532 nm injuries, the closure rate during this phase was  $-890 \pm 820 \mu\text{m}^2/\text{hour}$  ( $p < 0.001$  compared to knife). For 1064 nm injuries, the closure rate during this first phase was  $-870 \pm 390 \mu\text{m}^2/\text{hour}$  ( $p < 0.001$  compared to knife). During the closure phase, the closure rates were not significantly different between injury modes (Fig 3.2C, right). Together, these data suggest that a prolonged opening phase, rather than an impaired closure phase delayed gap closure in laser ablated wounds.

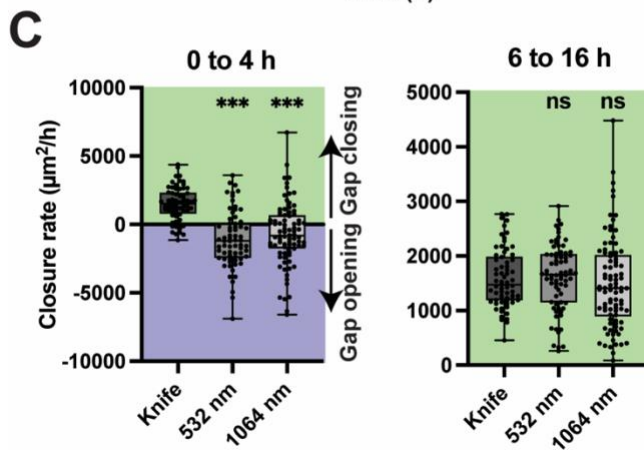
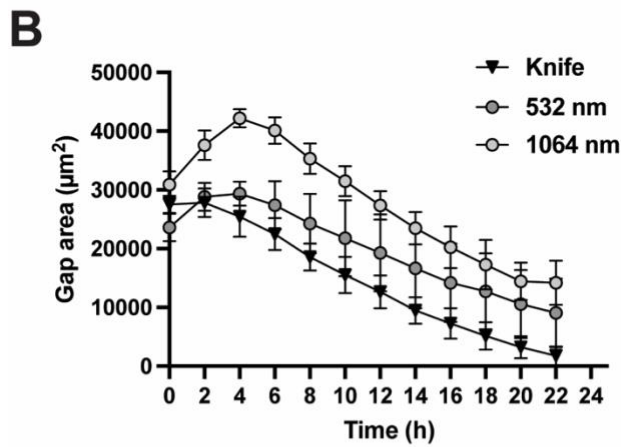
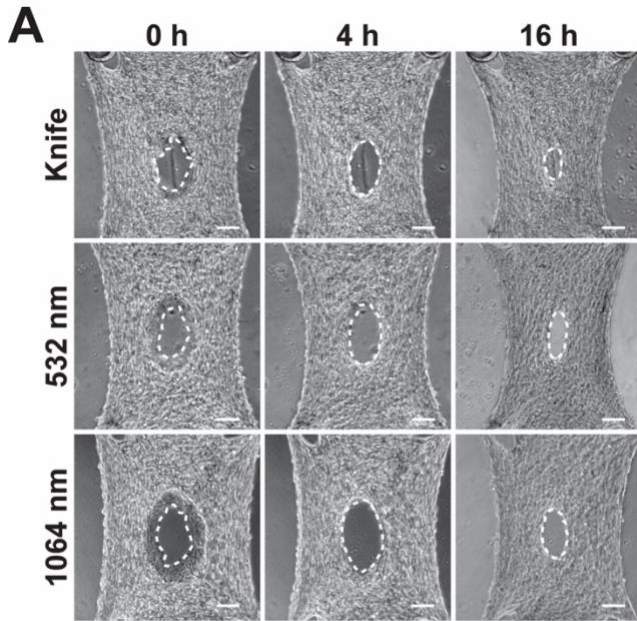


**Figure 3.2: Closure of injured microtissues.**

(A) Time-lapse images are shown at 0 hours, 4 hours, and 16 hours for each injury mode. The white dotted line indicates gap edges. Scale bars 100 μm. (B) Gap area as a function of time for each injury mode. Mean and standard deviation for n=4 tissues per mode with comparable starting areas. (C) Closure rate for the initial phase during the first 4 hours of the time-lapse (left) and between 6 and 16 hours (right). Data are compared to knife condition using Dunnett's test with control. \*\*\* p<0.001, ns: not significant.

### **3.2.3. Characterization of fiber damage and movement at gap periphery**

To investigate the gap opening in laser inflicted wounds, we carefully analyzed the time lapse phase contrast images during the opening phase and observed a darker band of damaged tissue at the periphery of the gap (Fig 3.2A) that corresponded to the area of dead cells (Fig 3.1C, Fig 3.S1). In phase contrast microscopy, changes in apparent brightness are due to phase shifts in light that occur when light passes through the sample. Therefore, visually darker tissue indicates that a different phase shift occurred in these parts of the tissue, potentially due to altered topography or density (increased or decreased density relative to the bulk tissue could both cause this visual distinction). This band of damaged tissue was present in most ablated tissues; very few knife-injured tissues contained a small patch of damaged tissue, but not a band (Fig 3.S1). During the initial opening phase, this band grew smaller (Fig 3.2A) as the gap area increased (Fig 3.2A, white dotted lines, B). We did not observe significant differences between the two laser wavelengths in the clearance and repair process. Although not statistically significant, the laser seems to generate more peripheral tissue damage at 1064 nm. For these reasons, and to simplify experiments, the laser was used in 1064 nm mode from this point onward in the study.

From the time-lapse images in Figure 3.2, we postulated that the that the ECM at the gap periphery was compromised and therefore cleared by the remaining

fibroblasts in the microtissue. In order to characterize the mechanical damage to surrounding ECM caused by each type of injury, we sought to visualize the microstructure of the fibrous matrix. We used high-resolution, reflection microscopy to capture z-stack images of the matrix topography at the wound edges. From these images, we made two main observations. First, the depth of the tissues in z was significantly smaller for knife ( $110 \mu\text{m} \pm 14 \mu\text{m}$ ) than for laser ( $152 \mu\text{m} \pm 18 \mu\text{m}$ ) injuries ( $p < 0.001$ ). Qualitatively, the knife-injured tissues appear to have a higher density of fibers than do ablated tissues (Fig 3.3A), suggesting that the mechanical injury compacts the microtissue, likely due to the pressure from the microdissection knife. To quantify fiber density, the  $25 \mu\text{m}$  region closest to the gap edge was divided into subregions and the density of each calculated. The histogram showing fiber density within these subregions reveals that laser injuries contain more empty space than do knife injuries (Fig 3.3B, left,  $p < 0.001$ ). Second, the fiber structure at the gap edge appeared disrupted in ablated tissues. We used an established algorithm (Bose, Eyckmans, Nguyen, Chen, & Reich, 2019) based on the Fibril Tool method (Boudaoud et al., 2014) to determine the distribution of fiber orientation angles within  $25 \mu\text{m}$  of the gap edge. This analysis revealed that the majority of fibers in knife-injured tissues aligned along the long axis of the tissue, parallel to the direction of movement of the knife. The peak alignment angle shifts to about  $-20$  degrees, and a wider spread of orientation angles is observed for ablation injuries compared to mechanical injuries (Fig 3.3B, right,  $p < 0.001$ ). Together,

these data suggest that tissue gaps made with laser ablation are surrounded by damaged tissue that is composed of dead cells and compromised ECM.

We wondered next how the fibrous matrix structure changes as the fibroblasts remodel the microtissue at the gap edge. Using reflection microscopy, we performed live microscopy and captured images every 10 minutes (Fig 3.3C, Supplemental Movie 3.2). In mechanical injuries, the gap edge smooths and begins closure within 4 hours. For ablation injuries, we observed the tissue from the damaged gap periphery moving into the bulk tissue over a period of 4-10 hours. In order to maximize the amount of damaged tissue that we could observe, wounds in this experiment only were made roughly three times larger than those in Figure 2. Therefore, they take roughly three times longer to complete the clearance phase and reach their maximum wound size. In some places, fiber breakages occurred as the damaged matrix was remodeled (Fig 3.3C'-C''', white arrows). At the conclusion of this tissue clearance phase, we observed compacted tissue at the wound edges (Fig 3.3C, yellow arrows).

Given the fiber breakages and compaction of the damaged matrix, we postulated that actomyosin contractile forces were required for tissue clearance/opening (Fig 3.3D). The data in Figure 3D are reported as relative opening rate for each treatment compared to the vehicle control (DMSO). Laser ablation was used for all conditions; because we sought to observe changes in damaged tissue

clearance, and knife injuries did not display this clearance phase, the knife condition was not included in these experiments. To decrease cellular contractility, the myosin-2 inhibitor blebbistatin (100  $\mu\text{M}$ ), myosin light chain kinase (MLCK) inhibitor peptide 18 (P18, 10  $\mu\text{M}$ ) or Y27632 (10  $\mu\text{M}$ ), a Rho-associated kinase (ROCK) inhibitor were added prior to microtissue ablation. Interestingly, blebbistatin and P18 did not significantly affect the tissue opening rate, while Y27632 significantly decreased the mean tissue opening rate to  $50\% \pm 1\%$  of the vehicle control, DMSO ( $p < 0.001$ ). These results suggest that ROCK activity, but not cellular contractility, is required for wound clearance. In addition to modulating cellular contractility, ROCK II activity is also an important regulator of phagocytosis of FN-coated beads in fibroblasts (Yoneda, Multhaupt, & Couchman, 2005). To investigate if fibroblasts cleared the wound by engulfing damaged matrix, we added dynasore (60  $\mu\text{M}$ ) to inhibit dynamin activity, which is necessary for phagocytosis (Gold et al., 1999; Praefcke & McMahon, 2004) and clathrin-mediated endocytosis (Praefcke & McMahon, 2004). Indeed, addition of dynasore lowered the mean opening rate to  $57\% \pm 9\%$  of control ( $p < 0.001$ ), suggesting that ECM ingestion may play a role in damaged tissue clearance by fibroblasts.

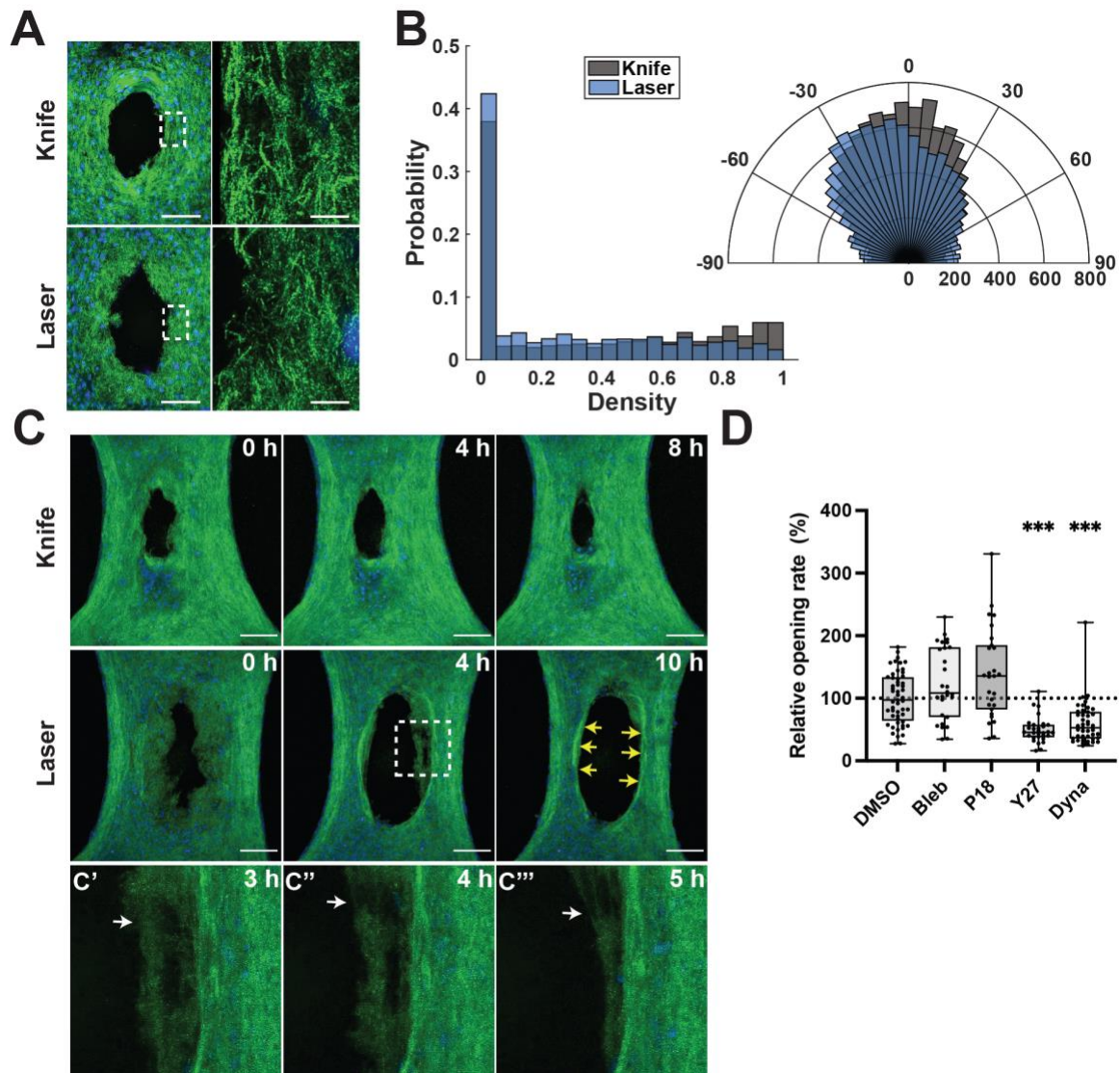


**Figure 3.3: Fiber disruption and breakage following ablation.**

(A) Hoechst dye (blue) and reflected 488 nm illumination (green). (Left) Max projection of tissue z-stacks. Scale bars 100  $\mu\text{m}$ . White box correlates to region shown on right. (Right) Single z-slices of 75X images. Scale bars 10  $\mu\text{m}$ . (B) Histogram in polar coordinates showing frequency (r-axis) of net fiber orientations ( $\theta$ -axis) of 10 pixel<sup>2</sup> subregions for 25  $\mu\text{m}$  of tissue adjacent to the gap long edge. Histograms are significantly different according to Kolmogorov-Smirnov test,  $p < 0.001$ . (C) Max z-projections of time-lapse reflection microscopy. Yellow arrows show compacted tissue at gap edge at the conclusion of the clearance phase. Scale bars 200  $\mu\text{m}$ . (C'-

C''') Enlargement of area inside white box from C, laser injured tissue, showing fiber breakage at 3 hours (C'), 4 hours (C''), and 5 hours (C'''). White arrows indicate breakage site. (D) Opening rate, normalized to the mean control (DMSO) rate within each biological replicate, during the first 4 hours following ablation. Non-parametric Steel test with control. \*\*\*  $p < 0.001$

### **3.2.4. Transmission electron microscopy reveals intracellular fibrillar structures, suggesting phagocytosis of ECM after ablation**

To further corroborate the hypothesis that fibroblasts clear wounds by engulfing ECM, we performed transmission electron microscopy (TEM) on uninjured microtissues and at the wound edge of laser injured microtissues at 0, 4, and 20 hours post injury (Fig 3.4). Immediately following ablation, cells at the wound edge displayed fragmented or misshapen nuclei and showed cellular blebbing (Fig 4B,B', red arrows). Other cells showed the formation of numerous, apparently vacant, cytoplasmic vacuoles, a reduction in cell size, and chromatin condensation at the edge of the nucleus (Fig 3.4B') which is reminiscent of a necrotic or oncotic cell (Balvan et al., 2015; Trump, Berezsky, Chang, & Phelps, 1997). At 4 hours after ablation, cells at the wound edge contained vacuoles with distinct fibrillar structures (Fig 3.4C, yellow arrows, C'). These vacuoles were relatively large ( $>1 \mu\text{m}$  in diameter) and the fibrillar structures appeared to have a similar morphology to those of the surrounding damaged extracellular matrix. At 20 hours after ablation, cells at the wound edge lacked vacuoles, but instead contained numerous organelles, including mitochondria, suggesting an increased metabolic demand, as would be expected of activated fibroblasts that are

undergoing transcription and translation to produce new ECM, and are utilizing actomyosin contractility to actively migrate through and remodel ECM. Close inspection of the cell surfaces near the wound edge revealed that fibrillar structures appear to be emanating from the cell (Fig 3.4D', blue arrowheads), which is in line with our previous observations that fibroblasts close wounds by producing a provisional matrix (Das et al., 2021; Sakar et al., 2016; Tefft et al., 2021). Fluorescence staining in previous studies confirm that this provisional matrix is composed of fibronectin. Remnants of necrotic cells can still be seen at 20 hours after injury, suggesting that dead cell debris is not phagocytosed by fibroblasts in our microtissues (Fig 3.4D', red arrowheads).

In order to determine if ECM phagocytosis occurred at all times in the microtissues, or if it was an injury-specific response, we quantified the number of vacuoles that contained distinct fibrillar structures (as in Figure 3.4C') for 10 fields of view at each timepoint. In uninjured tissues, 6 such vacuoles were observed, and in tissues 4 hours post injury, 17 such vacuoles were observed. Only vacant vacuoles were seen immediately following injury, and thus not included in this quantification. No vacuoles were observed at 20 hours post injury. Due to differences in number of cells and cell sizes, the number of fiber-containing vacuoles was normalized to cellular area (Fig 3.4E).

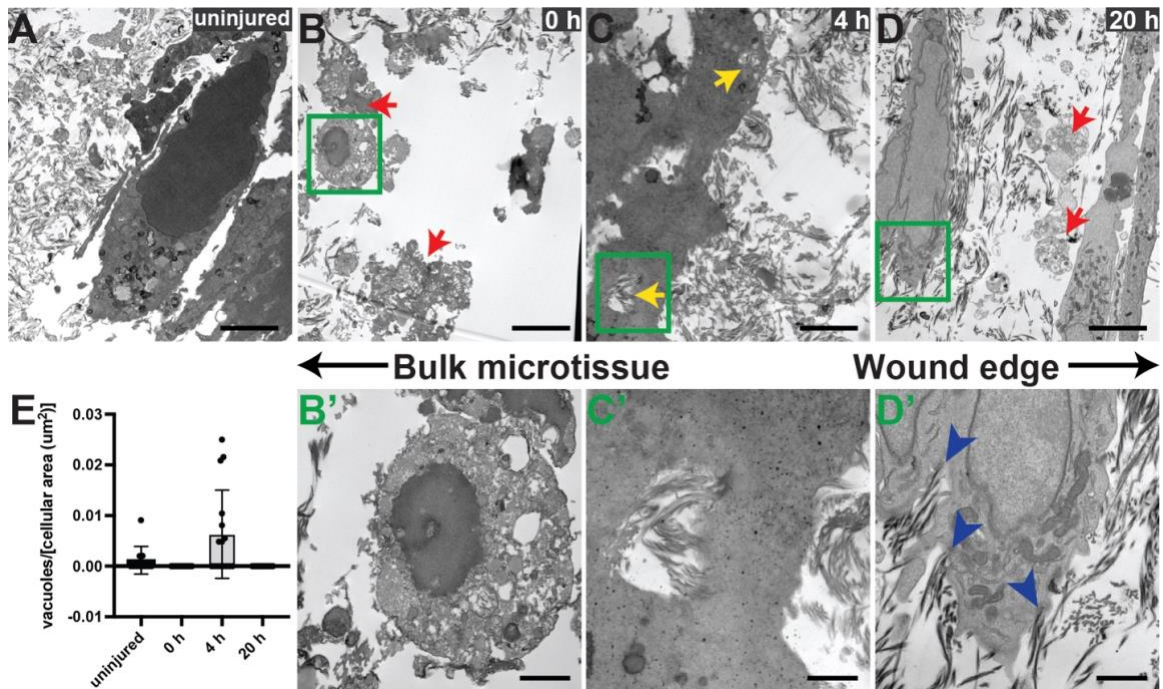


**Figure 3.4: Transmission electron microscopy suggests ECM fiber uptake after ablation.**

(A) Uninjured microtissue. (B) Fibroblasts at gap edge fixed immediately after ablation. Red arrows indicate dying cells, characterized by reduction in cell size, fragmented nuclei, many vacuoles, and blebbing. (C) Cells at gap edge 4 hours after injury. Yellow arrows indicate vacuoles containing ECM fibers. (D) Cells at gap edge 20 hours after ablation. Red arrows indicate nonviable cells. The cell on the left has an enlarged nucleus and many mitochondria. (A-D) Scale bars 4  $\mu\text{m}$ . (B-D) Wound edge is out of frame to the right. (E) Quantification of number of vacuoles containing distinct fibrillar structures normalized to cellular area for uninjured tissue and tissue 0, 4, or 20 hours after ablation.  $n=10$  fields of view. (B') Magnified view of the green box from B, immediately following ablation. An oncotic or necrotic cell, characterized by reduction in cell size, chromatin condensation at nucleus edge, and the formation of many cytoplasmic vacuoles. (C') Magnified view of the green box from C, 4 hours after ablation. An intracellular vacuole containing fibrillar structures matching the distinct appearance of the extracellular matrix. (D') Magnified view of the green box from D, 20 hours after ablation. Blue arrowheads indicate extracellular matrix fibers that appear to be emanating from the cell. (B'-D') Scale bars 1  $\mu\text{m}$ .

### 3.3. DISCUSSION

In this study, we explored laser ablation as a method to create full thickness wounds in engineered stromal microtissues and found that fibroblasts first clear the wound from damaged ECM before a new provisional matrix is assembled to close the wound. Previous studies have established a critical role for phagocytic macrophages (Chen et al., 2015; Sindrilaru et al., 2009) and non-professional phagocytic epithelial cells (J. Lee et al., 2010; E. J. Park et al., 2018; Seeberg et al., 2019) to participate in the removal of cell debris and apoptotic cells, but it is unclear if these cells actively remove damaged ECM from the wound site. In our experiments, dead cells remained present during the healing of microtissues, but the ECM at the site of injury was engulfed by fibroblasts via a process that was dependent on ROCK and dynamin activity. These data are line with other studies showing that, in non-wound healing settings, fibrillar collagen can be digested by cells integrin-dependent phagocytosis (W. Lee et al., 1996; Sprangers, Behrendt, Engelholm, Cao, & Everts, 2017; Sprangers & Everts, 2019), nonspecific macropinocytosis (Amyere et al., 2000; Sprangers & Everts, 2019), and Endo180/uPARAP-mediated endocytosis (Madsen et al., 2011; Sprangers & Everts, 2019). While further studies need to be conducted to delineate the mechanisms by which damaged collagen fibers are removed from the injury site in our model system, our data highlight a new role for fibroblasts in wound clearance.

In vitro wound healing models have been instrumental tools to parse out mechanisms of cell migration (Liang et al., 2007), vascularization (Grambow et al., 2021), and tissue assembly (Maione et al., 2015; Sakar et al., 2016; Shamis et al., 2012) during wound healing. In these model systems wounds are often generated by removing cells or tissue with a scalpel, pipet tip or biopsy punch leaving a clean wound with limited cell death or devitalized tissue present in the wound bed. Similar to what others have reported in these clean wounds, in this study, microtissues injured with a microdissection knife showed limited cell death or tissue damage, resulting in the immediate onset of tissue closure. In contrast, microtissues subjected to laser ablation showed open wounds surrounded by a zone of damaged ECM that contained elevated numbers of dead cells. This wound morphology is likely caused by a fast microscale thermal explosion in the focal point of the laser pulse that removes tissue in the center of the microtissue with the ensuing heat dissipation denaturing the surrounding tissue (Müller, Dörschel, & Kar, 1991; Vogel & Venugopalan, 2003). Hence, laser ablated wounds show similarities to thermal injuries such as burns.

Analogous to the healing dynamics of burn wounds in animals (Hell & Lawrence, 1979; Monsaingeon & Molimard, 1976), the presence of devitalized tissue in our model delayed the onset of wound closure. During this period of delay, fibroblasts were found to be actively clearing the wound of denatured ECM prior to assembling a provisional matrix to close the gap. The coordination between

ECM clearance and deposition of new matrix is critical for normal healing as imbalances between these two processes are implicated in pathological healing such as fibrosis (McCulloch & Knowles, 1993; Tsai, Ma, & Shieh, 1999) and chronic healing (Barman & Koh, 2020). In these settings, the surgeon removes the compromised wound bed by performing a surgical or enzymatic debridement in order for healing to proceed (Falabella, 2006). Understanding how to increase natural (autolytic) debridement or identifying mechanisms underlying regulation of ECM clearance could prove useful in treating chronic and fibrotic wounds. Bioengineered models of wound healing that capture both processes, ECM clearance and assembly, could be powerful in vitro platforms to gain such insights and to identify new therapeutic targets for chronic healing and fibrotic diseases.

### **3.4. METHODS**

#### **PDMS device fabrication**

As previously described (Legant et al., 2009; Sakar et al., 2016), standard photolithography was used to create an SU8 model of the microtissue device. A negative mold of the device was cast using poly-dimethyl siloxane (PDMS, Sylgard 184, Dow-Corning). Finally, the negative mold was used to generate devices of PDMS in 35 mm culture dishes. One device consisted of 80 rectangular microwells, each containing four cylindrical pillars with an overhanging cap near the top to constrain microtissues. Microwells were 1.12

mm × 1.5 m, and pillars had 0.62 mm and 1.0 mm between pillar centers. Pillar diameter was 120 μm for the first layer with a height of 110 μm, and cap diameter was 180 μm with a height of 80 μm.

### **Cell culture and microtissue seeding**

3T3 cells (ATCC #CCL-92) were grown in Dulbecco's modified eagle medium (DMEM, Fisher Scientific #10-013-CV) with 10% bovine (Sigma #B9433) or calf serum (ATCC #30-2030) and 1% penicillin/streptomycin (Life Technologies #15140-122). Cells were mixed with rat tail tendon collagen I (Corning #356236) at a final concentration of 2.2 mg/ml (pH ~7.5). 900K cells were added to each device and centrifuged to drive cells into the microwells. Excess collagen solution was removed, and collagen in the microwells was allowed to polymerize at room temperature for 10 minutes, then at 37°C for 10 minutes. Microtissues were cultured at 3°C with 5% CO<sub>2</sub> in growth medium for 16-20 hours prior to injury, during which time they spontaneously compact, as previously described. (Sakar et al., 2016) Compacted tissues suspended between the PDMS pillars contain about 2,000 cells per tissue (Sakar et al., 2016).

### **Knife injury and laser ablation of microtissues**

For knife injury, a diamond dissection knife (type MDL, Electron Microscopy Systems, #72029) mounted to an XYZ-micromanipulator (SLC-2040, SmarAct GmbH) was used to tear a full-thickness wound in the microtissues (Fig 3.1A).

Laser ablation was performed using a q-switched nanosecond-pulsed Nd:YAG laser (Minilite I, Continuum), which emits at 1064 nm. For experiments shown in Figures 3.1 and 3.2, the beam was first passed through a Potassium Titanyl Phosphate (KTP) crystal to generate the second-harmonic at 532 nm. The beam is enlarged by a beam expander (Edmund Optics #39-739) from 3 mm to 9 mm, directed through a dichroic mirror suitable for 1064 or 532 nm, and focused into the tissue through a 10x objective. Laser energy is measured directly after the beam expander, and was adjusted between 0.25 mJ and 0.7 mJ for 532 nm, and between 1.5 mJ and 3 mJ for 1064 nm. Phase images with an Axiovert inverted microscope (Zeiss) at 10x equipped with a 20Mp Blackfly camera (FLIR) were taken immediately following injury to quantify gap starting area. Hoechst 33342 (Sigma #14533) and Ethidium homodimer-1 (Thermo Fisher #E1169) were added to each device for 30 min, and epifluorescence images of tissues were captured at 10x with a Nikon TE-200 inverted microscope equipped with a color digital camera. Cell death was quantified as the fraction of dead cell area over total tissue area.

### **Live microscopy and closure rate measurements**

For closure experiments, time-lapse images were taken every 30 minutes for 18 hours on a Nikon Ti Eclipse microscope, fitted with an environmental chamber (37°C, 5% CO<sub>2</sub>). Gap area was measured every hour in ImageJ, manually, using the polygon selection tool. The closure rate was determined as the slope of the

line of best fit through data from 0 hours to 4 hours and from 0 hours to 16 hours.

### **Reflection microscopy and fiber alignment analysis**

Reflection microscopy was performed at 488 nm using a 25x water immersion objective with 0.75x digital zoom on an upright Leica SP8 confocal microscope. Samples were excited at 488 nm, and reflected light was captured between 484-492 nm. For fiber alignment experiments, tissues were fixed in 4% paraformaldehyde and Hoechst 33342 was added to visualize cell nuclei prior to imaging. For reflection time-lapse experiments, the microscope chamber was maintained at 37°C. Tissues were maintained in CO<sub>2</sub>-independent L15 Leibovitz's media. A layer of mineral oil was added atop the growth media to prevent evaporation. Z-stacks of about 30 slices with a z-step size of 4 μm were captured every 10 minutes for 4 hours to 10 hours.

The fiber alignment analysis was performed in MATLAB (MathWorks, Natick, MA) using a previously-reported MATLAB code that was based on the Fibril Tool (Bose et al., 2019; Boudaoud et al., 2014). First, each tissue stack was divided into 6 equal sections, and the max projection for each section was taken. Second, the rectangular region to be analyzed was defined for each image as the height of the field of view (148 μm) parallel to the tissue long axis, and a width of 25 μm adjacent to the gap edge. Next, a Gaussian blur was applied to images to reduce pixelation effects, then the local pixel intensity gradient was used to

determine a perpendicular normalized vector, which was then used to calculate the local nematic tensor for each pixel. The region was then subdivided into 10-pixel  $\times$  10-pixel subregions and the average nematic tensor for each subregion was calculated. The largest eigenvector corresponding to the largest eigenvalue of this average describes the alignment direction. Data are reported as a histogram of subregion alignment angles for all  $25 \times 148 \mu\text{m}$  regions. For fiber density, an automatic threshold was applied in ImageJ, and the pixel density for the same 10 pixels  $\times$  10 pixels subregions was calculated. Data are reported as a histogram of subregion signal density for all  $25 \times 148 \mu\text{m}$  regions.

### **Inhibitor experiments**

Inhibitors were added in fresh growth medium 30 minutes prior to injury. DMSO (Fisher Scientific #BP231) was added at 0.2% (v/v) as a vehicle control.

Blebbistatin (Cayman Chemical #24171) was used at  $100 \mu\text{M}$ . Myosin light chain kinase inhibitory peptide 18 (P18, Cayman Chemical #19181) was used at  $10 \mu\text{M}$ . ROCK inhibitor Y27632 (Cayman Chemical #10005583) was used at  $10 \mu\text{M}$ . Nocodazole (Cell Signaling #2190s) was used at  $100 \text{ nM}$ . Dynasore (Sigma #D7693) was used at  $60 \mu\text{M}$ .

### **Transmission electron microscopy**

For transmission electron microscopy (TEM) samples were fixed at specified time-points in 2% PFA/2.5% glutaraldehyde overnight. The samples were

washed thrice in 0.1M phosphate buffer (PB) and a secondary (post) fixation was performed in a 1.5% Potassium Ferricyanide:1% Osmium in 0.1M PB in a Pelco® Biowave (Ted Pella, Inc.) at 100W for 4 mins. A subsequent incubation in 1% osmium in 0.1M PB in the Biowave was performed and samples were then subject to a gradual ethanol dehydration sequence: 50% ethanol for 10 mins, 2% Uranyl Acetate in 70% Ethanol for 40 mins, 85% ethanol for 10 mins, 95% for 10 mins and 100% for 30 mins. Samples were embedded in EM812 Epoxy resin (Electron Microscopy Sciences) with 2,4,6-Tris-(dimethylaminomethyl) phenol (DMP-30) and cured at 60°C for 48-72 hours. Samples were sectioned with a Leica UCT Ultracut Ultramicrotome into 1 µm sections and imaged JEOL JEM-1400 Flash TEM. The TEM embedding, sectioning, and imaging were performed by the Integrated Biomedical Imaging Services (IBIS) at the Boston University Medical School Campus. The Transmission Electron Microscope was funded by the NIH Award Number S10OD028571.

### **Statistical analyses**

Statistical tests were performed in JMP Pro 15 software. First, the Shapiro-Wilkes test was performed on each data set to determine if the data were normally distributed. The specific statistical tests used are specified in figure captions; generally, the Dunnett's test with control was performed for normally distributed data and the Steel test with control was performed for non-normally distributed data. A p-value < 0.05 was considered significant. For Figures 3.1,

3.2, and S1, at least 3 biological replicates were performed with at least 5 tissues per condition in each replicate. For Figure 3.3B, 1 biological replicate was performed that included 3 tissues per condition. For Figure 3.3D, at least 2 biological replicates were performed with at least 10 tissues per condition in each replicate. For Figure 3.4, 1 tissue was imaged per condition with at least 10 fields of view per tissue. Values given in the text are expressed as mean  $\pm$  standard error of the mean.

### 3.5. SUPPLEMENTAL MATERIAL

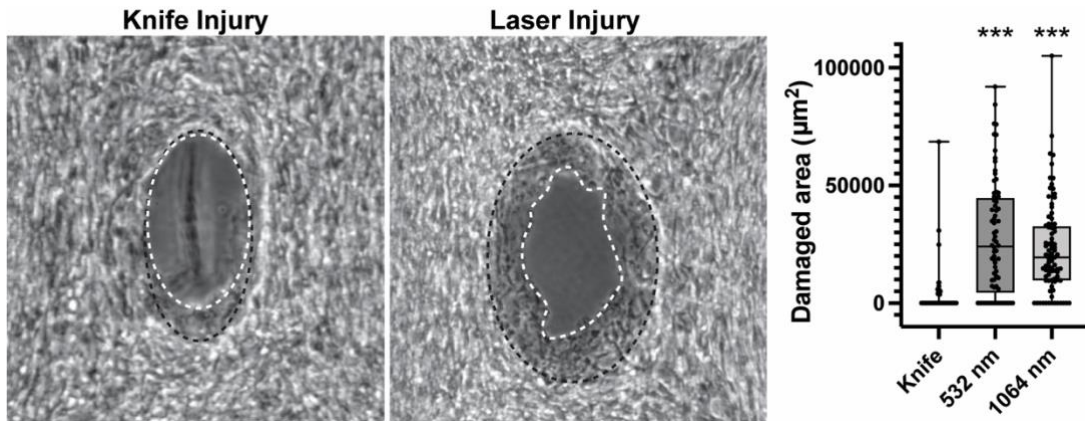


**Figure 3.S1: Quantification of damaged tissue area.**

(Left, Center) Sample phase contrast images of injured tissues. The black and white dotted lines delineate the outside and inside, respectively, of the damaged tissue area. (Right) Box and whisker plot showing the quantification of damaged tissue area for the microtissues included in Figure 3.2. For the knife condition, the majority of data points are at  $0 \mu\text{m}^2$ , therefore the box and lower whisker are not visible.

#### **Calculation of laser fluence**

The fluence, or energy density, of the laser pulse at the focal point of a microscope objective is a critical parameter for laser ablation. When the fluence exceeds the ablation threshold of the microtissue, the tissue is decomposed by ablation. Several factors such as the diameter of the entrance beam, the wavelength of the laser pulse, the focal length of the objective, and the transmittance of light at the wavelength of the laser pulse determine the fluence in the focal point. In our system, a Nd:YAG laser generates a laser pulse at a wavelength of 1064 nm (or 532 nm when the beam is steered through a KTP

crystal) with a diameter of 3 mm. The laser pulse passes a 3x beam expander that diverges the pulse diameter to 9 mm. Next, the laser pulse passes a Focal Flat Top Beam Shaper (Edmund Optics) which is then converged through a 10x EC Plan-Neofluar objective (Zeiss) before hitting the sample (Figure S2A). The shape of the laser pulse where it is focused into the microtissue is shown (Figure S2B).

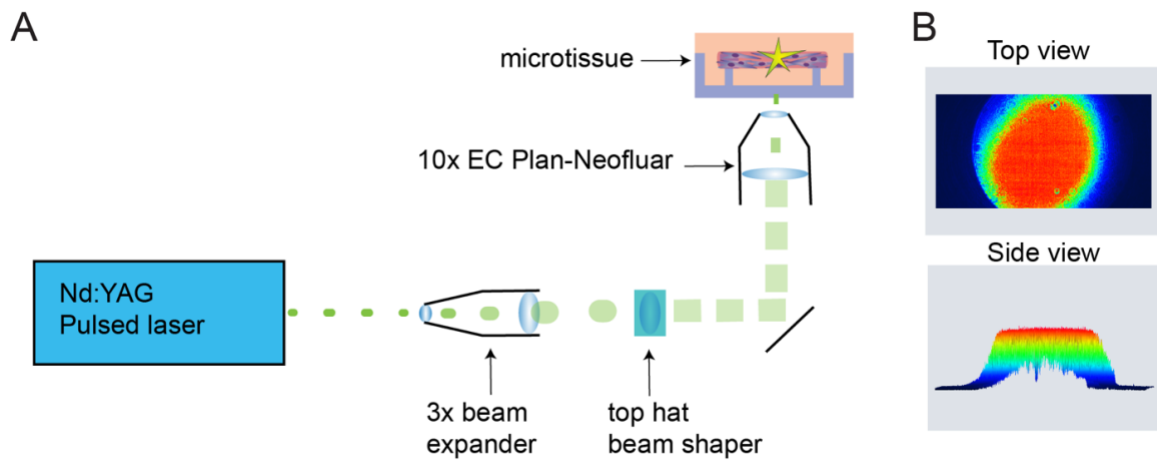


**Figure 3.S2: Details of laser ablation system.**

(A) Schematic overview of the laser ablation setup. (B) A laser intensity color map ranging from 0 (dark blue) to 100% (red) laser intensity shows the top-hat profile of the laser pulse. The laser intensity for 1 mJ pulse was measured 3-4 mm above the focal point using a BeamPro 3.0 laser beam profiler (Edmund Optics).

To estimate the fluence, we first calculate the spot size in the focal point using the following formula:

$$2\omega_0 = \frac{4M^2\lambda f}{\pi D}$$

In which  $\omega_0$  is the radius of the focal spot size,  $M$  the beam quality ( $\sim 1$ ),  $\lambda$  the wavelength of the laser pulse (532 nm and 1064 nm),  $f$  the focal length of the objective (16.5 mm), and  $D$  the beam diameter of the laser pulse before entering the objective (9 mm). Using this formula, we obtained a spot diameter of 1.24  $\mu\text{m}$  and 2.48  $\mu\text{m}$  for a wavelength of 532 nm and 1064 nm respectively.

The fluence is calculated as the pulse power divided by the beam area. Given that the laser beam has a top hat profile, we can approximate the beam area as  $\pi r^2$  which results in  $1.2076\text{e}^{-8} \text{ cm}^2$  and  $4.8305\text{e}^{-8} \text{ cm}^2$  for 532 nm and 1064 nm respectively. Using these numbers, we calculated the fluence for each used laser power (Table S1). The pulse power is measured before it passes through the objective. Given that the transmittance of light through the objective is different for each wavelength, the calculated fluence need to be corrected. Based on the transmission specifications for a representative sample of the 10x EC Plan-Neofluar objective (<https://www.micro-shop.zeiss.com/en/us/shop/objectives/420340-9901-000/Objective-EC-Plan-Neofluar-10x-0.30-M27>), the transmission for 532 nm is approximately 92% and 57 % for 1064 nm.

**Table 3.S1: Measured laser power and calculated laser fluence**

	<b>Laser Power</b>	<b>Fluence (J/cm<sup>2</sup>)</b>	<b>Corrected fluence (J/cm<sup>2</sup>)</b>
<b>532nm</b>	0.25 mJ	20700	19044
	0.4 mJ	33110	30461.2
	0.55 mJ	45530	41887.6
	0.7 mJ	57950	53314
<b>1064nm</b>	1.5 mJ	31050	17698.5
	2 mJ	41400	23598
	3 mJ	62100	35397

## **CHAPTER FOUR: Effects of fibroblast phenotype and ECM composition on repair potential in engineered stromal microtissues**

### **4.1. INTRODUCTION**

In the adult human body, the healing process is nearly always occurring somewhere. The purpose and general progression of the injury-response is considered the same regardless of the anatomical site, although there are many organ- and tissue-specific distinctions in this process. One main difference lies in the outcome of the healing process: repair or regeneration. Regeneration refers to a full recovery of the tissue function, and is considered the ideal result. The adult liver has an incredible capacity for regeneration (perhaps better called “compensatory growth”), capable of growing new, functional hepatic tissue (Braun & Sandgren, 1998; Diehl & Rai, 1996; Kan, Junghans, & Belmonte, 2009; Michalopoulos, 2013). Some tissues have notably low capacities for regeneration, including cardiac and central nervous tissue (Modo, 2019). Tissue damage, such as that caused by a stroke or heart attack, undergoes a repair process in an attempt to preserve mechanical integrity, but the result is mostly non-functional scar-tissue (Curtis & Russell, 2009; Hasan et al., 2015; E. H. Lo, 2008; Radhakrishnan, Krishnan, & Sethuraman, 2014; Tuladhar & Shoichet, 2018). Healing in the skin can have varying results. Some cutaneous wounds, particularly those in young and otherwise healthy individuals, heal relatively scar-free and with full function restored. However, many cutaneous wounds fall short of regeneration in favor of repair, creating scar tissue. Scar tissue consists of

thick, highly aligned fibers of collagen type I. Although this tissue fulfills the most important purpose of skin, to serve as a barrier to pathogens and fluid loss, it fails to recapitulate other functions. Scar tissue only regains up to 70% of its tensile strength compared to healthy skin, has minimal elasticity, and lacks sweat and sebaceous glands (Corr, Gallant-Behm, Shrive, & Hart, 2009; Hollander et al., 2003; Hollinsky & Sandberg, 2007).

Fibroblasts, and their activated counterparts, myofibroblasts, are important throughout the healing process. Shortly after hemostasis, and overlapping with the inflammatory phase, fibroblasts proliferate and migrate into the wound bed, where they begin to replace the fibrin clot with provisional matrix consisting of (predominantly) fibronectin and collagen type III. This process is critical because it results in a substrate over which epithelial cells can migrate in order to restore tissue barrier (Rittié, 2016). Around the third to fourth day of healing, some fibroblasts (could also be circulating fibrocytes or epithelial/endothelial cells having undergone EMT/EndoMT) in the wound bed become activated into myofibroblasts. Myofibroblasts are highly contractile cells that produce a large amount of ECM. They contribute to wound closure by contracting the tissue to draw the wound margins closer together, and by producing abundant, highly aligned ECM fibers consisting of predominantly collagen type I. This remodeling phase can last months to years, and is mainly carried out by myofibroblasts. At wound resolution, the myofibroblasts disappear, classically thought to occur via

apoptosis. More recently, myofibroblasts have been shown to revert to a quiescent phenotype or transdifferentiate into another cell type, such as adipose cells (Plikus et al., 2017). However, under pathological conditions, myofibroblasts can persist and remain active. This often leads to hypertrophic scarring (of the skin) or fibrosis (of internal organs). The long-term effects of fibrosis are serious, and can become fatal as non-functional fibrotic tissue replaces healthy tissue.

The behavior of fibroblasts and myofibroblasts is guided by several factors. The presence of inflammatory cytokines can jumpstart a positive feedback loop that results in chronic inflammation. In these settings, pro-inflammatory macrophages (M1 type) do not correctly convert to the anti-inflammatory M2 type. As a result of continued pro-inflammatory signaling, the abundance of myofibroblasts in the tissue increases (Hesketh, Sahin, West, & Murray, 2017; Ploeger et al., 2013; Tang, Nikolic-Paterson, & Lan, 2019). The extracellular matrix can also guide the behavior of cells, including fibroblasts. For example, the mechanical interactions of fibroblasts with stiff matrices regulate myofibroblast differentiation (Hinz et al., 2019). In turn, myofibroblasts stiffen the surrounding matrix. This reciprocity between (myo)fibroblasts and the ECM has become of increasing interest in the last few decades (K. Liu, Wiendels, Yuan, Ruan, & Kouwer, 2022; Schultz, Davidson, Kirsner, Bornstein, & Herman, 2011; Xu, Boudreau, & Bissell, 2009). The composition of the ECM alters which integrins and adhesion molecules are activated in cells. The stiffness and compliance of the ECM can differentially

contribute to focal adhesion formation and activation of mechanotransduction pathways. The topography (including alignment and fiber diameter) can also affect cell behavior, polarization, and migration. Additionally, the ECM can serve as a reservoir for bound and latent growth factors. Each of these components affects the behavior of the cells that interact with the matrix. In turn, the cells accordingly alter the ECM, thus propagating the cycle.

In this chapter, I describe a series of pilot experiments that were performed to begin to understand the relationships between fibroblast type and phenotype, ECM composition, and tissue repair potential. In Pilot Study 1, I examined repair responses in several fibroblast types from normal adult tissues: marrow-derived stromal cells (MSC), human lung fibroblasts (HLF), human cardiac fibroblasts (HCF), and human dermal fibroblasts (HDF). Additionally, human dermal fibroblasts from neonatal tissue (HDFneo) were compared to adult HDF. In Pilot Study 2, the initial composition of the ECM hydrogel was altered slightly, and changes in injury closure rate and tissue compaction were observed. In Pilot Study 3, the activation of fibroblast to myofibroblast phenotype in 2D cell culture was examined. Different cell types displayed varying activation potential.

## **4.2. PILOT STUDY 1: Fibroblasts from different tissues have varying in vitro repair potentials**

### **4.2.1. Motivation**

Different organs have different repair potentials. For example, the liver has amazing capacity for regeneration, whereas cardiac tissue repairs via scarring and fibrosis. Tissue repair is mainly carried out by local mesenchymal cells. There can be many differences in the local microenvironment (biochemical cues, ECM composition, stiffness, architecture, and alignment) and in the cells themselves (different epigenetics, transcriptomes, proteomes, etc.) that all affect the tissue repair potential. In order to determine cell-type specific factors affecting repair potential, we compare several primary human cells from multiple sources in a common physical environment using our biomimetic stromal healing model.

### **4.2.2. Methods**

**PDMS device fabrication.** As previously described (Legant et al., 2009), standard photolithography was used to create an SU8 model of the microtissue device. A negative mold of the device was cast using poly-dimethyl siloxane (PDMS, Sylgard 184, Dow-Corning). Finally, the negative mold was used to generate devices of PDMS in 35 mm culture dishes. One device consisted of 80 rectangular microwells, each containing four cylindrical pillars with an overhanging cap near the top to constrain microtissues. Microwells were

1.12 mm × 1.5 m, and pillars had 0.62 mm and 1.0 mm between pillar centers. Pillar diameter was 120 µm for the first layer with a height of 110 µm, and cap diameter was 180 µm with a height of 80 µm.

**Cell culture.** Cells were cultured in humidified incubators at 37°C with 5% CO<sub>2</sub>. Standard growth media (sGM) was DMEM with 10% fetal bovine serum (FBS) and 1% penicillin/streptomycin. FGM2 (Lonza) consists of a proprietary basal media, FBM, with 2% FBS and gentamicin. FGM3 (Lonza) consists of FBM with 10% FBS and gentamicin. Cells were passaged with 0.05% trypsin-EDTA once they reached 80-90% confluence and seeded into new tissue culture plastic (TCP) dishes at a density of 5,000 cells/cm<sup>2</sup>. Cells were used between passages 3 and 10. Specific cell types and their corresponding growth media are shown in Table 4.1.

**Table 4.1: Cell sources and growth medias used in Pilot Study 1.**

Cell Type	Cell Source	Growth Media
Human lung fibroblasts (HLF)	A: Lonza	FGM2
	B: collaborator	FGM2
Human dermal fibroblasts (HDF)	A: collaborator	FGM2
	B: Lonza lot A	FGM2
	C: Lonza lot B	FGM2
Human neonatal dermal fibroblasts (HDFneo)	A: Lonza lot A	FGM2
	B: Lonza lot B	FGM2
Marrow-derived stromal cells (MSC)	A: MSC – donor 3	sGM
	B: MSC – donor 2	sGM
Human cardiac fibroblasts (HCF)	A: Lonza	FGM3

**Microtissue seeding.** Cells were mixed with rat tail tendon collagen I (Corning #356236) at a final concentration of 2 mg/ml (pH ~8). Final collagen solution contained 2 mg/ml collagen I, 10mM HEPES, 0.035% (w/v) NaHCO<sub>3</sub>, 1X M199, and an empirically determined volume of NaOH to reach pH 8. 600,000 – 800,000 cells were added to each device and centrifuged to drive cells into the microwells. Excess collagen solution was removed, and collagen in the microwells was allowed to polymerize at room temperature for 10 minutes, then at 37°C for 10 minutes. Microtissues were cultured at 3°C with 5% CO<sub>2</sub> in growth medium for 16-20 hours prior to injury, during which time they spontaneously compact, as previously described (Sakar et al., 2016).

**Knife injury of microtissues.** For knife injury, a diamond dissection knife (type MDL, Electron Microscopy Systems, #72029) mounted to an XYZ-micromanipulator (SLC-2040, SmarAct GmbH) was used to tear a full-thickness wound in the microtissues.

**Live microscopy and closure rate measurements.** For closure experiments, time-lapse images were taken every 30 minutes for 22 hours on a Nikon Ti Eclipse microscope with a 10x objective, fitted with an environmental chamber (37°C, 5% CO<sub>2</sub>). Gap area was measured every other hour in ImageJ, manually, using the polygon selection tool. The closure rate was determined as the slope of the line of best fit through data from 0 hours until closure or the end of timelapse data.

**Statistical analysis.** Statistical tests were performed in JMP Pro 15 software. First, the Shapiro-Wilkes test was performed on each data set to determine if the data were normally distributed; the data shown in Figure 4.1 are not. Next, the data for each cell type were compared using the non-parametric Wilcoxon test for each pair.

### 4.2.3. Results

Microtissues were made from primary cell types: normal adult human lung fibroblasts (HLF), human dermal fibroblasts (HDF), marrow-derived stromal cells (MSC) from adult donors, and human cardiac fibroblasts (HCF) from a normal adult left ventricle. As can be seen in Figure 4.1, there are organ specific differences in repair potential of adult cells. HLF fail to repair tissues, either stalling before completing closure (Fig 4.1A, bottom), or occasionally tearing the microtissue wound much larger. HCF repair tissues quickly, within 10 hours for small-size wounds, whereas adult HDF and MSC heal much more slowly, completing closure within 20-24 hours for similar size wounds (Fig 4.1A,B).

Neonatal and adult cells, both from dermal tissues, were also compared. HDFneo microtissues healed much faster than did adult HDF microtissues (Fig 4.1A,B). Adult closure rates were about three times lower than neonatal, with a mean closure rate of  $910 \pm 380 \mu\text{m}^2/\text{hour}$  for HDF compared to  $2710 \pm 1500 \mu\text{m}^2/\text{hour}$  for HDFneo ( $p < 0.05$ , Fig 4.1C). MSC closure rates, mean  $1240 \pm 700 \mu\text{m}^2/\text{hour}$ , were a little faster than HDF ( $p < 0.05$ ). HCF performed similarly to HDFneo, with a mean closure rate of  $3000 \pm 1200 \mu\text{m}^2/\text{hour}$  (not statistically different from HDFneo). HLF exhibited a slightly slower mean closure rate than HDF ( $870 \pm 830 \mu\text{m}^2/\text{hour}$  compared to  $910 \pm 380 \mu\text{m}^2/\text{hour}$ ), although the data does not reach statistical significance ( $p = 0.06$ ). However, the standard deviation for HLF closure rate is much greater, which is likely because many HLF tissues

stalled and did not complete closure and some HLF tissues tore the wound large, resulting in negative closure rates (Fig 4.1C).

With the exception of HCF, at least two sources were tested for each cell type. Details can be found in Table 4.1 in Methods Subsection 4.2.2. Data from Figure 4.1C colored to indicate cell source can be found in Figure 4.S1. (NOTE: Data collected from HCF are from colleague Anish Vasani. These data were collected from microtissues that were made in a 96-well plate format and laser ablation was used to inflict wounds in HCF tissues only.)

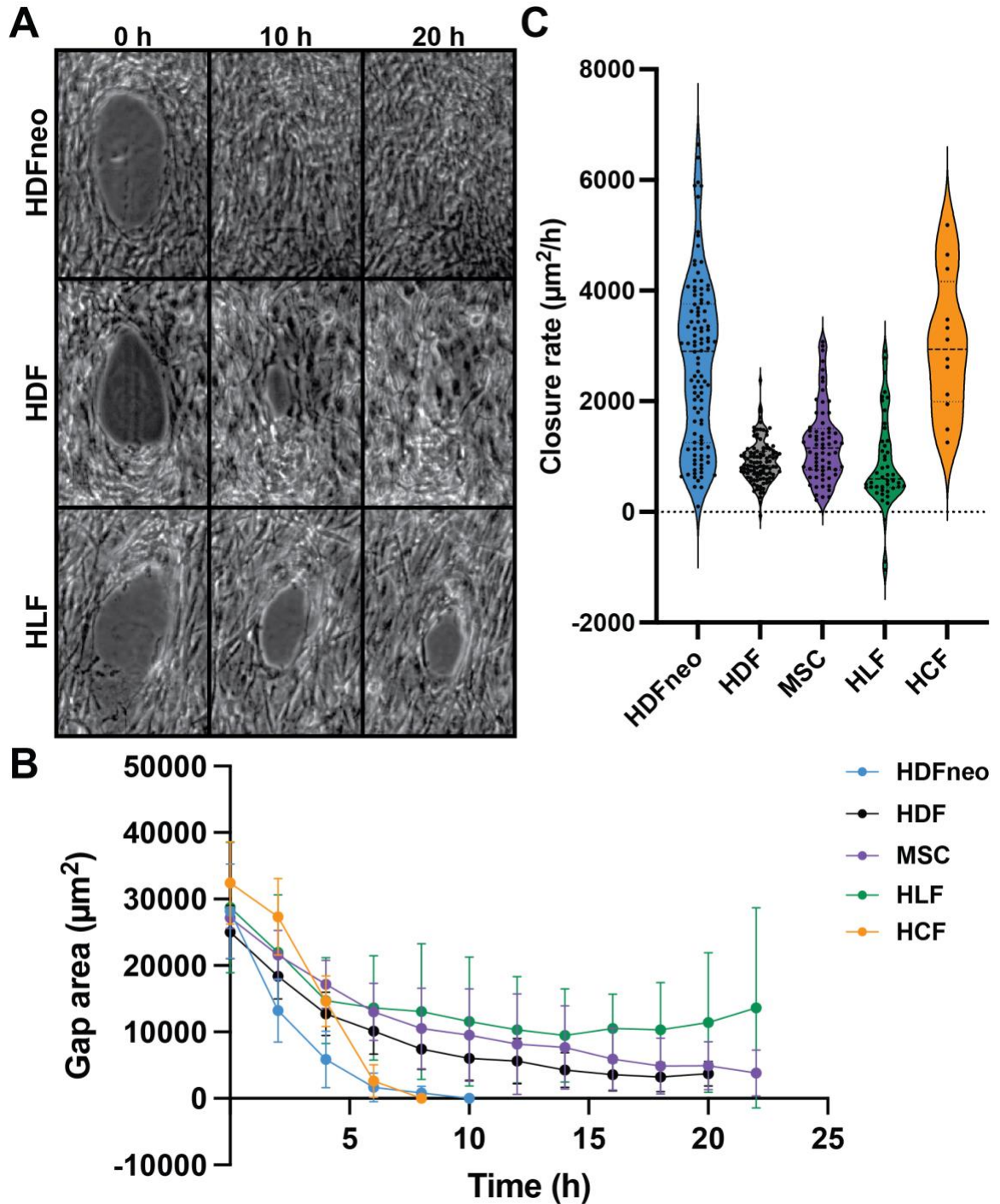


**Figure 4.1: Injury responses in microtissues of various human cell types.**

(A) Time-lapse images are shown at 0 hours, 10 hours, and 20 hours post injury for representative tissues composed of three human cell types: neonatal dermal fibroblasts

(HDFneo), adult dermal fibroblasts (HDF), and adult lung fibroblasts (HLF). (B) Gap area as a function of time for each cell type. Mean and standard deviation for  $n=6$  tissues per cell type with comparable starting areas. (C) Closure rate following injury for each cell type. The differences between each pair are statistically significant ( $p<0.05$ ), with two exceptions: HDFneo and HCF are not statistically different, and HDF and HLF are not statistically different.

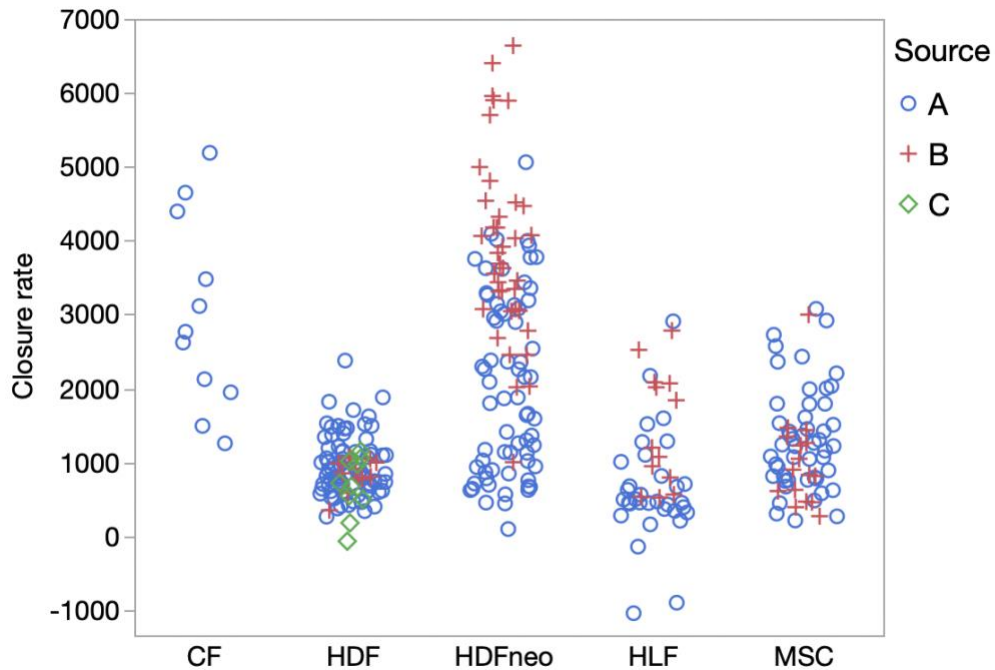


**Figure 4.S1: Closure rates for various cell types colored by cell source.**

Figure includes the same data shown in Figure 4.1C. The source (A, B, or C) corresponds to the cell sources listed in Table 4.1: Cell sources and growth medias used in Pilot Study 1.

#### 4.2.4. Discussion

Our stromal microtissue healing model was developed with 3T3 cells, which are mouse embryonic fibroblasts. We expected that all fibroblast and mesenchymal cell types would similarly be able to repair “wounds” or gaps in 3D soft tissues. However, experiments revealed that different cell types have varying repair potentials in our microtissues. Marrow-derived stromal cells performed similarly to 3T3 cells (data not shown in this chapter, but is included under “knife” in Figure 3.2). In comparison to MSC, adult HDF repaired tissues a little slower. One confounding factor when comparing MSC and HDF data is the differences in media conditions. MSC had 10% serum, whereas HDF had only 2% serum. It is possible that the greater amount of stimulatory growth factors in the media with more serum contributed to the differences observed in closure rates.

Lung fibroblasts were about as slow as HDF, with some instances of wound tearing/enlargement that were not observed in other cell types. HLF and HDF were grown in the same media. Morphologically, there are some differences between the two cell types. Both cells are spindle shaped in 2D cell culture, but HLF generally spread much more length-wise and tend to exhibit greater alignment between neighboring cells. These differences can be seen to some extent by the different textures of the tissues in Figure 4.1A. These observations, coupled with failed microtissue repair, suggest higher cell contractility in HLF compared to HDF. In Pilot Study 3, these cells display different potentials to

differentiate into myofibroblasts, a phenomenon that is also dependent on cellular contractility.

Surprisingly, cardiac fibroblasts exhibited a much faster closure rate than other adult cells compared here. Although HCF media, FGM3, contains 10% serum, this may only explain differences between HCF and HDF. MSC GM also contains 10% FBS, so there are likely other factors contributing to the accelerated closure rates of HCF. Preliminary data from Anish Vasan suggests that these differences can be at least partially attributed to differences in ECM production. Further experiments controlling for serum level will need to be performed to parse the differences between serum-driven and inherent to cell type differences in ECM production and tissue repair.

Neonatal fibroblasts had very fast closure rates, comparable to HCF. Given the scar-free wound healing observed in embryos and neonates, it is perhaps unsurprising that HDFneo exhibited much faster tissue repair in vitro than did adult HDF. There are many changes that occur in cells with age. Aged cells experience reduced migratory and proliferative capacities. Tissues become stiffer and less elastic with age. ECM production also changes. For example, the portion of collagen type III in skin tissue is known to decrease with age. In Pilot Study 2, a simple addition of collagen type III increases microtissue closure rate in 3T3 tissues. These collective data are discussed further in Chapter 5.

### **4.3. PILOT STUDY 2: Effect of ECM composition on fibrous tissue healing in microtissues**

#### **4.3.1. Motivation**

Embryonic and neonatal tissues exhibit the desired but elusive quality of flawless, scar-free wound healing. There are many factors that likely contribute to the decrease in regeneration potential observed as tissues age (Ferguson & O’Kane, 2004). Damage due to sun exposure, increased tissue stiffness, reduced proliferative capacities of cells, cellular senescence, depleted stem cell populations, and underlying conditions such as diabetes may all contribute to the poorer wound healing prognoses seen in older populations (Gosain & DiPietro, 2004). Changes in ECM due to aging are an important factor affecting healing outcome. For example, in aged skin, collagen type I content and glycosylation increase whereas collagen type III and proteoglycan abundances decrease. Additionally, production of the EDA splice variant of fibronectin, known to promote fibrosis, increases with age (Kapetanaki, Mora, & Rojas, 2013). Together, these observations suggest an important role of ECM in determining healing outcomes.

In this pilot study, we investigated whether the composition of the ECM affects microtissue repair potential. We hypothesized that microtissue repair would be altered in the presence of additional fibrillar ECM proteins. To address this hypothesis, collagen type III was added to collagen type I made 3T3

microtissues. Upon compaction, tissues were injured and observed with live microscopy, and closure rates calculated. Interestingly, addition of only 10% collagen type III accelerated microtissue closure rate.

Additionally, the presence of network forming collagens was investigated.

Preliminary data from experiments performed by Jeroen Eyckmans and Laurie Kelleher showed increased tissue compaction when network forming collagen type VIII was added to microtissues. Based on these preliminary observations, we hypothesized that inclusion of network forming ECM proteins would increase microtissue compaction. To address this hypothesis, network forming collagen type IV was added to microtissues and, contrary to our expectations, decreased tissue compaction.

#### **4.3.2. Methods**

**PDMS device fabrication.** As previously described (Legant et al., 2009), standard photolithography was used to create an SU8 model of the microtissue device. A negative mold of the device was cast using poly-dimethyl siloxane (PDMS, Sylgard 184, Dow-Corning). Finally, the negative mold was used to generate devices of PDMS in 35 mm culture dishes. One device consisted of 80 rectangular microwells, each containing four cylindrical pillars with an overhanging cap near the top to constrain microtissues. Microwells were 1.12 mm × 1.5 m, and pillars had 0.62 mm and 1.0 mm between pillar centers.

Pillar diameter was 120  $\mu\text{m}$  for the first layer with a height of 110  $\mu\text{m}$ , and cap diameter was 180  $\mu\text{m}$  with a height of 80  $\mu\text{m}$ .

**Cell culture.** 3T3 cells (ATCC #CCL-92) were grown in Dulbecco's modified eagle medium (DMEM, Fisher Scientific #10-013-CV) with 10% bovine serum (Sigma #B9433) and 1% penicillin/streptomycin (Life Technologies #15140-122). Cells were cultured in humidified incubators at 37°C with 5% CO<sub>2</sub>. Cells were passaged with 0.05% trypsin-EDTA once they reached 80-90% confluence and seeded into new tissue culture plastic (TCP) dishes at a density of 5,000 cells/cm<sup>2</sup>. Cells were used between passages 5 and 18.

**Microtissue seeding.** Cells were mixed with rat tail tendon collagen I (Corning #356236). Final collagen solutions contained 2.2 mg/ml total collagen, 10mM HEPES, 0.035% (w/v) NaHCO<sub>3</sub>, 1X M199, and an empirically determined volume of NaOH to reach pH 8. For tissues containing only collagen type I, 2.2 mg/ml of collagen I was used. For tissues containing collagen type III or IV, 2 mg/ml of collagen I with 0.2 mg/ml of collagen III or collagen IV was added, and mixtures were adjusted to about pH 8 with NaOH. 900,000 cells were added to each device in collagen mixture and centrifuged to drive cells into the microwells. Excess collagen solution was removed, and collagen in the microwells was allowed to polymerize at room temperature for 10 minutes, then at 37°C for 10 minutes. Microtissues were cultured at 37°C with 5% CO<sub>2</sub> in growth medium for

16-20 hours prior to injury, during which time they spontaneously compact, as previously described. Compacted tissues suspended between the PDMS pillars contain about 2,000 cells per tissue (Sakar et al., 2016).

**Knife injury of microtissues.** For knife injury, a diamond dissection knife (type MDL, Electron Microscopy Systems, #72029) mounted to an XYZ-micromanipulator (SLC-2040, SmarAct GmbH) was used to tear a full-thickness wound in the microtissues.

**Live microscopy and closure rate measurements.** For closure experiments, time-lapse images were taken every 30 minutes for 22 hours on a Nikon Ti Eclipse microscope with a 10x objective, fitted with an environmental chamber (37°C, 5% CO<sub>2</sub>). Gap area was measured every other hour in ImageJ, manually, using the polygon selection tool. The closure rate was determined as the slope of the line of best fit through data from 0 hours until closure or the end of timelapse data.

**Statistical analyses.** Statistical tests were performed in JMP Pro 15 software. First, the Shapiro-Wilkes test was performed on each data set to determine if the data were normally distributed. Closure data is non-normal, and compaction data is normal. Then, the Steel test with control was used for closure data, and Dunnett's test with control was used for compaction data.

### 4.3.3. Results

As described in previous sections, microtissues were made, injured, and imaged to observe the injury closure responses. Microtissues composed of collagen types I and III had an accelerated closure rate compared to microtissues composed of only collagen type I ( $1040 \pm 390 \mu\text{m}^2/\text{hour}$  compared to  $720 \pm 420 \mu\text{m}^2/\text{hour}$ ). The width of tissues immediately following injury and 24 hours later was measured as a proxy for overall tissue compaction. Compaction, expressed as a percent change in tissue width, was significantly decreased for microtissues composed of collagen types I and IV compared to microtissues composed of only collagen type I (mean compaction  $15\% \pm 3\%$  compared to  $20\% \pm 4\%$ ).

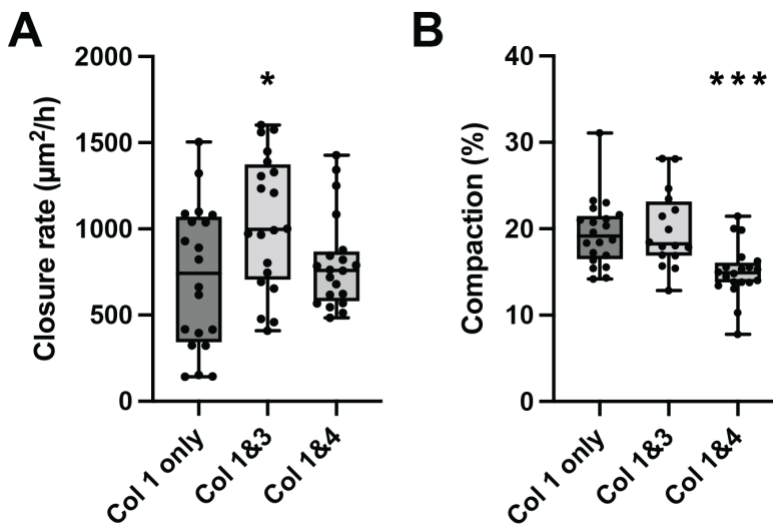


**Figure 4.2: ECM composition alters microtissue closure and compaction.**

(A) Closure rate for microtissues composed of only collagen I, collagen I and III, or collagen I and IV. \*  $p < 0.05$ , non-parametric Steel test with control. (B) Compaction for microtissues composed of only collagen I, collagen I and III, or collagen I and IV. \*\*\*  $p < 0.001$ , Dunnett's Test with control.

#### 4.3.4. Discussion

Collagen types I and III are both fibrillar collagens, whereas collagen type IV is a network-forming collagen often found in basement membranes. Collagen type III is more abundant in fetal skin (up to 50%) whereas adult skin contains only 10-20% of collagen type III (Cheung, Tong, Perelman, Ertl, & Nimni, 1990). This difference is believed to contribute to the scar-less healing observed in fetal skin (D. D. Lo, Zimmermann, Nauta, Longaker, & Lorenz, 2012). In our experiments, including collagen III in microtissues accelerated the closure rate. In this study, only 10% collagen III was added. Experiments with relative amounts of collagen III closer to that in fetal skin (>30%) may yield more dramatic results and provide more insight into the contribution of each collagen type to tissue repair. Further experimentation is needed to determine the mechanism by which collagen composition affects healing in this model. The microtissues repair by generating a provisional matrix composed of fibronectin (Sakar et. al., 2016). Therefore, it is unlikely that addition of collagen III directly alters the provisional matrix. Collagen III may contribute indirectly to tissue repair, perhaps by altering the mechanical properties of the surrounding tissue. Bulk rheology and local atomic force microscopy could be performed to determine if and how collagen III affects microtissue mechanical properties.

The decreased compaction with collagen type IV present is an interesting result, especially when compared to the preliminary data with collagen type VIII, where

compaction was dramatically increased. A potential explanation for the decreased compaction with collagen IV is that collagen IV may alter the mechanical properties of the tissue, causing increased crosslinking and therefore increased stiffness and preventing cell-mediated tissue compaction. Interestingly, it has been reported that collagen type IV abundance increases with age in several tissues, including lung and kidney (Onursal, Dick, Angelidis, Schiller, & Staab-Weijnitz, 2021). Since tissue compaction aids in tissue repair, it is possible that an increased abundance of collagen type IV alters healing in aged tissues by affecting compaction. Further experimentation is needed to parse the effects of ECM composition on mechanical properties of tissues and the subsequent healing response.

#### **4.4. PILOT STUDY 3: Fibroblast activation to myfibroblast phenotype in standard cell culture**

##### **4.4.1. Motivation**

Myfibroblasts are important for proper and timely tissue repair. They are characterized by de novo alpha smooth muscle actin ( $\alpha$ SMA) expression and organization into stress fibers. Myfibroblasts are highly contractile, a characteristic which is attributed to  $\alpha$ SMA expression, although other actin isoforms can compensate when  $\alpha$ SMA is knocked out. Myfibroblasts also produce a large amount of ECM and are primarily responsible for modifying ECM during the remodeling phase of healing (Darby, Laverdet, Bonté, & Desmoulière, 2014; Gabbiani, 2003). In pathological settings like fibrosis or hypertrophic scarring, myfibroblasts are implicated in depositing excess collagenous matrix that can prevent functioning of parenchymal tissue. Because of their role in fibrosis, myfibroblasts are of great interest to biomedical researchers (Teng et al., 2022).

Fibroblasts, upon biochemical activation, will first differentiate into proto-myfibroblasts, and then into myfibroblasts. The distinction between these phenotypes is important, but is often blurred or ignored. In standard cell culture, transforming growth factor beta (TGF $\beta$ ) is typically used to initiate this biochemical activation (Gabbiani, 2003; Kis, Liu, & Hagood, 2011). However, activation with TGF $\beta$  requires time – on the order of days – and can be prevented

by serum and basic fibroblast growth factor (bFGF or FGF2) (Cushing, Mariner, Liao, Sims, & Anseth, 2008; Sun et al., 2022; Svystonyuk et al., 2015a). On the other hand, maintaining a true fibroblast phenotype in cell culture is also difficult. When cultured in serum conditions on stiff substrates like tissue culture plastic, fibroblasts tend to develop stress fibers, indicating they have activated into proto-myofibroblasts. Native fibroblasts do not exhibit stress fibers (Tomasek et al., 2002). In this pilot study, we looked at three primary cell types, MSC, HDF, and HLF, and their responses to TGF $\beta$  under various media conditions. We found that each cell type had different propensities for activation.

#### **4.4.2. Methods**

**Cell culture.** Cells were cultured in humidified incubators at 37°C with 5% CO<sub>2</sub>. Standard growth media (sGM) was DMEM with 10% fetal bovine serum (FBS) and 1% penicillin/streptomycin. FGM2 (Lonza) consists of a proprietary basal media, FBM, with 2% FBS and gentamicin. The growth media (GM) used for MSC D2 and D3 was sGM. The GM for HDFneo, HDF, and HLF was FGM2. In this Pilot Study, the cells correspond to Table 4.1 as follows. HLF and HDF are Source A, and HDFneo are Source B.

**Growth factor studies.** B27 media consists of 2% v/v Supplement B27 (Gibco) in DMEM/F12 (Gibco) with 1% penicillin/streptomycin. Supplement B27 contains essential vitamins, amino acids, hormones and enzymes to support a serum-free

(and growth factor-free) cell culture. Recombinant human TGF $\beta$ 1 (R&D Systems) and recombinant bFGF (R&D Systems) were both used at 10 ng/ml. Cells were incubated with growth factors for 4 days, with fresh media and growth factors every 48 hours.

**Immunofluorescence.** Cells were fixed in 4% paraformaldehyde in PBS for 15 minutes at room temperature, then washed 3 times in phosphate buffered saline (PBS). Blocking was performed with 5% goat serum and 0.1% saponin in PBS for 1 hour at room temperature. The primary antibody for  $\alpha$ SMA (Abcam 7817) was diluted 1:400 in the blocking buffer, and incubated with cells overnight at 4°C, then washed 3 times in PBS. The secondary antibody (goat anti-mouse 488), phalloidin, and DAPI were diluted 1:500 in blocking buffer, and incubated with cells for 1-2 hours at room temperature, then washed 3 times in PBS.

**Fluorescence microscopy and image quantification.** Stained cells were imaged using a 20X objective on a spinning disc confocal microscope. Quantification was performed in MATLAB. First, DAPI images were thresholded and masked, and masks overlaid with  $\alpha$ SMA images. Any nuclei which had  $\alpha$ SMA stress fibers present underneath were considered  $\alpha$ SMA positive cells. Cells with  $\alpha$ SMA signal that was not arranged in stress fibers were not considered positive (as in Figure 4.3A, top center).

**Quantitative PCR.** Cells were lysed with Trizol (LifeTechnologies) followed by homogenization using a 20-gauge needle. RNA extraction was performed using the Qiagen RNeasy Mini kit according to the manufacturer's protocol. Next, 1  $\mu$ g of total RNA was converted to cDNA using qScript cDNA Supermix (Quanta Sciences) following the manufacturer's protocol. Quantitative PCR was performed in 20- $\mu$ l reactions using the SYBR Green Mastermix I (Roche) and a LightCycler480 (Roche), with 40 cycles of 95 °C for 3 s, 60 °C for 10 s, and 72 °C for 20 s. Specific gene targets were detected with the primers listed in Table 4.2. Relative gene expression is expressed as  $-\Delta\Delta C_t$ , in which  $\Delta C_t$  is the difference in  $C_t$  value between the gene of interest and the housekeeping gene proteasome subunit beta type-2 (PSMB2).

**Table 4.2: qPCR primer sequences used in Pilot Study 3.**

Gene	Forward (5' -> 3')	Reverse (5' -> 3')
PSMB2	ACTATGTTCTTGTCGCCTCCG	CTGTACAGTGTCTCCAGCCTC
ACTA2	GGCACC ACTATGACCCTGG	CTGCTGGAAGGTGGACAGAG
COL1A1	AGGCTGGTGTGATGGGATTC	CCAGCCTCTCCATCTTTGCC
COL3A1	AGCTGGCTACTTCTCGCTCT	GCAGAGAACGGATCCTGAGTC
FN1	AACCTTGCTCCTGACAGCTC	CTGAGCTGGTCTGCTTGTC A
CTGF	GTGGAGTATGTACCGACGGC	TCCGGGACAGTTGTAATGGC
P4H	GGCTAAACACAGACTGGCCT	TCTCA TCAGGGCTTTGGCAG

#### 4.4.3. Results

Attempts to activate fibroblasts by adding TGF $\beta$  to growth media resulted in little to no activation, as determined by  $\alpha$ SMA staining, in several cell types even after 4 days (Figure 4.3B). HDF, HDFneo, and HLF in particular lack stress fibers in their growth media, FGM2, and thus maintain a fibroblast phenotype. MSC, on the other hand, always display stress fibers in standard growth media, some of which are  $\alpha$ SMA positive, indicating that these cells are mixed proto-myofibroblasts and myofibroblasts (Figure 4.3A, left). In order to render cells more responsive to growth factors, they were grown instead in a serum-free media supplemented with B27 to support growth. In most cell types tested (with the exception of HDF) some cells became  $\alpha$ SMA positive in serum-free media.

The degree of basal activation was different for each cell source. About 10% of HDFneo, 50% of HLF and MSC from Donor 2 (D2), and 80% of MSC from Donor 3 (D3) differentiated to myofibroblasts in serum-free media. Addition of TGF $\beta$  to serum-free media caused further myofibroblast differentiation in almost all cells (Figure 4.3B). HDFneo increased from 10% to 40%, HDF from 0% to 8%, MSC D3 from 80% to 95%, and HLF from 50% to 70%. Morphologically, these cells look very different upon TGF $\beta$  stimulation; they are much larger, polygonal in shape, with very large and distinct stress fibers (Figure 4.3A, center), suggestive of a highly contractile phenotype. In B27+TGF $\beta$ , all cells, including HDF, showed

$\alpha$ SMA-positive stress fibers suggesting differentiation towards proto-myofibroblasts or myofibroblasts.

Next, to determine if FGM2 maintains a quiescent fibroblast phenotype due to some factor(s) in the serum or due to the supplemented bFGF, leave-one-out experiments were performed on HLF, in which serum or bFGF were omitted from the medium. Some activation was observed when serum or bFGF were removed (data not shown), suggesting that both serum and bFGF likely contribute to the suppression of activation. Literature supports that bFGF inhibits TGF $\beta$ -mediated myofibroblast differentiation by preventing SMAD3 from locating to the nucleus (Cushing et al., 2008; Shimbori et al., 2016; Svystonyuk et al., 2015b). Indeed, addition of bFGF to serum-free media lowered the degree of myofibroblast activation almost to the GM baseline in most cell types (Figure 4.3B), and reverted cell morphology to smaller, more spindle-shaped cells (Figure 4.3A, right).

To confirm the activated myofibroblast phenotype, qPCR was performed to determine the relative expression level of several genes associated with myofibroblast differentiation and fibrosis. Several of these are ECM genes: collagen type 1 (COL1A1), collagen type III (COL3A1), and fibronectin. ACTA2 (the gene encoding for  $\alpha$ SMA), connective tissue growth factor (CTGF), and collagen maturation enzyme, prolyl-4 hydroxylase (P4H) were also included.

When compared to growth media condition, TGF $\beta$  in serum-free media increased the expression of each gene tested here in both HDF and MSC D3. Interestingly, HDF had an 8-fold increase in ACTA2 expression, even though very few cells with  $\alpha$ SMA positive stress fibers were observed.

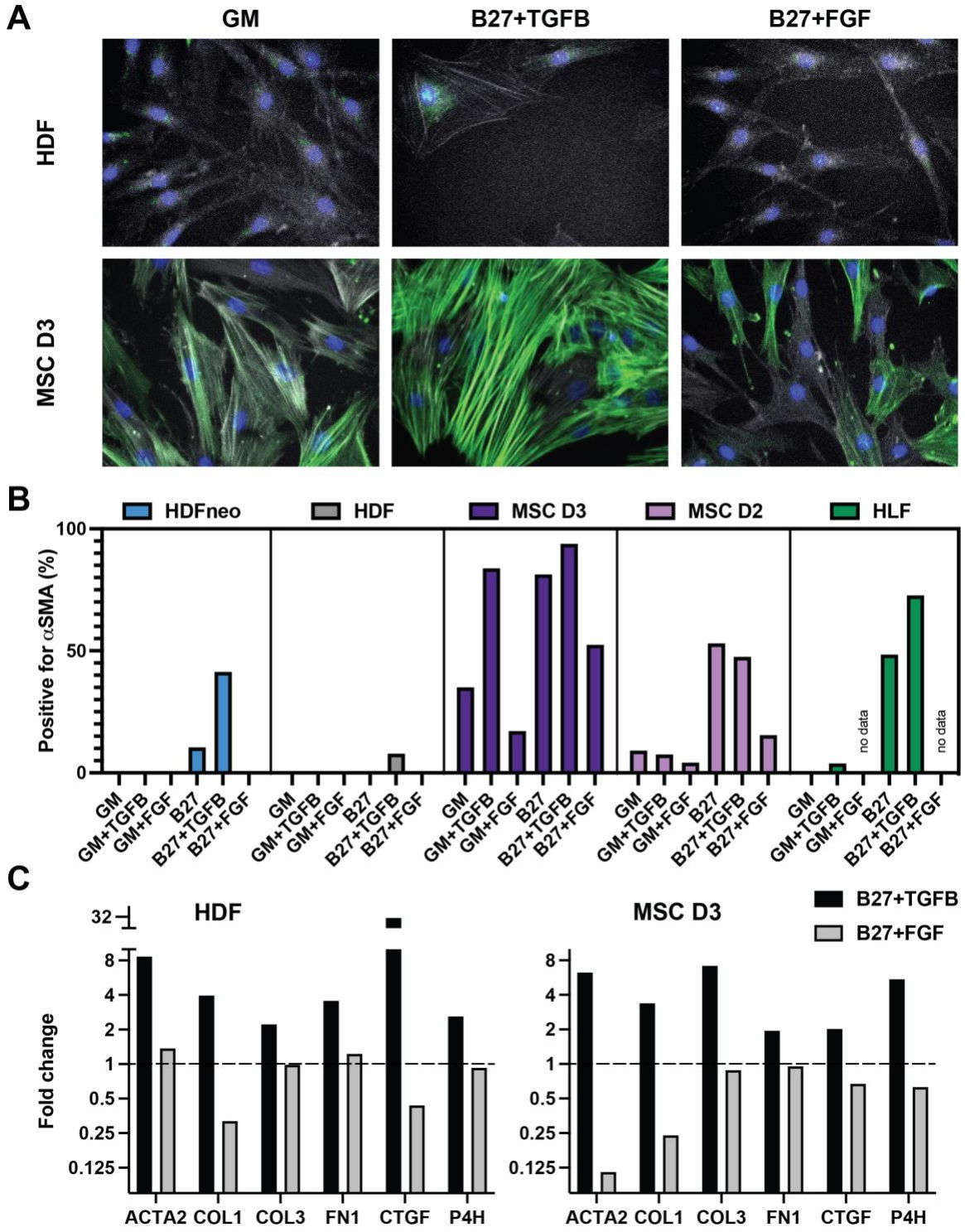


**Figure 4.3: Fibroblast activation in standard cell culture.**

(A) Representative images of  $\alpha$ SMA (green) for HDF and MSC in GM, B27+TGFB, and B27+FGF

after 4 days of stimulation. Cells are counterstained with phalloidin (white) and DAPI (blue). (B) Percent of cells that are positive for  $\alpha$ SMA stress fibers in several cell types. Quantification is of 10 randomly selected fields of view for each condition. (C) Relative expression of several genes after 4 days of stimulation with TGF $\beta$  or bFGF, shown as fold change over the GM condition for both HDF and MSC.

#### 4.4.4. Discussion

The data gathered in this pilot study suggest that different mesenchymal cell types have different inherent capacities for activation and myofibroblast differentiation. HDF, both adult and neonatal, display minimal activation in all conditions. HLF showed some basal activation in serum free media that can be further increased using TGF $\beta$ . Interestingly, the two MSC seemed to show donor-dependent capacities for activation. Cells from Donor 3 showed great activation in serum-free media and almost complete differentiation towards myofibroblasts when treated with TGF $\beta$ . Cells from Donor 2 had lower levels of activation that were apparently unaffected (or slightly lowered) by TGF $\beta$ .

Together, these data suggest that  $\alpha$ SMA expression increases upon differentiation to proto-myofibroblasts, although some cue is missing or insufficient for this  $\alpha$ SMA to be incorporated into stress fibers. For this reason, it is important that researchers wishing to study myofibroblasts do not rely upon Western blot or qPCR data alone. Additionally, researchers wishing to study

fibroblasts should take care to confirm that their culture conditions sufficiently prevent proto-myofibroblast activation.

## **CHAPTER FIVE: Perspectives**

### **5.1. PERSPECTIVES: Fibroblast clearance after laser ablation (Chapter 3)**

#### **5.1.1. Summary of findings**

Implementing a laser ablation system to injure microtissues has enabled us to study tissue repair in response to multiple injury types. We found that, compared to laceration, ablation created more damage to surrounding tissue. The presence of devitalized tissue delayed the onset of microtissue healing, as fibroblasts first had to navigate and remodel the damaged ECM. This process was dependent on dynamin and ROCK activity, and unaffected by blocking myosin II activity. TEM imaging revealed large intracellular vacuoles containing fibrillar ECM structures. These data together suggest a phagocytic or endocytic process that depends on actin polymerization, but not actomyosin contractility. Further investigation is needed to determine the precise mechanism of ECM uptake, or if multiple routes of ECM ingestion are active concurrently. Imbalances between ECM degradation and deposition are implicated in chronic wounding and fibrosis. Therefore, our model, which captures both processes in a 3D soft tissue, will be a valuable addition to the study of these diseases.

In addition to enabling study of ECM clearance by fibroblasts, the laser ablation system also enables study of tissue repair in a variety of experimental setups where mechanical laceration cannot be easily performed. For example, epithelial cells form tight junctions with their neighbors in microtissues, which make them

very challenging to injure mechanically. However, the laser can easily generate wounds in epithelial tissues. Furthermore, our laser ablation setup is very amenable to a multi-well plate format, and it reduces variability between users. Whereas ability to injure by microdissection knife and injury size are subjective to each user, ablation is a user-independent method of injury. The size of injury is controlled by laser energy, which can be objectively measured. In the next section, I will discuss a few of the remaining questions from our study of ECM clearance.

### **5.1.2. Remaining questions**

The most pressing question remaining from the study in Chapter 3 is regarding the mechanism of ECM uptake. There are three main processes by which collagen is ingested by cells: phagocytosis, macropinocytosis, and endocytosis.

Phagocytosis is an integrin dependent mechanism of extracellular material ingestion. For collagen phagocytosis,  $\beta 1$  integrins first bind collagen fibrils prior to ingestion (Segal et al., 2001). Collagen fibril phagocytosis also requires MT1-MMP (a membrane-bound MMP) to cleave fibrils before ingestion (H. Lee, Overall, McCulloch, & Sodek, 2006). Collagen-coated bead internalization does not require NMMIIA, but does require MLCK activity (Arora et al., 2008). It had been assumed that this phagocytic process was dependent on uPARAP, but a recent study has identified the uPARAP-independent mechanism of collagen

phagocytosis in vivo (Sprangers et al., 2017).

Macropinocytosis is the non-specific cell “drinking” of extracellular materials. This process requires Rac1 and dynamin-2 activity, as well as PI3K/AKT signaling (Koivusalo et al., 2010). Macropinocytosis is typically controlled via growth factor signaling, particularly EGF, although constitutive macropinocytosis has also been reported (Sprangers & Everts, 2019). Interestingly, in an inflammatory environment, macrophages switch from receptor-dependent phagocytosis to non-specific macropinocytosis (BoseDasgupta & Pieters, 2014).

The endocytic pathway for ingestion of soluble collagens (already cleaved by MMPs extracellularly) is dependent on collagen binding to uPARAP/Endo180 receptor. The receptor and bound material is then endocytosed in a clathrin-mediated process (Sprangers & Everts, 2019). A study in which several established cell-lines were examined revealed that all cells capable of efficient collagen uptake used the uPARAP method (Madsen et al., 2011).

In our model system, further experimentation is needed to determine the mechanism(s) by which ECM uptake occurs. In order to rule out the endocytic pathway, an inhibitor of genetic knockdown for the uPARAP/Endo 180 receptor could be used. If tissue clearance is not impaired, we can rule out the endocytic pathway. However, distinguishing between phagocytosis and macropinocytosis is

more complicated. When considering either process alone, Rac1 activity is harnessed to alter the degree of ECM ingestion. Up- and down-regulation of Rac1 increased and decreased, respectively, both phagocytosis (Kim et al., 2017) and macropinocytosis (Koivusalo et al., 2010; Lin, Mintern, & Gleeson, 2020). However, as both processes are affected by altering Rac1 activity, this strategy does not enable independent study of either process. In order to inhibit only phagocytosis, the binding of  $\beta 1$  integrins to collagen could be blocked, However, as these integrins are necessary for fibroblast interaction with collagen beyond phagocytosis, this strategy is not ideal, as many other aspects of the microtissue repair process would be affected. Ideally, better methods to independently control macropinocytosis and phagocytosis will be developed and can then be adapted for mechanistic studies in our model.

Two remaining interesting questions are regarding the fates of compromised ECM and of apoptotic cells. Does ingested ECM undergo lysosomal digestion (Kjøller et al., 2004), or are the fibroblasts able to reuse or redirect any material to aid in building the provisional matrix? Recently, neutrophils have been shown to utilize pre-existing matrix for tissue repair (Fischer et al., 2022). If the cells in our system were able to use the cleared ECM similarly, this would provide a valuable system for studying ECM recycling. The last main question from our study is are fibroblasts able to ingest dead cells? Recent evidence in a dermal model shows that fibroblasts phagocytose dead cells and then activate towards a

myofibroblast phenotype (Romana-Souza, Chen, Leonardo, Chen, & DiPietro, 2021). However, in our system, the fibroblasts appear to move around dead cells, rather than ingesting them. Future work may investigate the factors regulating non-professional phagocytosis of dead cells, and why some fibroblasts perform this function whereas others do not.

### **5.1.3. Broader context**

To conclude these perspectives of the study presented in Chapter 3, I briefly place our work in a broader context. Clinically, novel strategies to improve wound healing are becoming increasingly necessary, as the prevalence of comorbidities associated with chronic wounds are on the rise. Historically, much focus has been placed on understanding and promoting reepithelialization of the epidermis. However, proper assembly of granulation tissue is crucial for reepithelialization. For this reason, biomimetic models that capture the 3D assembly of granulation tissue are an active area of wound healing research. Our model of stromal tissue repair is particularly useful in this context because it captures both clearance of ECM from the wound bed and provisional matrix assembly. The imbalance between these processes is implicated in several pathologic healing outcomes. Therefore, our model should prove useful for detailed study of the balance between ECM degradation and deposition in a 3D soft tissue.

## **5.2. PERSPECTIVES: Fibroblast type and ECM composition (Chapter 4)**

### **5.2.1. Summary of findings**

In order to increase clinical relevance, we aimed to alter our microtissue system to use primary human cells rather than mouse embryonic 3T3 cells. In this effort, I screened several human cell types from normal tissues: human lung fibroblasts (HLF), marrow-derived human stromal cells (MSC), and human dermal fibroblasts (HDF). Data generated by Anish Vasani for human cardiac fibroblasts (HCF) were also included. We found that each type of stromal cell had differing closure rates in the microtissues. HCF microtissues healed very quickly. MSC rates were similar to 3T3, and HDF were considerably slower. HLF mostly failed to heal, either stalling or tearing the wound larger. We also compared healing rates in microtissues composed of two distinct ages of HDF: neonatal (HDFneo) and adult HDF. HDFneo microtissues closed dramatically faster than did adult HDF microtissues. These data raise interesting questions about the differences between fibroblasts from different anatomical sites, as well as differences that occur in healing with age.

We next investigated the effect of ECM composition in microtissues on the healing rate post-injury. We found that presence of collagen III (10% of total collagen) accelerated closure rates of 3T3-laden microtissues. Addition of collagen IV did not affect the closure rate of microtissues, but did decrease the overall compaction of tissues during healing. While it is known that fetal and

neonatal skin contain more collagen III than adult skin, and that fetal skin heals without scarring, it is not known if the relationship between these observations is one of causality or simply correlation. Our microtissue platform can be used to further investigate the relationship between ECM composition and rate of provisional matrix assembly in an otherwise homogenous environment.

Lastly, we probed the biochemical activation of multiple stromal cell types in standard culture. We measured differentiation to myofibroblasts using  $\alpha$ SMA-positive stress fibers as our primary marker. We found that each cell type had differing degrees of basal activation in their respective growth medias. Culture in serum-free media increased the amount of activation in all cell types, either to proto-myofibroblast or myofibroblast phenotype. Addition of bFGF was sufficient to prevent this activation, and TGF $\beta$  further increased fibroblast activation.

Having a biochemical handle on activation enables future comparisons between fibroblasts and myofibroblasts in the microtissue platform.

### **5.2.2. Future directions**

The pilot experiments examined in Chapter 4 raise many interesting questions about stromal tissue repair and provide preliminary data to motivate future projects. Several of these questions were stated briefly in Chapter 4. Here, I will elaborate on a couple of these questions and future experiments that could be performed to begin to address these questions.

A broad question raised by Pilot Study 1: What drives the differences in tissue repair rates between different cell types in our model? There are several potential explanations for these differences, and likely multiple factors contribute to the observed differences in microtissue repair. One potential explanation is that each cell type has a different level of ECM protein production. As has been discussed, fibronectin is particularly important for the generation of provisional ECM (Sakar et al., 2016; Sottile & Hocking, 2002; Sottile et al., 2007). Preliminary Western Blot data generated by Anish Vasan suggests that the amount of fibronectin produced by the cells directly correlates with speed of wound closure. He compared HCF, neonatal HDF, and adult HDF and found that HCF closed wounds the quickest and had the highest fibronectin expression, followed by neonatal HDF, with adult HDF trailing behind. While these experiments need to be repeated in serum-controlled media, the data suggest a clear link between fibronectin expression level and rate of tissue repair. Future work should include quantification of fibronectin expression in each of the cell types used in this study. Additionally, the composition of the provisional matrix generated by each cell type should be characterized. Previous work has shown that mouse 3T3 fibroblasts repair microtissues with fibronectin (Sakar et al., 2016), but this observation has yet to be confirmed in humanized microtissues.

Another potential explanation for the differences in repair rates is differences in cellular contractility between cell types. The microtissue devices can be adapted

to quantify tissue level forces, and future experiments should incorporate these measurements. Additionally, traction force microscopy could be used to determine cell contractility at the single-cell level (Legant et al., 2010; Polacheck & Chen, 2016), and any differences between cell and tissue forces correlated with repair rates in the microtissues.

Myofibroblast differentiation affects both ECM production and cell contractility, which, as discussed above, may both contribute to differences in microtissue repair potential. As demonstrated in Pilot Study 3, stromal cells in culture display different amounts of myofibroblast activation. Therefore, comparative studies of microtissues composed of different cell sources should include an evaluation of myofibroblasts. As demonstrated by Kollmannsberger et. al., tissue tension in hydrogels can transiently cause myofibroblast activation (Kollmannsberger et al., 2018). It is currently unknown if this phenomenon occurs during tissue repair in our microtissues. In addition to characterizing mechanically-driven myofibroblast activation in the microtissues, this activation can be induced biochemically, as demonstrated in Pilot Study 3. This strategy can be used in order to investigate differences in the tissue repair process between fibroblasts and myofibroblasts. There is much interest in studying scar tissue in vitro, and the use of myofibroblasts in our microtissues may be a useful tool in this endeavor.

### **5.3. CONCLUSION**

In this dissertation, I have described the processes within physiological wound healing and the many cell players involved. In Chapter 2, I described *in vitro* strategies available to study the various phases of wound healing, with an emphasis on 3D biomimetic models. In this context, I introduced our model of stromal tissue repair, which relies on injury of engineered microtissues to capture the subsequent generation of a fibrous provisional matrix. In Chapter 3, we introduced an alternate method of injury, laser ablation, which resulted in wounds surrounded by damaged tissue. We demonstrated the clearance of damaged tissue by fibroblasts, and provided data that suggest fibroblasts are able to phagocytose ECM fibers during the tissue repair process. In Chapter 4, I explored a few factors that may affect tissue repair potential, including cell type, microtissue ECM composition, and myofibroblast activation. Lastly, I concluded with a discussion of remaining questions and future directions of this work.

As is the nature of scientific research, the work presented in this dissertation raised many more questions than it answered. It is my hope that others in my lab and in the field will continue to build on the model presented here to explore these questions, and that the study of wound healing will improve the treatments available and the quality of life for patients.

## **APPENDIX: Supplemental Movies**

### **Supplemental Movie 3.1: Closure of injured microtissues.**

Timelapses of microtissue closure following (top) knife injury, (middle) laser ablation at 532 nm, and (bottom) laser ablation at 1064 nm.

### **Supplemental Movie 3.2: Fiber clearance and breakage following laser ablation.**

Reflection microscopy timelapse imaging following (top) knife injury and (bottom) injury by laser ablation. Green: reflected light from 488 nm illumination. Blue: cell nuclei stained with Hoechst dye.

## REFERENCES

- Abazari, M., Ghaffari, A., Rashidzadeh, H., Badeleh, S. M., & Maleki, Y. (2022). A Systematic Review on Classification, Identification, and Healing Process of Burn Wound Healing. *International Journal of Lower Extremity Wounds*, 21(1), 18–30. <https://doi.org/10.1177/1534734620924857>
- Adra, S., Sun, T., MacNeil, S., Holcombe, M., & Smallwood, R. (2010). Development of a three dimensional multiscale computational model of the human epidermis. *PLoS ONE*, 5(1), e8511. <https://doi.org/10.1371/journal.pone.0008511>
- Amadeu, T. P., Coulomb, B., Desmouliere, A., & Costa, A. M. A. (2003). Cutaneous Wound Healing: Myofibroblastic Differentiation and in Vitro Models. *The International Journal of Lower Extremity Wounds*, 2(2), 60–68. <https://doi.org/10.1177/1534734603256155>
- Amyere, M., Payraastre, B., Krause, U., Van Der Smissen, P., Veithen, A., & Courtoy, P. J. (2000). Constitutive macropinocytosis in oncogene-transformed fibroblasts depends on sequential permanent activation of phosphoinositide 3-kinase and phospholipase C. *Molecular Biology of the Cell*, 11(10), 3453–3467. <https://doi.org/10.1091/mbc.11.10.3453>
- Ansell, D. M., Holden, K. A., & Hardman, M. J. (2012). Animal models of wound repair: Are they cutting it? *Experimental Dermatology*, 21(8), 581–585. <https://doi.org/10.1111/j.1600-0625.2012.01540.x>
- Aragona, M., Dekoninck, S., Rulands, S., Lenglez, S., Mascré, G., Simons, B. D., & Blanpain, C. (2017). Defining stem cell dynamics and migration during wound healing in mouse skin epidermis. *Nature Communications*, 8(1), 1–14. <https://doi.org/10.1038/ncomms14684>
- Arora, P. D., Conti, M. A., Ravid, S., Sacks, D. B., Kapus, A., Adelstein, R. S., ... McCulloch, C. A. (2008). Rap1 activation in collagen phagocytosis is dependent on nonmuscle myosin II-A. *Molecular Biology of the Cell*, 19(12), 5032–5046. <https://doi.org/10.1091/mbc.E08-04-0430>
- Aumailley, M. (2021). Laminins and interaction partners in the architecture of the basement membrane at the dermal-epidermal junction. *Experimental Dermatology*, 30(1), 17–24. <https://doi.org/10.1111/exd.14239>
- Balvan, J., Krizova, A., Gumulec, J., Raudenska, M., Sladek, Z., Sedlackova, M., ... Masarik, M. (2015). Multimodal holographic microscopy: Distinction between apoptosis and oncosis. *PLoS ONE*, 10(3), e0121674. <https://doi.org/10.1371/journal.pone.0121674>

- Barman, P. K., & Koh, T. J. (2020, June 26). Macrophage Dysregulation and Impaired Skin Wound Healing in Diabetes. *Frontiers in Cell and Developmental Biology*, 8, 528. <https://doi.org/10.3389/fcell.2020.00528>
- Baroni, A., Buommino, E., De Gregorio, V., Ruocco, E., Ruocco, V., & Wolf, R. (2012). Structure and function of the epidermis related to barrier properties. *Clinics in Dermatology*, 30(3), 257–262. <https://doi.org/10.1016/j.clindermatol.2011.08.007>
- Bechetoille, N., Dezutter-Dambuyant, C., Damour, O., André, V., Orly, I., & Perrier, E. (2007). Effects of solar ultraviolet radiation on engineered human skin equivalent containing both langerhans cells and dermal dendritic cells. *Tissue Engineering*, 13(11), 2667–2679. <https://doi.org/10.1089/ten.2006.0405>
- Bell, E., Ivarsson, B., & Merrill, C. (1979). Production of a tissue-like structure by contraction of collagen lattices by human fibroblasts of different proliferative potential in vitro. *Proceedings of the National Academy of Sciences of the United States of America*, 76(3), 1274–1278. <https://doi.org/10.1073/PNAS.76.3.1274>
- Bereiter-Hahn, J. (1986). Epidermal Cell Migration and Wound Repair. In *Biology of the Integument* (pp. 443–471). Springer, Berlin, Heidelberg. [https://doi.org/10.1007/978-3-662-00989-5\\_23](https://doi.org/10.1007/978-3-662-00989-5_23)
- Bergmeier, V., Etich, J., Pitzler, L., Frie, C., Koch, M., Fischer, M., ... Brachvogel, B. (2018). Identification of a myofibroblast-specific expression signature in skin wounds. *Matrix Biology*, 65, 59–74. <https://doi.org/10.1016/j.matbio.2017.07.005>
- Biglari, S., Le, T. Y. L., Tan, R. P., Wise, S. G., Zambon, A., Codolo, G., ... Dehghani, F. (2019). Simulating Inflammation in a Wound Microenvironment Using a Dermal Wound-on-a-Chip Model. *Advanced Healthcare Materials*, 8(1), 1801307. <https://doi.org/10.1002/adhm.201801307>
- Bose, P., Eyckmans, J., Nguyen, T. D., Chen, C. S., & Reich, D. H. (2019). Effects of Geometry on the Mechanics and Alignment of Three-Dimensional Engineered Microtissues. *ACS Biomaterials Science and Engineering*, 5(8), 3843–3855. <https://doi.org/10.1021/acsbiomaterials.8b01183>
- BoseDasgupta, S., & Pieters, J. (2014). Inflammatory Stimuli Reprogram Macrophage Phagocytosis to Macropinocytosis for the Rapid Elimination of Pathogens. *PLoS Pathogens*, 10(1), e1003879. <https://doi.org/10.1371/journal.ppat.1003879>

- Boudaoud, A., Burian, A., Borowska-Wykręt, D., Uyttewaal, M., Wrzalik, R., Kwiatkowska, D., & Hamant, O. (2014). FibrilTool, an ImageJ plug-in to quantify fibrillar structures in raw microscopy images. *Nature Protocols*, *9*(2), 457–463. <https://doi.org/10.1038/nprot.2014.024>
- Braun, K. M., & Sandgren, E. P. (1998). Liver disease and compensatory growth: Unexpected lessons from genetically altered mice. *International Journal of Developmental Biology*, *42*(7), 935–942. <https://doi.org/10.1387/IJDB.9853824>
- Breuss, J. M., Gallo, J., DeLisser, H. M., Klimanskaya, I. V., Folkessons, H. G., Pittet, J. F., ... Pytela, R. (1995). Expression of the  $\beta 6$  integrin subunit in development, neoplasia and tissue repair suggests a role in epithelial remodeling. *Journal of Cell Science*, *108*(6), 2241–2251. <https://doi.org/10.1242/jcs.108.6.2241>
- Broughton, G., Janis, J. E., & Attinger, C. E. (2006, June). The basic science of wound healing. *Plastic and Reconstructive Surgery*, *117*(7S), 12S–34S. <https://doi.org/10.1097/01.prs.0000225430.42531.c2>
- Buck, R. C. (1979). Cell migration in repair of mouse corneal epithelium. *Investigative Ophthalmology and Visual Science*, *18*(8), 767–784.
- Buganza Tepole, A., & Kuhl, E. (2013, January 11). Systems-based approaches toward wound healing. *Pediatric Research*, *73*, 553–563. <https://doi.org/10.1038/pr.2013.3>
- Butler, P. D., Ly, D. P., Longaker, M. T., & Yang, G. P. (2008). Use of organotypic coculture to study keloid biology. *American Journal of Surgery*, *195*(2), 144–148. <https://doi.org/10.1016/j.amjsurg.2007.10.003>
- Caley, M. P., Martins, V. L. C., & O'Toole, E. A. (2015). Metalloproteinases and Wound Healing. *Advances in Wound Care*, *4*(4), 225–234. <https://doi.org/10.1089/wound.2014.0581>
- Cañedo-Dorantes, L., & Cañedo-Ayala, M. (2019). Skin acute wound healing: A comprehensive review. *International Journal of Inflammation*, *2019*, 3706315. <https://doi.org/10.1155/2019/3706315>
- Carlson, M. A., & Longaker, M. T. (2004, March 1). The fibroblast-populated collagen matrix as a model of wound healing: A review of the evidence. *Wound Repair and Regeneration*, *12*(2), 134–147. <https://doi.org/10.1111/j.1067-1927.2004.012208.x>

- Chau, D. Y. S., Johnson, C., Macneil, S., Haycock, J. W., & Ghaemmaghami, A. M. (2013). The development of a 3D immunocompetent model of human skin. *Biofabrication*, 5(3), 035011. <https://doi.org/10.1088/1758-5082/5/3/035011>
- Chen, H., Shi, R., Luo, B., Yang, X., Qiu, L., Xiong, J., ... Wu, Y. (2015). Macrophage peroxisome proliferator-activated receptor B deficiency delays skin wound healing through impairing apoptotic cell clearance in mice. *Cell Death and Disease*, 6(1), e1597–e1597. <https://doi.org/10.1038/cddis.2014.544>
- Cheung, D. T., Tong, D., Perelman, N., Ertl, D., & Nimni, M. E. (1990). Mechanism of crosslinking of proteins by glutaraldehyde IV: In vitro and in vivo stability of a crosslinked collagen matrix. *Connective Tissue Research*, 25(1), 27–34. <https://doi.org/10.3109/03008209009009810>
- Chung, E., Choi, H., Lim, J. E., & Son, Y. (2014). Development of skin inflammation test model by co-culture of reconstituted 3D skin and RAW264.7 cells. *Tissue Engineering and Regenerative Medicine*, 11(1), 87–92. <https://doi.org/10.1007/s13770-013-1113-x>
- Clark, R. A. F. (1993). Basics of Cutaneous Wound Repair. *The Journal of Dermatologic Surgery and Oncology*, 19(8), 693–706. <https://doi.org/10.1111/j.1524-4725.1993.tb00413.x>
- Corr, D. T., Gallant-Behm, C. L., Shrive, N. G., & Hart, D. A. (2009). Biomechanical behavior of scar tissue and uninjured skin in a porcine model. *Wound Repair and Regeneration*, 17(2), 250–259. <https://doi.org/10.1111/j.1524-475X.2009.00463.x>
- Costantini, E., Aielli, L., Serra, F., De Dominicis, L., Falasca, K., Di Giovanni, P., & Reale, M. (2022). Evaluation of Cell Migration and Cytokines Expression Changes under the Radiofrequency Electromagnetic Field on Wound Healing In Vitro Model. *International Journal of Molecular Sciences*, 23(4), 2205. <https://doi.org/10.3390/ijms23042205>
- Costantini, E., Sinjari, B., D'Angelo, C., Murmura, G., Reale, M., & Caputi, S. (2019). Human gingival fibroblasts exposed to extremely low-frequency electromagnetic fields: In vitro model of wound-healing improvement. *International Journal of Molecular Sciences*, 20(9), 2108. <https://doi.org/10.3390/ijms20092108>
- Curtis, M. W., & Russell, B. (2009). Cardiac Tissue Engineering. *Journal of Cardiovascular Nursing*, 24(2), 87–92. <https://doi.org/10.1097/01.JCN.0000343562.06614.49>

- Cushing, M. C., Mariner, P. D., Liao, J.-T., Sims, E. A., & Anseth, K. S. (2008). Fibroblast growth factor represses Smad-mediated myofibroblast activation in aortic valvular interstitial cells. *The FASEB Journal*, 22(6), 1769. <https://doi.org/10.1096/FJ.07-087627>
- Darby, I. A., Laverdet, B., Bonté, F., & Desmoulière, A. (2014, November 6). Fibroblasts and myofibroblasts in wound healing. *Clinical, Cosmetic and Investigational Dermatology*, 7, 301–311. <https://doi.org/10.2147/CCID.S50046>
- Das, S. L., Bose, P., Lejeune, E., Reich, D. H., Chen, C., & Eyckmans, J. (2021). Extracellular Matrix Alignment Directs Provisional Matrix Assembly and Three Dimensional Fibrous Tissue Closure. *Tissue Engineering - Part A*, 27(23–24), 1447–1457. <https://doi.org/10.1089/ten.tea.2020.0332>
- Diehl, A. M., & Rai, R. M. (1996). Regulation of signal transduction during liver regeneration. *The FASEB Journal*, 10(2), 215–227. <https://doi.org/10.1096/fasebj.10.2.8641555>
- Doyle, A. D., Carvajal, N., Jin, A., Matsumoto, K., & Yamada, K. M. (2015). Local 3D matrix microenvironment regulates cell migration through spatiotemporal dynamics of contractility-dependent adhesions. *Nature Communications*, 6(1), 1–15. <https://doi.org/10.1038/ncomms9720>
- Doyle, A. D., Petrie, R. J., Kutys, M. L., & Yamada, K. M. (2013, October 1). Dimensions in cell migration. *Current Opinion in Cell Biology*, 25(5), 642–649. <https://doi.org/10.1016/j.ceb.2013.06.004>
- Driskell, R. R., & Watt, F. M. (2015, February 1). Understanding fibroblast heterogeneity in the skin. *Trends in Cell Biology*, 25(2), 92–99. <https://doi.org/10.1016/j.tcb.2014.10.001>
- Enoch, S., & Leaper, D. J. (2008). Basic science of wound healing. *Surgery*, 26(2), 31–37. <https://doi.org/10.1016/j.mpsur.2007.11.005>
- Estève, D., Boulet, N., Belles, C., Zakaroff-Girard, A., Decaunes, P., Briot, A., ... Galitzky, J. (2019). Lobular architecture of human adipose tissue defines the niche and fate of progenitor cells. *Nature Communications*, 10(1), 1–16. <https://doi.org/10.1038/s41467-019-09992-3>
- Falabella, A. F. (2006). Debridement and wound bed preparation. *Dermatologic Therapy*, 19(6), 317–325. <https://doi.org/10.1111/j.1529-8019.2006.00090.x>
- Ferguson, M. W. J., & O’Kane, S. (2004). Scar-free healing: from embryonic mechanisms to adult therapeutic intervention. *Philosophical Transactions of*

- the Royal Society B: Biological Sciences*, 359(1445), 839–850.  
<https://doi.org/10.1098/rstb.2004.1475>
- Fetz, A. E., Radic, M. Z., & Bowlin, G. L. (2021, April 1). Neutrophils in Biomaterial-Guided Tissue Regeneration: Matrix Reprogramming for Angiogenesis. *Tissue Engineering - Part B: Reviews*, 27(2), 95–106.  
<https://doi.org/10.1089/ten.teb.2020.0028>
- Fischer, A., Wannemacher, J., Christ, S., Koopmans, T., Kadri, S., Zhao, J., ... Rinkevich, Y. (2022). Neutrophils direct preexisting matrix to initiate repair in damaged tissues. *Nature Immunology*, 23(4), 518–531.  
<https://doi.org/10.1038/s41590-022-01166-6>
- Frahs, S. M., Oxford, J. T., Neumann, E. E., Brown, R. J., Keller-Peck, C. R., Pu, X., & Lujan, T. J. (2018). Extracellular Matrix Expression and Production in Fibroblast-Collagen Gels: Towards an In Vitro Model for Ligament Wound Healing. *Annals of Biomedical Engineering*, 46(11), 1882–1895.  
<https://doi.org/10.1007/s10439-018-2064-0>
- Gabbiani, G. (2003, July 1). The myofibroblast in wound healing and fibrocontractive diseases. *Journal of Pathology*, 200(4), 500–503  
<https://doi.org/10.1002/path.1427>
- Galiano, R. D., Michaels V, J., Dobryansky, M., Levine, J. P., & Gurtner, G. C. (2004). Quantitative and reproducible murine model of excisional wound healing. *Wound Repair and Regeneration*, 12(4), 485–492.  
<https://doi.org/10.1111/j.1067-1927.2004.12404.x>
- Geer, D. J., Swartz, D. D., & Andreadis, S. T. (2002). Fibrin promotes migration in a three-dimensional in vitro model of wound regeneration. *Tissue Engineering*, 8(5), 787–798. <https://doi.org/10.1089/10763270260424141>
- Ghibaudo, M., Trichet, L., Le Digabel, J., Richert, A., Hersen, P., & Ladoux, B. (2009). Substrate topography induces a crossover from 2D to 3D behavior in fibroblast migration. *Biophysical Journal*, 97(1), 357–368.  
<https://doi.org/10.1016/j.bpj.2009.04.024>
- Gibbins, J. R. (1978). Epithelial migration in organ culture. A morphological and time lapse cinematographic analysis of migrating stratified squamous epithelium. *Pathology*, 10(3), 207–218.  
<https://doi.org/10.3109/00313027809063503>
- Gold, E. S., Underhill, D. M., Morrissette, N. S., Guo, J., McNiven, M. A., & Aderem, A. (1999). Dynamin 2 is required for phagocytosis in macrophages. *Journal of Experimental Medicine*, 190(12), 1849–1856.

<https://doi.org/10.1084/jem.190.12.1849>

Gosain, A., & DiPietro, L. A. (2004, March). Aging and Wound Healing. *World Journal of Surgery*, 28, 321–326. <https://doi.org/10.1007/s00268-003-7397-6>

Gouzos, M., Ramezanpour, M., Bassiouni, A., Psaltis, A. J., Wormald, P. J., & Vreugde, S. (2020). Antibiotics Affect ROS Production and Fibroblast Migration in an In-vitro Model of Sinonasal Wound Healing. *Frontiers in Cellular and Infection Microbiology*, 10, 110. <https://doi.org/10.3389/fcimb.2020.00110>

Grambow, E., Sorg, H., Sorg, C. G. G., & Strüder, D. (2021). Experimental Models to Study Skin Wound Healing with a Focus on Angiogenesis. *Medical Sciences*, 9(3), 55. <https://doi.org/10.3390/medsci9030055>

Grinnell, F. (2003, May 1). Fibroblast biology in three-dimensional collagen matrices. *Trends in Cell Biology*, 13(5), 264–269. [https://doi.org/10.1016/S0962-8924\(03\)00057-6](https://doi.org/10.1016/S0962-8924(03)00057-6)

Grinnell, F., B. Rocha, L., Iucu, C., Rhee, S., & Jiang, H. (2006). Nested collagen matrices: A new model to study migration of human fibroblast populations in three dimensions. *Experimental Cell Research*, 312(1), 86–94. <https://doi.org/10.1016/j.yexcr.2005.10.001>

Guerra, A., Belinha, J., & Jorge, R. N. (2018, December 14). Modelling skin wound healing angiogenesis: A review. *Journal of Theoretical Biology*, 459, 1–17. <https://doi.org/10.1016/j.jtbi.2018.09.020>

Gurtner, G. C., Werner, S., Barrandon, Y., & Longaker, M. T. (2008). Wound repair and regeneration. *Nature*, 453(7193), 314–321. <https://doi.org/10.1038/nature07039>

Gutierrez, E., Petrich, B. G., Shattil, S. J., Ginsberg, M. H., Groisman, A., & Kasirer-Friede, A. (2008). Microfluidic devices for studies of shear-dependent platelet adhesion. *Lab on a Chip*, 8(9), 1486–1495. <https://doi.org/10.1039/b804795b>

Hakkinen, K. M., Harunaga, J. S., Doyle, A. D., & Yamada, K. M. (2011). Direct comparisons of the morphology, migration, cell adhesions, and actin cytoskeleton of fibroblasts in four different three-dimensional extracellular matrices. *Tissue Engineering - Part A*, 17(5–6), 713–724. <https://doi.org/10.1089/ten.tea.2010.0273>

Häkkinen, L., Larjava, H., & Koivisto, L. (2011). Granulation tissue formation and remodeling. *Endodontic Topics*, 24(1), 94–129.

<https://doi.org/10.1111/ETP.12008>

- Han, G., & Ceilley, R. (2017, March 1). Chronic Wound Healing: A Review of Current Management and Treatments. *Advances in Therapy*, 34, 599–610. <https://doi.org/10.1007/s12325-017-0478-y>
- Hansen, R. R., Wufsus, A. R., Barton, S. T., Onasoga, A. A., Johnson-Paben, R. M., & Neeves, K. B. (2013). High content evaluation of shear dependent platelet function in a microfluidic flow assay. *Annals of Biomedical Engineering*, 41(2), 250–262. <https://doi.org/10.1007/s10439-012-0658-5>
- Hasan, A., Khattab, A., Islam, M. A., Hweij, K. A., Zeitouny, J., Waters, R., ... Paul, A. (2015, November 1). Injectable Hydrogels for Cardiac Tissue Repair after Myocardial Infarction. *Advanced Science*, 2(11), 1500122. <https://doi.org/10.1002/advs.201500122>
- Hell, E., & Lawrence, J. C. (1979). The initiation of epidermal wound healing in cuts and burns. *British Journal of Experimental Pathology*, 60(2), 171–179.
- Hesketh, M., Sahin, K. B., West, Z. E., & Murray, R. Z. (2017, July 17). Macrophage phenotypes regulate scar formation and chronic wound healing. *International Journal of Molecular Sciences*, 18(7), 1545. <https://doi.org/10.3390/ijms18071545>
- Hinz, B., Celetta, G., Tomasek, J. J., Gabbiani, G., & Chaponnier, C. (2001). Alpha-Smooth Muscle Actin Expression Upregulates Fibroblast Contractile Activity. *Molecular Biology of the Cell*, 12(9), 2730–2741. <https://doi.org/10.1091/mbc.12.9.2730>
- Hinz, B., McCulloch, C. A., & Coelho, N. M. (2019, June 1). Mechanical regulation of myofibroblast phenoconversion and collagen contraction. *Experimental Cell Research*, 379(1), 119–128. <https://doi.org/10.1016/j.yexcr.2019.03.027>
- Hollander, D. A., Erli, H. J., Theisen, A., Falk, S., Kreck, T., & Müller, S. (2003). Standardized qualitative evaluation of scar tissue properties in an animal wound healing model. *Wound Repair and Regeneration*, 11(2), 150–157. <https://doi.org/10.1046/j.1524-475X.2003.11212.x>
- Hollinsky, C., & Sandberg, S. (2007). Measurement of the tensile strength of the ventral abdominal wall in comparison with scar tissue. *Clinical Biomechanics*, 22(1), 88–92. <https://doi.org/10.1016/j.clinbiomech.2006.06.002>

- Hosseini, M., Koehler, K. R., & Shafiee, A. (2022, November 1). Biofabrication of Human Skin with Its Appendages. *Advanced Healthcare Materials*, 11(22), 2201626. <https://doi.org/10.1002/adhm.202201626>
- Hu, J. J., Liu, Y. C., Chen, G. W., Wang, M. X., & Lee, P. Y. (2013). Development of fibroblast-seeded collagen gels under planar biaxial mechanical constraints: A biomechanical study. *Biomechanics and Modeling in Mechanobiology*, 12(5), 849–868. <https://doi.org/10.1007/s10237-012-0448-x>
- Humphrey, J. D., Dufresne, E. R., & Schwartz, M. A. (2014, October 22). Mechanotransduction and extracellular matrix homeostasis. *Nature Reviews Molecular Cell Biology*, 15, 802–812. <https://doi.org/10.1038/nrm3896>
- Ilijas, J. D., Röhl, J., McGovern, J. A., Moromizato, K. H., Parker, T. J., & Cuttle, L. (2021). A human skin equivalent burn model to study the effect of a nanocrystalline silver dressing on wound healing. *Burns*, 47(2), 417–429. <https://doi.org/10.1016/J.BURNS.2020.07.007>
- Illouz, Y. G. (1990). Study of Subcutaneous Fat. *Aesthetic Plastic Surgery*, 14, 165–177.
- John, J., Thom Quinlan, A., Silvestri, C., & Billiar, K. (2010, March 10). Boundary stiffness regulates fibroblast behavior in collagen gels. *Annals of Biomedical Engineering*, 38, 658–673. <https://doi.org/10.1007/s10439-009-9856-1>
- Jorgensen, S. N., & Sanders, J. R. (2016, September 1). Mathematical models of wound healing and closure: a comprehensive review. *Medical & Biological Engineering & Computing*, 54, 1297–1316. <https://doi.org/10.1007/s11517-015-1435-z>
- Kan, N. G., Junghans, D., & Belmonte, J. C. I. (2009). Compensatory growth mechanisms regulated by BMP and FGF signaling mediate liver regeneration in zebrafish after partial hepatectomy. *The FASEB Journal*, 23(10), 3516–3525. <https://doi.org/10.1096/fj.09-131730>
- Kapetanaki, M. G., Mora, A. L., & Rojas, M. (2013, January 1). Influence of age on wound healing and fibrosis. *Journal of Pathology*, 229(2), 310–322. <https://doi.org/10.1002/path.4122>
- Karamichos, D., Lakshman, N., & Petroll, W. M. (2009). An experimental model for assessing fibroblast migration in 3-D collagen matrices. *Cell Motility and the Cytoskeleton*, 66(1), 1–9. <https://doi.org/10.1002/CM.20326>

- Kasugai, S., Suzuki, S., Shibata, S., Yasui, S., Amano, H., & Ogura, H. (1990). Measurements of the isometric contractile forces generated by dog periodontal ligament fibroblasts in vitro. *Archives of Oral Biology*, *35*(8), 597–601. [https://doi.org/10.1016/0003-9969\(90\)90025-6](https://doi.org/10.1016/0003-9969(90)90025-6)
- Kaur, T., Dumoga, S., Koul, V., & Singh, N. (2020). Modulating neutrophil extracellular traps for wound healing. *Biomaterials Science*, *8*(11), 3212–3223. <https://doi.org/10.1039/d0bm00355g>
- Kawasumi, A., Sagawa, N., Hayashi, S., Yokoyama, H., & Tamura, K. (2012). Wound Healing in Mammals and Amphibians: Toward Limb Regeneration in Mammals. In: Heber-Katz, E., Stocum, D. (eds.) *New Perspectives in Regeneration. Current Topics in Microbiology and Immunology*, vol. 367. (pp. 33–49). Springer, Berlin, Heidelberg. [https://doi.org/10.1007/82\\_2012\\_305](https://doi.org/10.1007/82_2012_305)
- Kim, S. Y., Kim, S., Bae, D. J., Park, S. Y., Lee, G. Y., Park, G. M., & Kim, I. S. (2017). Coordinated balance of Rac1 and RhoA plays key roles in determining phagocytic appetite. *PLoS ONE*, *12*(4), e0174603. <https://doi.org/10.1371/journal.pone.0174603>
- Kis, K., Liu, X., & Hagood, J. S. (2011). Myofibroblast differentiation and survival in fibrotic disease. *Expert Reviews in Molecular Medicine*, *13*, e27. <https://doi.org/10.1017/S1462399411001967>
- Kjøller, L., Engelholm, L. H., Høyer-Hansen, M., Danø, K., Bugge, T. H., & Behrendt, N. (2004). uPARAP/endo180 directs lysosomal delivery and degradation of collagen IV. *Experimental Cell Research*, *293*(1), 106–116. <https://doi.org/10.1016/j.yexcr.2003.10.008>
- Klingberg, F., Hinz, B., & White, E. S. (2013, January 1). The myofibroblast matrix: Implications for tissue repair and fibrosis. *Journal of Pathology*, *229*(2), 298–309. <https://doi.org/10.1002/path.4104>
- Koivusalo, M., Welch, C., Hayashi, H., Scott, C. C., Kim, M., Alexander, T., ... Grinstein, S. (2010). Amiloride inhibits macropinocytosis by lowering submembranous pH and preventing Rac1 and Cdc42 signaling. *Journal of Cell Biology*, *188*(4), 547–563. <https://doi.org/10.1083/jcb.200908086>
- Kollmannsberger, P., Bidan, C. M., Dunlop, J. W. C., Fratzl, P., & Vogel, V. (2018). Tensile forces drive a reversible fibroblast-to-myofibroblast transition during tissue growth in engineered clefts. *Science Advances*, *4*(1), eaao4881. <https://doi.org/10.1126/sciadv.aao4881>

- Korosec, A., Frech, S., Gesslbauer, B., Vierhapper, M., Radtke, C., Petzelbauer, P., & Lichtenberger, B. M. (2019). Lineage Identity and Location within the Dermis Determine the Function of Papillary and Reticular Fibroblasts in Human Skin. *Journal of Investigative Dermatology*, *139*(2), 342–351. <https://doi.org/10.1016/j.jid.2018.07.033>
- Kosten, I. J., Spiekstra, S. W., de Gruijl, T. D., & Gibbs, S. (2015). MUTZ-3 derived Langerhans cells in human skin equivalents show differential migration and phenotypic plasticity after allergen or irritant exposure. *Toxicology and Applied Pharmacology*, *287*(1), 35–42. <https://doi.org/10.1016/j.taap.2015.05.017>
- Krawczyk, W. S. (1971). A pattern of epidermal cell migration during wound healing. *Journal of Cell Biology*, *49*(2), 247–263. <https://doi.org/10.1083/jcb.49.2.247>
- Kreimendahl, F., Marquardt, Y., Apel, C., Bartneck, M., Zwadlo-Klarwasser, G., Hepp, J., ... Baron, J. M. (2019). Macrophages significantly enhance wound healing in a vascularized skin model. *Journal of Biomedical Materials Research Part A*, *107*(6), 1340–1350. <https://doi.org/10.1002/JBM.A.36648>
- Krieg, T., & Aumailley, M. (2011, August 1). The extracellular matrix of the dermis: Flexible structures with dynamic functions. *Experimental Dermatology*, *20*(8), 689–695. <https://doi.org/10.1111/j.1600-0625.2011.01313.x>
- Kühbacher, A., Henkel, H., Stevens, P., Grumaz, C., Finkelmeier, D., Burger-Kentischer, A., ... Rupp, S. (2017). Central Role for Dermal Fibroblasts in Skin Model Protection against *Candida albicans*. *The Journal of Infectious Diseases*, *215*(11), 1742–1752. <https://doi.org/10.1093/INFDIS/JIX153>
- Kuhl, E., & Steinmann, P. (2004). Computational modeling of healing: An application of the material force method. *Biomechanics and Modeling in Mechanobiology*, *2*(4), 187–203. <https://doi.org/10.1007/S10237-003-0034-3>
- Kunz-Schughart, L. A., Wenninger, S., Neumeier, T., Seidl, P., & Knuechel, R. (2003). Three-dimensional tissue structure affects sensitivity of fibroblasts to TGF- $\beta$ 1. *American Journal of Physiology - Cell Physiology*, *284*(1), C209–C219. <https://doi.org/10.1152/ajpcell.00557.2001>
- Laplante, A. F., Germain, L., Auger, F. A., & Moulin, V. (2001). Mechanisms of wound reepithelialization: hints from a tissue-engineered reconstructed skin to long-standing questions. *The FASEB Journal*, *15*(13), 2377–2389. <https://doi.org/10.1096/fj.01-0250com>

- Laubach, V., Zöller, N., Rossberg, M., Görg, K., Kippenberger, S., Bereiter-Hahn, J., ... Bernd, A. (2011). Integration of Langerhans-like cells into a human skin equivalent. *Archives of Dermatological Research*, *303*(2), 135–139. <https://doi.org/10.1007/s00403-010-1092-x>
- Lee, H., Overall, C. M., McCulloch, C. A., & Sodek, J. (2006). A critical role for the membrane-type 1 matrix metalloproteinase in collagen phagocytosis. *Molecular Biology of the Cell*, *17*(11), 4812–4826. <https://doi.org/10.1091/mbc.E06-06-0486>
- Lee, J., Wang, Y. L., Ren, F., & Lele, T. P. (2010). Stamp wound assay for studying coupled cell migration and cell debris clearance. *Langmuir*, *26*(22), 16672–16676. <https://doi.org/10.1021/la103542y>
- Lee, W., Sodek, J., & McCulloch, C. A. G. (1996). Role of integrins in regulation of collagen phagocytosis by human fibroblasts. *Journal of Cellular Physiology*, *168*(3), 695–704. [https://doi.org/10.1002/\(SICI\)1097-4652\(199609\)168:3<695::AID-JCP22>3.0.CO;2-X](https://doi.org/10.1002/(SICI)1097-4652(199609)168:3<695::AID-JCP22>3.0.CO;2-X)
- Legant, W. R., Miller, J. S., Blakely, B. L., Cohen, D. M., Genin, G. M., & Chen, C. S. (2010). Measurement of mechanical tractions exerted by cells in three-dimensional matrices. *Nature Methods*, *7*(12), 969–971. <https://doi.org/10.1038/nmeth.1531>
- Legant, W. R., Pathak, A., Yang, M. T., Deshpande, V. S., McMeeking, R. M., & Chen, C. S. (2009). Microfabricated tissue gauges to measure and manipulate forces from 3D microtissues. *Proceedings of the National Academy of Sciences of the United States of America*, *106*(25), 10097–10102. <https://doi.org/10.1073/pnas.0900174106>
- Liang, C. C., Park, A. Y., & Guan, J. L. (2007). In vitro scratch assay: A convenient and inexpensive method for analysis of cell migration in vitro. *Nature Protocols*, *2*(2), 329–333. <https://doi.org/10.1038/nprot.2007.30>
- Lin, X. P., Mintern, J. D., & Gleeson, P. A. (2020, August 3). Macropinocytosis in different cell types: Similarities and differences. *Membranes*, *10*(8), 177. <https://doi.org/10.3390/membranes10080177>
- Linde, N., Gutschalk, C. M., Hoffmann, C., Yilmaz, D., & Mueller, M. M. (2012). Integrating macrophages into organotypic co-cultures: A 3D in vitro model to study tumor-associated macrophages. *PLoS ONE*, *7*(7), e40058. <https://doi.org/10.1371/journal.pone.0040058>
- Liu, C., Rinderknecht, H., Histing, T., Kolbensschlag, J., Nussler, A. K., & Ehnert, S. (2022). Establishment of an In Vitro Scab Model for Investigating Different

- Phases of Wound Healing. *Bioengineering*, 9(5).  
<https://doi.org/10.3390/bioengineering9050191>
- Liu, K., Wiendels, M., Yuan, H., Ruan, C., & Kouwer, P. H. J. (2022, March 1). Cell-matrix reciprocity in 3D culture models with nonlinear elasticity. *Bioactive Materials*, 9, 316–331.  
<https://doi.org/10.1016/j.bioactmat.2021.08.002>
- Lo, D. D., Zimmermann, A. S., Nauta, A., Longaker, M. T., & Lorenz, H. P. (2012). Scarless fetal skin wound healing update. *Birth Defects Research Part C - Embryo Today: Reviews*, 96(3), 237–247.  
<https://doi.org/10.1002/bdrc.21018>
- Lo, E. H. (2008, May 7). A new penumbra: Transitioning from injury into repair after stroke. *Nature Medicine*, 14, 497–500. <https://doi.org/10.1038/nm1735>
- Loomis, T., Hu, L. Y., Wohlgemuth, R. P., Chellakudam, R. R., Muralidharan, P. D., & Smith, L. R. (2022). Matrix stiffness and architecture drive fibro-adipogenic progenitors' activation into myofibroblasts. *Scientific Reports*, 12(1), 1–15. <https://doi.org/10.1038/s41598-022-17852-2>
- Lorthoix, I., Simard, M., Morin, S., & Pouliot, R. (2019). Infiltration of T cells into a three-dimensional psoriatic skin model mimics pathological key features. *International Journal of Molecular Sciences*, 20(7), 1670.  
<https://doi.org/10.3390/ijms20071670>
- Madsen, D. H., Ingvarsen, S., Jørgensen, H. J., Melander, M. C., Kjølner, L., Moyer, A., ... Engelholm, L. H. (2011). The non-phagocytic route of collagen uptake: A distinct degradation pathway. *Journal of Biological Chemistry*, 286(30), 26996–27010.  
<https://doi.org/10.1074/JBC.M110.208033/ATTACHMENT/CC528A92-0FF2-4AE8-81EB-12805B543F3F/MMC1.PDF>
- Mailand, E., Li, B., Eyckmans, J., Bouklas, N., & Sakar, M. S. (2019). Surface and Bulk Stresses Drive Morphological Changes in Fibrous Microtissues. *Biophysical Journal*, 117(5), 975–986.  
<https://doi.org/10.1016/j.bpj.2019.07.041>
- Maione, A. G., Brudno, Y., Stojadinovic, O., Park, L. K., Smith, A., Tellechea, A., ... Garlick, J. A. (2015). Three-dimensional human tissue models that incorporate diabetic foot ulcer-derived fibroblasts mimic in vivo features of chronic wounds. *Tissue Engineering - Part C: Methods*, 21(5), 499–508.  
<https://doi.org/10.1089/ten.tec.2014.0414>

- Maione, A. G., Smith, A., Kashpur, O., Yanez, V., Knight, E., Mooney, D. J., ... Garlick, J. A. (2016). Altered ECM deposition by diabetic foot ulcer-derived fibroblasts implicates fibronectin in chronic wound repair. *Wound Repair and Regeneration*, 24(4), 630–643. <https://doi.org/10.1111/wrr.12437>
- Marquardt, Y., Amann, P. M., Heise, R., Czaja, K., Steiner, T., Merk, H. F., ... Baron, J. M. (2015). Characterization of a novel standardized human three-dimensional skin wound healing model using non-sequential fractional ultrapulsed CO2 laser treatments. *Lasers in Surgery and Medicine*, 47(3), 257–265. <https://doi.org/10.1002/lsm.22341>
- Martin, P. (1997). Wound healing - Aiming for perfect skin regeneration. *Science*, 276(5309), 75–81. <https://doi.org/10.1126/science.276.5309.75>
- Mastrullo, V., Cathery, W., Velliou, E., Madeddu, P., & Campagnolo, P. (2020, March 20). Angiogenesis in Tissue Engineering: As Nature Intended? *Frontiers in Bioengineering and Biotechnology*, 8, 188. <https://doi.org/10.3389/fbioe.2020.00188>
- McCulloch, C. A. G., & Knowles, G. C. (1993). Deficiencies in collagen phagocytosis by human fibroblasts in vitro: A mechanism for fibrosis? *Journal of Cellular Physiology*, 155(3), 461–471. <https://doi.org/10.1002/jcp.1041550305>
- Menke, N. B., Cain, J. W., Reynolds, A., Chan, D. M., Segal, R. A., Witten, T. M., ... Ward, K. R. (2010). An in silico approach to the analysis of acute wound healing. *Wound Repair and Regeneration*, 18(1), 105–113. <https://doi.org/10.1111/j.1524-475X.2009.00549.x>
- Menon, M. B., Ronkina, N., Schwermann, J., Kotlyarov, A., & Gaestel, M. (2009). Fluorescence-based quantitative scratch wound healing assay demonstrating the role of MAPKAPK-2/3 in fibroblast migration. *Cell Motility and the Cytoskeleton*, 66(12), 1041–1047. <https://doi.org/10.1002/cm.20418>
- Menon, R., Krzyszczyk, P., & Berthiaume, F. (2017). Pro-Resolution Potency of Resolvins D1, D2 and E1 on Neutrophil Migration and in Dermal Wound Healing. *Nano LIFE*, 07(01), 1750002. <https://doi.org/10.1142/s1793984417500027>
- Michalopoulos, G. K. (2013). Principles of liver regeneration and growth homeostasis. *Comprehensive Physiology*, 3(1), 485–513. <https://doi.org/10.1002/cphy.c120014>
- Miron-Mendoza, M., Lin, X., Ma, L., Ririe, P., & Petroll, W. M. (2012). Individual versus collective fibroblast spreading and migration: Regulation by matrix

- composition in 3D culture. *Experimental Eye Research*, 99(1), 36–44.  
<https://doi.org/10.1016/j.exer.2012.03.015>
- Miskolci, V., Squirrell, J., Rindy, J., Vincent, W., Sauer, J. D., Gibson, A., ... Huttenlocher, A. (2019). Distinct inflammatory and wound healing responses to complex caudal fin injuries of larval zebrafish. *ELife*, 8.  
<https://doi.org/10.7554/eLife.45976>
- Modo, M. (2019, November 7). Bioscaffold-Induced Brain Tissue Regeneration. *Frontiers in Neuroscience*, 13, 1156.  
<https://doi.org/10.3389/fnins.2019.01156>
- Monfared, G. S., Ertl, P., & Rothbauer, M. (2021, May 26). Microfluidic and lab-on-a-chip systems for cutaneous wound healing studies. *Pharmaceutics*, 13(6), 793. <https://doi.org/10.3390/pharmaceutics13060793>
- Monsaingeon, A., & Molimard, R. (1976). Wound healing: Comparison of healing rates of burn wounds and of excisional wounds. *European Surgical Research*, 8(4), 337–343. <https://doi.org/10.1159/000127878>
- Monsuur, H. N., Boink, M. A., Weijers, E. M., Roffel, S., Breetveld, M., Gefen, A., ... Gibbs, S. (2016). Methods to study differences in cell mobility during skin wound healing in vitro. *Journal of Biomechanics*, 49(8), 1381–1387.  
<https://doi.org/10.1016/j.jbiomech.2016.01.040>
- Moore, E. M., & West, J. L. (2019, February 15). Harnessing Macrophages for Vascularization in Tissue Engineering. *Annals of Biomedical Engineering*, 47, 354–365. <https://doi.org/10.1007/s10439-018-02170-4>
- Müller, G., Dörschel, K., & Kar, H. (1991). Biophysics of the photoablation process. *Lasers in Medical Science*, 6(3), 241–254.  
<https://doi.org/10.1007/BF02030877>
- Oda, D., Gown, A. M., Vande Berg, J. S., & Stern, R. (1990). Instability of the myofibroblast phenotype in culture. *Experimental and Molecular Pathology*, 52(2), 221–234. [https://doi.org/10.1016/0014-4800\(90\)90007-Z](https://doi.org/10.1016/0014-4800(90)90007-Z)
- Olsen, A. L., Bloomer, S. A., Chan, E. P., Gaça, M. D. A., Georges, P. C., Sackey, B., ... Wells, R. G. (2011). Hepatic stellate cells require a stiff environment for myofibroblastic differentiation. *American Journal of Physiology - Gastrointestinal and Liver Physiology*, 301(1), G110–G118.  
<https://doi.org/10.1152/ajpgi.00412.2010>
- Onursal, C., Dick, E., Angelidis, I., Schiller, H. B., & Staab-Weijnitz, C. A. (2021, May 20). Collagen Biosynthesis, Processing, and Maturation in Lung Ageing.

*Frontiers in Medicine*, 8, 593874. <https://doi.org/10.3389/fmed.2021.593874>

- Opneja, A., Kapoor, S., & Stavrou, E. X. (2019, July 1). Contribution of platelets, the coagulation and fibrinolytic systems to cutaneous wound healing. *Thrombosis Research*, 179, 56–63. <https://doi.org/10.1016/j.thromres.2019.05.001>
- Ouwehand, K., Spiekstra, S. W., Waaijman, T., Breetveld, M., Scheper, R. J., de Gruijl, T. D., & Gibbs, S. (2012). CCL5 and CCL20 mediate immigration of Langerhans cells into the epidermis of full thickness human skin equivalents. *European Journal of Cell Biology*, 91(10), 765–773. <https://doi.org/10.1016/j.ejcb.2012.06.004>
- Ouwehand, K., Spiekstra, S. W., Waaijman, T., Scheper, R. J., de Gruijl, T. D., & Gibbs, S. (2011). Technical Advance: Langerhans cells derived from a human cell line in a full-thickness skin equivalent undergo allergen-induced maturation and migration. *Journal of Leukocyte Biology*, 90(5), 1027–1033. <https://doi.org/10.1189/jlb.0610374>
- Pakshir, P., & Hinz, B. (2018). The big five in fibrosis: Macrophages, myofibroblasts, matrix, mechanics, and miscommunication. *Matrix Biology*, 68–69, 81–93. <https://doi.org/10.1016/j.matbio.2018.01.019>
- Park, E. J., Park, S. J., Kim, S., Lee, K., & Chang, J. (2018). Lung fibroblasts may play an important role in clearing apoptotic bodies of bronchial epithelial cells generated by exposure to PHMG-P-containing solution. *Toxicology Letters*, 286, 108–119. <https://doi.org/10.1016/j.toxlet.2018.01.003>
- Park, J. E., & Barbul, A. (2004). Understanding the role of immune regulation in wound healing. *American Journal of Surgery*, 187(5 SUPPL. 1), S11–S16. [https://doi.org/10.1016/S0002-9610\(03\)00296-4](https://doi.org/10.1016/S0002-9610(03)00296-4)
- Percival, N. J. (2002). Classification of Wounds and their Management. *Surgery (Oxford)*, 20(5), 114–117. <https://doi.org/10.1383/surg.20.5.114.14626>
- Pierce, M. C., Sheridan, R. L., Hyle Park, B., Cense, B., & De Boer, J. F. (2004). Collagen denaturation can be quantified in burned human skin using polarization-sensitive optical coherence tomography. *Burns*, 30(6), 511–517. <https://doi.org/10.1016/j.burns.2004.02.004>
- Plikus, M. V., Guerrero-Juarez, C. F., Ito, M., Li, Y. R., Dedhia, P. H., Zheng, Y., ... Cotsarelis, G. (2017). Regeneration of fat cells from myofibroblasts during wound healing. *Science*, 355(6326), 748–752. <https://doi.org/10.1126/science.aai8792>

- Ploeger, D. T., Hosper, N. A., Schipper, M., Koerts, J. A., De Rond, S., & Bank, R. A. (2013). Cell plasticity in wound healing: Paracrine factors of M1/ M2 polarized macrophages influence the phenotypical state of dermal fibroblasts. *Cell Communication and Signaling*, 11(1), 1–17. <https://doi.org/10.1186/1478-811X-11-29>
- Polacheck, W. J., & Chen, C. S. (2016). Measuring cell-generated forces: a guide to the available tools. *Nature Methods*, 13(5), 415–423. <https://doi.org/10.1038/nmeth.3834>
- Ponmozhi, J., Dhinakaran, S., Varga-medveczky, Z., Fónagy, K., Bors, L. A., Iván, K., & Erdő, F. (2021). Development of skin-on-a-chip platforms for different utilizations: Factors to be considered. *Micromachines*, 12(3), 294. <https://doi.org/10.3390/mi12030294>
- Porter, S. (2007). The role of the fibroblast in wound contraction and healing. *Wounds UK*, 3(1), 33–40. [https://www.woundsinternational.com/uploads/resources/content\\_9113.pdf](https://www.woundsinternational.com/uploads/resources/content_9113.pdf)
- Poujade, M., Grasland-Mongrain, E., Hertzog, A., Jouanneau, J., Chavrier, P., Ladoux, B., ... Silberzan, P. (2007). Collective migration of an epithelial monolayer in response to a model wound. *Proceedings of the National Academy of Sciences of the United States of America*, 104(41), 15988–15993. <https://doi.org/10.1073/pnas.0705062104>
- Poventud-Fuentes, I., Kwon, K. W., Seo, J., Tomaiuolo, M., Stalker, T. J., Brass, L. F., & Huh, D. (2021). A Human Vascular Injury-on-a-Chip Model of Hemostasis. *Small*, 17(15), 2004889. <https://doi.org/10.1002/sml.202004889>
- Praefcke, G. J. K., & McMahon, H. T. (2004, February). The dynamin superfamily: Universal membrane tubulation and fission molecules? *Nature Reviews. Molecular Cell Biology*, 5, 133–147. <https://doi.org/10.1038/nrm1313>
- Pupovac, A., Senturk, B., Griffoni, C., Maniura-Weber, K., Rottmar, M., & McArthur, S. L. (2018). Toward Immunocompetent 3D Skin Models. *Advanced Healthcare Materials*, 7(12), 1701405. <https://doi.org/10.1002/adhm.201701405>
- Quinlan, A. M. T., & Billiar, K. L. (2012). Investigating the role of substrate stiffness in the persistence of valvular interstitial cell activation. *Journal of Biomedical Materials Research - Part A*, 100 A(9), 2474–2482. <https://doi.org/10.1002/jbm.a.34162>

- Radhakrishnan, J., Krishnan, U. M., & Sethuraman, S. (2014, March 1). Hydrogel based injectable scaffolds for cardiac tissue regeneration. *Biotechnology Advances*, 32(2), 449–461. <https://doi.org/10.1016/j.biotechadv.2013.12.010>
- Radice, G. P. (1980). The spreading of epithelial cells during wound closure in *Xenopus* larvae. *Developmental Biology*, 76(1), 26–46. [https://doi.org/10.1016/0012-1606\(80\)90360-7](https://doi.org/10.1016/0012-1606(80)90360-7)
- Randall, M. J., Jüngel, A., Rimann, M., & Wuertz-Kozak, K. (2018, October 31). Advances in the biofabrication of 3D skin in vitro: Healthy and pathological models. *Frontiers in Bioengineering and Biotechnology*, 6, 154. <https://doi.org/10.3389/fbioe.2018.00154>
- Raziyeva, K., Kim, Y., Zharkinbekov, Z., Kassymbek, K., Jimi, S., & Saparov, A. (2021, May 8). Immunology of acute and chronic wound healing. *Biomolecules*, 11(5), 700. <https://doi.org/10.3390/biom11050700>
- Reddy, L. V. K., Murugan, D., Mullick, M., Begum Moghal, E. T., & Sen, D. (2019). Recent Approaches for Angiogenesis in Search of Successful Tissue Engineering and Regeneration. *Current Stem Cell Research & Therapy*, 15(2), 111–134. <https://doi.org/10.2174/1574888x14666191104151928>
- Rhee, S. (2009, December 31). Fibroblasts in three dimensional matrices: Cell migration and matrix remodeling. *Experimental and Molecular Medicine*, 41, 858–865. <https://doi.org/10.3858/emm.2009.41.12.096>
- Rippa, A. L., Kalabusheva, E. P., & Vorotelyak, E. A. (2019). Regeneration of Dermis: Scarring and Cells Involved. *Cells*, 8(6), 607. <https://doi.org/10.3390/CELLS8060607>
- Rittié, L. (2016, June 1). Cellular mechanisms of skin repair in humans and other mammals. *Journal of Cell Communication and Signaling*, 10, 103–120. <https://doi.org/10.1007/s12079-016-0330-1>
- Romana-Souza, B., Chen, L., Leonardo, T. R., Chen, Z., & DiPietro, L. A. (2021). Dermal fibroblast phagocytosis of apoptotic cells: A novel pathway for wound resolution. *FASEB Journal*, 35(4), e21443. <https://doi.org/10.1096/fj.202002078R>
- Rousselle, P., Braye, F., & Dayan, G. (2019). Re-epithelialization of adult skin wounds: Cellular mechanisms and therapeutic strategies. *Advanced Drug Delivery Reviews*, 146, 344–365. <https://doi.org/10.1016/j.addr.2018.06.019>
- Rousselle, P., Montmasson, M., & Garnier, C. (2019). Extracellular matrix contribution to skin wound re-epithelialization. *Matrix Biology*, 75–76, 12–26.

<https://doi.org/10.1016/j.matbio.2018.01.002>

- Rouwkema, J., & Khademhosseini, A. (2016, September 1). Vascularization and Angiogenesis in Tissue Engineering: Beyond Creating Static Networks. *Trends in Biotechnology*, 34(9), 733–745. <https://doi.org/10.1016/j.tibtech.2016.03.002>
- Safferling, K., Sütterlin, T., Westphal, K., Ernst, C., Breuhahn, K., James, M., ... Grabe, N. (2013). Wound healing revised: A novel reepithelialization mechanism revealed by in vitro and in silico models. *Journal of Cell Biology*, 203(4), 691–709. <https://doi.org/10.1083/jcb.201212020>
- Sakar, M. S., Eyckmans, J., Pieters, R., Eberli, D., Nelson, B. J., & Chen, C. S. (2016). Cellular forces and matrix assembly coordinate fibrous tissue repair. *Nature Communications*, 7, 1–8. <https://doi.org/10.1038/ncomms11036>
- Sakurai, Y., Hardy, E. T., Ahn, B., Tran, R., Fay, M. E., Ciciliano, J. C., ... Lam, W. A. (2018). A microengineered vascularized bleeding model that integrates the principal components of hemostasis. *Nature Communications*, 9(1), 1–9. <https://doi.org/10.1038/s41467-018-02990-x>
- Sami, D. G., Heiba, H. H., & Abdellatif, A. (2019, March 1). Wound healing models: A systematic review of animal and non-animal models. *Wound Medicine*, 24(1), 8–17. <https://doi.org/10.1016/j.wndm.2018.12.001>
- Scheja, L., & Heeren, J. (2019, July 11). The endocrine function of adipose tissues in health and cardiometabolic disease. *Nature Reviews. Endocrinology*, 15, 507–524. <https://doi.org/10.1038/s41574-019-0230-6>
- Schroeder, A. B., Karim, A., Ocotl, E., Dones, J. M., Chacko, J. V, Liu, A., ... Eliceiri, K. W. (2020). Optical imaging of collagen fiber damage to assess thermally injured human skin. *Wound Repair and Regeneration*, 28(6), 848–855. <https://doi.org/10.1111/wrr.12849>
- Schultz, G. S., Davidson, J. M., Kirsner, R. S., Bornstein, P., & Herman, I. M. (2011, March 1). Dynamic reciprocity in the wound microenvironment. *Wound Repair and Regeneration*, 19(2), 134–148. <https://doi.org/10.1111/j.1524-475X.2011.00673.x>
- Seaton, M., Hocking, A., & Gibran, N. S. (2015). Porcine models of cutaneous wound healing. *ILAR Journal*, 56(1), 127–138. <https://doi.org/10.1093/ilar/ilv016>
- Seeberg, J. C., Loibl, M., Moser, F., Schwegler, M., Büttner-Herold, M., Daniel, C., ... Distel, L. V. (2019). Non-professional phagocytosis: a general feature

- of normal tissue cells. *Scientific Reports*, 9(1), 1–8.  
<https://doi.org/10.1038/s41598-019-48370-3>
- Segal, G., Lee, W., Arora, P. D., McKee, M., Downey, G., & McCulloch, C. A. G. (2001). Involvement of actin filaments and integrins in the binding step in collagen phagocytosis by human fibroblasts. *Journal of Cell Science*, 114(1), 119–129. <https://doi.org/10.1242/jcs.114.1.119>
- Sen, C. K. (2019, February 2). Human Wounds and Its Burden: An Updated Compendium of Estimates. *Advances in Wound Care*, 8(2), 39–48.  
<https://doi.org/10.1089/wound.2019.0946>
- Seok, J., Warren, H. S., Alex, G. C., Michael, N. M., Henry, V. B., Xu, W., ... Tompkins, R. G. (2013). Genomic responses in mouse models poorly mimic human inflammatory diseases. *Proceedings of the National Academy of Sciences of the United States of America*, 110(9), 3507–3512.  
<https://doi.org/10.1073/pnas.1222878110>
- Shamis, Y., J. Hewitt, K., Bear, S. E., Addy, A. H., Qari, H., Margvelashvili, M., ... Garlick, J. A. (2012). iPSC-derived fibroblasts demonstrate augmented production and assembly of extracellular matrix proteins. *In Vitro Cellular and Developmental Biology - Animal*, 48(2), 112–122.  
<https://doi.org/10.1007/s11626-011-9478-4>
- Shimbori, C., Bellaye, P. S., Xia, J., Gauldie, J., Ask, K., Ramos, C., ... Kolb, M. (2016). Fibroblast growth factor-1 attenuates TGF- $\beta$ 1-induced lung fibrosis. *The Journal of Pathology*, 240(2), 197–210.  
<https://doi.org/10.1002/PATH.4768>
- Shin, J. U., Abaci, H. E., Herron, L., Guo, Z., Sallee, B., Pappalardo, A., ... Christiano, A. M. (2020). Recapitulating T cell infiltration in 3D psoriatic skin models for patient-specific drug testing. *Scientific Reports*, 10(1), 1–12.  
<https://doi.org/10.1038/s41598-020-60275-0>
- Shravani, K. S., Agrawal, P., & Raksha, M. (2021). Recent trends in microfluidics-based skin-on-a-chip models and applications. *International Journal of Advance Research, Ideas and Innovations in Technology*, 7(3), 729–737.
- Sindrilaru, A., Peters, T., Schymeinsky, J., Oreshkova, T., Wang, H., Gompf, A., ... Scharffetter-Kochanek, K. (2009). Wound healing defect of Vav3<sup>-/-</sup> mice due to impaired  $\beta$ 2-integrin-dependent macrophage phagocytosis of apoptotic neutrophils. *Blood*, 113(21), 5266–5276.  
<https://doi.org/10.1182/blood-2008-07-166702>

- Smith, S. A., Travers, R. J., & Morrissey, J. H. (2015, July 4). How it all starts: Initiation of the clotting cascade. *Critical Reviews in Biochemistry and Molecular Biology*, 50(4), 326–336.  
<https://doi.org/10.3109/10409238.2015.1050550>
- Smithmyer, M. E., Sawicki, L. A., & Kloxin, A. M. (2014, April 1). Hydrogel scaffolds as in vitro models to study fibroblast activation in wound healing and disease. *Biomaterials Science*, 2, 634–650.  
<https://doi.org/10.1039/c3bm60319a>
- Song, H. H. G., Rumma, R. T., Ozaki, C. K., Edelman, E. R., & Chen, C. S. (2018). Vascular Tissue Engineering: Progress, Challenges, and Clinical Promise. *Cell Stem Cell*, 22(3), 340–354.  
<https://doi.org/10.1016/j.stem.2018.02.009>
- Sottile, J., & Hocking, D. C. (2002). Fibronectin polymerization regulates the composition and stability of extracellular matrix fibrils and cell-matrix adhesions. *Molecular Biology of the Cell*, 13(10), 3546–3559.  
<https://doi.org/10.1091/mbc.E02-01-0048>
- Sottile, J., Shi, F., Rublyevska, I., Chiang, H. Y., Lust, J., & Chandler, J. (2007). Fibronectin-dependent collagen I deposition modulates the cell response to fibronectin. *American Journal of Physiology - Cell Physiology*, 293(6).  
<https://doi.org/10.1152/ajpcell.00130.2007>
- Sprangers, S., Behrendt, N., Engelholm, L., Cao, Y., & Everts, V. (2017). Phagocytosis of Collagen Fibrils by Fibroblasts In Vivo Is Independent of the uPARAP/Endo180 Receptor. *Journal of Cellular Biochemistry*, 118(6), 1590–1595. <https://doi.org/10.1002/jcb.25821>
- Sprangers, S., & Everts, V. (2019, January 1). Molecular pathways of cell-mediated degradation of fibrillar collagen. *Matrix Biology*, 75–76, 190–200.  
<https://doi.org/10.1016/j.matbio.2017.11.008>
- Staton, C. A., Stribbling, S. M., Tazzyman, S., Hughes, R., Brown, N. J., & Lewis, C. E. (2004, October 1). Current methods for assaying angiogenesis in vitro and in vivo. *International Journal of Experimental Pathology*, 85(5), 233–248.  
<https://doi.org/10.1111/j.0959-9673.2004.00396.x>
- Stryker, Z. I., Rajabi, M., Davis, P. J., & Mousa, S. A. (2019, May 16). Evaluation of angiogenesis assays. *Biomedicines*, 7(2), 37.  
<https://doi.org/10.3390/biomedicines7020037>
- Sullivan, T. P., Eaglstein, W. H., Davis, S. C., & Mertz, P. (2001, March 1). The pig as a model for human wound healing. *Wound Repair and Regeneration*,

9(2), 66–76. <https://doi.org/10.1046/j.1524-475X.2001.00066.x>

Sumagin, R., Brazil, J. C., Nava, P., Nishio, H., Alam, A., Luissint, A. C., ... Parkos, C. A. (2016). Neutrophil interactions with epithelial-expressed ICAM-1 enhances intestinal mucosal wound healing. *Mucosal Immunology*, 9(5), 1151–1162. <https://doi.org/10.1038/mi.2015.135>

Sun, C., Tian, X., Jia, Y., Yang, M., Li, Y., & Fernig, D. G. (2022). Functions of exogenous FGF signals in regulation of fibroblast to myofibroblast differentiation and extracellular matrix protein expression. *Open Biology*, 12(9). <https://doi.org/10.1098/RSOB.210356>

Svystonyuk, D. A., Ngu, J. M. C., Mewhort, H. E. M., Lipon, B. D., Teng, G., Guzzardi, D. G., ... Fedak, P. W. M. (2015a). Fibroblast growth factor-2 regulates human cardiac myofibroblast-mediated extracellular matrix remodeling. *Journal of Translational Medicine*, 13(1), 1–11. <https://doi.org/10.1186/s12967-015-0510-4>

Svystonyuk, D. A., Ngu, J. M. C., Mewhort, H. E. M., Lipon, B. D., Teng, G., Guzzardi, D. G., ... Fedak, P. W. M. (2015b). Fibroblast growth factor-2 regulates human cardiac myofibroblast-mediated extracellular matrix remodeling. *Journal of Translational Medicine*, 13(1), 1–11. <https://doi.org/10.1186/S12967-015-0510-4/FIGURES/5>

Tanaka, R., Fukushima, S.-I., Sasaki, K., Tanaka, Y., Murota, H., Matsumoto, K., ... Yasui, T. (2013). In vivo visualization of dermal collagen fiber in skin burn by collagen-sensitive second-harmonic-generation microscopy. *Journal of Biomedical Optics*, 18(06), 1. <https://doi.org/10.1117/1.jbo.18.6.061231>

Tang, P. M. K., Nikolic-Paterson, D. J., & Lan, H. Y. (2019, January 28). Macrophages: versatile players in renal inflammation and fibrosis. *Nature Reviews. Nephrology*, 15, 144–158. <https://doi.org/10.1038/s41581-019-0110-2>

Tefft, J. B., Chen, C. S., & Eyckmans, J. (2021). Reconstituting the dynamics of endothelial cells and fibroblasts in wound closure. *APL Bioengineering*, 5(1), 016102. <https://doi.org/10.1063/5.0028651>

Teng, Y. Y., Zou, M. L., Zhou, X. J., Wu, J. J., Liu, S. Y., Yuan, Z. D., ... Yuan, F. L. (2022, October 1). Novel prospects for scarless wound healing: The roles of myofibroblasts and adipocytes. *Journal of Cellular and Molecular Medicine*, 26(20), 5113–5121. <https://doi.org/10.1111/jcmm.17535>

Tiraravesit, N., Humbert, P., Robin, S., Tissot, M., Viennet, C., & Viyoch, J. (2017). Artocarpin-enriched (*Artocarpus altilis*) Heartwood Extract Provides

- Protection Against UVB-induced Mechanical Damage in Dermal Fibroblasts. *Photochemistry and Photobiology*, 93(5), 1232–1239. <https://doi.org/10.1111/php.12788>
- Tomasek, J. J., Gabbiani, G., Hinz, B., Chaponnier, C., & Brown, R. A. (2002). Myofibroblasts and mechano: Regulation of connective tissue remodelling. *Nature Reviews. Molecular Cell Biology*, 3, 349–363. <https://doi.org/10.1038/nrm809>
- Tomasek, J. J., Haaksma, C. J., Schwartz, R. J., & Howard, E. W. (2013). Whole animal knockout of smooth muscle alpha-actin does not alter excisional wound healing or the fibroblast-to-myofibroblast transition. *Wound Repair and Regeneration*, 21(1), 166–176. <https://doi.org/10.1111/WRR.12001>
- Tracy, L. E., Minasian, R. A., & Caterson, E. J. (2016). Extracellular Matrix and Dermal Fibroblast Function in the Healing Wound. *Advances in Wound Care*, 5(3), 119–136. <https://doi.org/10.1089/wound.2014.0561>
- Trump, B. F., Berezesky, I. K., Chang, S. H., & Phelps, P. C. (1997). The pathways of cell death: Oncosis, apoptosis, and necrosis. *Toxicologic Pathology*, 25(1), 82–88. <https://doi.org/10.1177/019262339702500116>
- Tsai, C. C., Ma, R. H., & Shieh, T. Y. (1999). Deficiency in collagen and fibronectin phagocytosis by human buccal mucosa fibroblasts in vitro as a possible mechanism for oral submucous fibrosis. *Journal of Oral Pathology and Medicine*, 28(2), 59–63. <https://doi.org/10.1111/j.1600-0714.1999.tb01997.x>
- Tuladhar, A., & Shoichet, M. S. (2018). Biomaterials driving repair after stroke. *Nature Materials*, 17(7), 573–574. <https://doi.org/10.1038/s41563-018-0124-3>
- Ud-Din, S., & Bayat, A. (2017). Non-animal models of wound healing in cutaneous repair: In silico, in vitro, ex vivo, and in vivo models of wounds and scars in human skin. *Wound Repair and Regeneration*, 25(2), 164–176. <https://doi.org/10.1111/wrr.12513>
- Ugurlu, B., & Karaoz, E. (2020, December 1). Comparison of similar cells: Mesenchymal stromal cells and fibroblasts. *Acta Histochemica*, 122(8), 151634. <https://doi.org/10.1016/j.acthis.2020.151634>
- Urciuolo, F., Passariello, R., Imparato, G., Casale, C., & Netti, P. A. (2022). Bioengineered Wound Healing Skin Models: The Role of Immune Response and Endogenous ECM to Fully Replicate the Dynamic of Scar Tissue Formation In Vitro. *Bioengineering*, 9(6), 233.

<https://doi.org/10.3390/bioengineering9060233>

- Usui, M. L., Underwood, R. A., Mansbridge, J. N., Muffley, L. A., Carter, W. G., & Olerud, J. E. (2005). Morphological evidence for the role of suprabasal keratinocytes in wound reepithelialization. *Wound Repair and Regeneration*, 13(5), 468–479. <https://doi.org/10.1111/j.1067-1927.2005.00067.x>
- van Putten, S., Shafieyan, Y., & Hinz, B. (2016, April 1). Mechanical control of cardiac myofibroblasts. *Journal of Molecular and Cellular Cardiology*, 93, 133–142. <https://doi.org/10.1016/j.yjmcc.2015.11.025>
- Vaughan, M. B., Ramirez, R. D., Brown, S. A., Yang, J. C., Wright, W. E., & Shay, J. W. (2004). A reproducible laser-wounded skin equivalent model to study the effects of aging in vitro. *Rejuvenation Research*, 7(2), 99–110. <https://doi.org/10.1089/1549168041552982>
- Vaughan, R. B., & Trinkaus, J. P. (1966). Movements of epithelial cell sheets in vitro. *Journal of Cell Science*, 1(4), 407–413. <https://doi.org/10.1242/jcs.1.4.407>
- Vedula, S. R. K., Peyret, G., Cheddadi, I., Chen, T., Brugués, A., Hirata, H., ... Ladoux, B. (2015). Mechanics of epithelial closure over non-adherent environments. *Nature Communications*, 6(1), 6111. <https://doi.org/10.1038/ncomms7111>
- Velnar, T., Bailey, T., & Smrkolj, V. (2009). The wound healing process: An overview of the cellular and molecular mechanisms. *Journal of International Medical Research*, 37(5), 1528–1542. <https://doi.org/10.1177/147323000903700531>
- Vidmar, J., Chingwaru, C., & Chingwaru, W. (2017, April 1). Mammalian cell models to advance our understanding of wound healing: a review. *Journal of Surgical Research*, 210, 269–280. <https://doi.org/10.1016/j.jss.2016.10.016>
- Vogel, A., & Venugopalan, V. (2003, February). Mechanisms of pulsed laser ablation of biological tissues. *Chemical Reviews*, 103(2), 577–644. <https://doi.org/10.1021/cr010379n>
- Wang, H., Haeger, S. M., Kloxin, A. M., Leinwand, L. A., & Anseth, K. S. (2012). Redirecting valvular myofibroblasts into dormant fibroblasts through light-mediated reduction in substrate modulus. *PLoS ONE*, 7(7), e39969. <https://doi.org/10.1371/journal.pone.0039969>
- Weng, T., Wu, P., Zhang, W., Zheng, Y., Li, Q., Jin, R., ... Wang, X. (2020, February 3). Regeneration of skin appendages and nerves: Current status

- and further challenges. *Journal of Translational Medicine*, 18, 53.  
<https://doi.org/10.1186/s12967-020-02248-5>
- Wickett, R. R., & Visscher, M. O. (2006). Structure and function of the epidermal barrier. *American Journal of Infection Control*, 34(10 SUPPL.), S98–S110.  
<https://doi.org/10.1016/j.ajic.2006.05.295>
- Winter, G. D. (1972). Epidermal regeneration studies in the domestic pig. *Epidermal Wound Healing*, 71–112.  
<https://cir.nii.ac.jp/crid/1570854174772619008>
- Wong, S. L., Demers, M., Martinod, K., Gallant, M., Wang, Y., Goldfine, A. B., ... Wagner, D. D. (2015). Diabetes primes neutrophils to undergo NETosis, which impairs wound healing. *Nature Medicine*, 21(7), 815–819.  
<https://doi.org/10.1038/nm.3887>
- Woodley, D. T. (1996). Reepithelialization. In Clark, R.A.F. (ed.) *The Molecular and Cellular Biology of Wound Repair* (pp. 339–354). Springer, Boston, MA.  
[https://doi.org/10.1007/978-1-4899-0185-9\\_10](https://doi.org/10.1007/978-1-4899-0185-9_10)
- Wufuer, M., Lee, G. H., Hur, W., Jeon, B., Kim, B. J., Choi, T. H., & Lee, S. H. (2016). Skin-on-a-chip model simulating inflammation, edema and drug-based treatment. *Scientific Reports*, 6(1), 1–12.  
<https://doi.org/10.1038/srep37471>
- Wynn, T. A. (2008, January 1). Cellular and molecular mechanisms of fibrosis. *Journal of Pathology*, 214(2), 199–210. <https://doi.org/10.1002/path.2277>
- Xie, Y., Rizzi, S. C., Dawson, R., Lynam, E., Richards, S., Leavesley, D. I., & Upton, Z. (2010). Development of a three-dimensional human skin equivalent wound model for investigating novel wound healing therapies. *Tissue Engineering - Part C: Methods*, 16(5), 1111–1123.  
<https://doi.org/10.1089/ten.tec.2009.0725>
- Xu, R., Boudreau, A., & Bissell, M. J. (2009, January 23). Tissue architecture and function: Dynamic reciprocity via extra- and intra-cellular matrices. *Cancer and Metastasis Reviews*, 28, 167–176. <https://doi.org/10.1007/s10555-008-9178-z>
- Yang, G., Mahadik, B., Choi, J. Y., & Fisher, J. P. (2020, January 9). Vascularization in tissue engineering: Fundamentals and state-of-art. *Progress in Biomedical Engineering*, 2, 012002.  
<https://doi.org/10.1088/2516-1091/ab5637>

- Yoneda, A., Multhaupt, H. A. B., & Couchman, J. R. (2005). The Rho kinases I and II regulate different aspects of myosin II activity. *Journal of Cell Biology*, *170*(3), 443–453. <https://doi.org/10.1083/jcb.200412043>
- Zhang, Q., Wang, P., Fang, X., Lin, F., Fang, J., & Xiong, C. (2022). Collagen gel contraction assays: From modelling wound healing to quantifying cellular interactions with three-dimensional extracellular matrices. *European Journal of Cell Biology*, *101*(3), 151253. <https://doi.org/10.1016/j.ejcb.2022.151253>
- Zhao, R., Liang, H., Clarke, E., Jackson, C., & Xue, M. (2016, December 11). Inflammation in chronic wounds. *International Journal of Molecular Sciences*, *17*(12), 2085. <https://doi.org/10.3390/ijms17122085>
- Zhu, Z., Ding, J., Shankowsky, H. A., & Tredget, E. E. (2013, December 18). The molecular mechanism of hypertrophic scar. *Journal of Cell Communication and Signaling*, *7*, 239–252. <https://doi.org/10.1007/s12079-013-0195-5>

**CURRICULUM VITAE**

